

**Wetting Phenomena and  
Interactions in Phase-Separated  
Colloid-Polymer Mixtures**

Promotor: Prof. dr. M. A. Cohen Stuart,  
hoogleraar fysische chemie, met bijzondere aandacht voor de  
kolloïdchemie

Copromotor: Dr. ir. N. A. M. Besseling,  
universitair docent bij de leerstoelgroep Fysische Chemie  
en Kolloïdkunde

#### Samenstelling promotiecommissie

Prof. dr. G. H. Findenegg	Technische Universität Berlin, Deutschland
Prof. dr. B. Vincent	University of Bristol, United Kingdom
Prof. dr. H. N. W. Lekkerkerker	Universiteit Utrecht, Nederland
Prof. dr. E. van der Linden	Wageningen Universiteit, Nederland

# Wetting Phenomena and Interactions in Phase-Separated Colloid-Polymer Mixtures

Willem Karel Wijting

Proefschrift

ter verkrijging van de graad van doctor

op gezag van de rector magnificus

van Wageningen Universiteit,

prof. dr. ir. L. Speelman,

in het openbaar te verdedigen

op maandag 10 mei 2004

des namiddags te half twee in de Aula.

ISBN 90-8504-018-3

*Aan Rob en Riet Wijting*



# Contents

<b>Chapter 1. Introduction</b>	1
1.1. Colloidal systems	1
1.2. Interactions in colloid-polymer mixtures	2
1.3. Phase behaviour of colloid-polymer mixtures	5
1.4. Wetting	11
1.5. Outline of this thesis	15
References	15
<b>Chapter 2. Depletion Interaction measured by Colloidal Probe Atomic Force Microscopy</b>	17
2.1. Introduction	18
2.2. Theories on depletion interaction	19
2.2.1. Derjaguin approximation	23
2.3. Experimental	23
2.3.1. Preparation of spheres and plates	23
2.3.2. Attaching a sphere to an AFM-cantilever	24
2.3.3. Force measurements	24
2.4. Results and Discussion	26
2.4.1. Force measurements between a hard sphere and a plate	26
2.4.2. Force measurements between a sphere and a plate in the presence of a polymer solution	27
2.5. Conclusions	34
Appendix 2A. Self-consistent field modelling of homopolymers in a slit	35
References	37
<b>Chapter 3. Wetting in a Colloidal Liquid-Gas System</b>	39
References	47
<b>Chapter 4. Wetting Behaviour in Colloid-Polymer Mixtures at Different Substrates</b>	49
4.1. Introduction	50
4.2. Experimental	52
4.2.1. Colloidal system	52
4.2.2. Wetting experiments	53
4.2.3. Substrates	54

4.3. Results and discussion	54
4.4. Conclusions	65
References	65
<b>Summary and Outlook</b>	67
Summary	67
Outlook	68
References	69
<b>Samenvatting voor niet-vakgenoten</b>	71
<b>List of publications</b>	77
<b>Dankwoord</b>	79
<b>Curriculum vitae</b>	81



# CHAPTER 1

## Introduction

The central theme of this thesis is the wetting behaviour of phase-separated mixtures of non-adsorbing polymer and spherical solid colloids dispersed in a liquid. The phase behaviour of this kind of colloid-polymer mixtures is regulated by depletion interactions. These depletion interactions exist between particles, but also between a particle and a flat substrate. Therefore, wetting behaviour is also regulated by these depletion interactions. Because both phase behaviour and wetting behaviour of colloid-polymer mixtures are regulated by depletion interactions it is important to quantify the depletion interaction. Therefore we also investigated this depletion interaction itself.

In this first chapter of this thesis, depletion interactions and phase behaviour of colloid-polymer mixtures will be reviewed. Furthermore, some concepts concerning wetting will be introduced. In the second chapter we present measurements of the depletion interaction between surfaces in the presence of a non-adsorbing polymer solution. The instrument used for these measurements is the colloidal probe atomic force microscope. In the third chapter, investigations on the wetting behaviour of phase separated colloid polymer mixtures near a hard wall are reported. In chapter four the latter theme is discussed in more detail and extended to wetting phenomena near a 'soft' (polymer-covered) wall.

### 1.1. Colloidal systems

Colloidal systems consist of particles of a size between  $\sim 1$  and  $\sim 1000$  nm. These particles are suspended in a medium. An important class of colloidal systems consist of solid or liquid particles dispersed in a liquid, but also a gas phase can be dispersed in a liquid phase (foam) or a solid or liquid phase in a gas phase (fume and fog). Examples of colloidal systems playing a role in every day life are paint, ink, and many food systems such as milk products or white beer. Many biological fluids, such as blood and protein solutions are also examples of colloidal systems. Colloidal systems have not just practical value; they are also scientifically interesting. For example, they have played an important role as model systems for molecular systems.<sup>1</sup> Because in colloidal systems the particles are larger than in molecular systems, relevant time and length scales are also larger. These larger time and length scales make colloidal systems in some respects more convenient for experimental studies than atomic or molecular materials. Colloidal particles can be prepared with variable sizes and shapes. Another important property of colloidal particles is that their interactions can be tuned, both in *range* and *strength*. Macroscopic properties of colloidal suspensions such as rheological and phase behaviour

are determined by these interactions. We therefore briefly discuss the most important interactions.

## 1.2. Interactions in colloid-polymer mixtures

In colloidal systems different types of interactions may occur. The first to be mentioned is the Van der Waals attraction. This is a long range attraction. Its origin is the polarizability of the individual atoms which make up the colloidal particles. This type of interaction occurs also in molecular systems. In molecular or atomic systems the Van der Waals interaction energy scales with the separation distance  $h$  as  $h^{-6}$ . For two identical spherical colloidal particles of radius  $R$ , the Van der Waals interaction energy is attractive and scales with  $h^{-1}$  if  $h \ll R$ . Van der Waals interactions play an important role in concentrated colloidal systems. However, the distance dependence of this attraction is determined by the shape of the particles and cannot be tuned. The strength can be changed by dispersing the particles in a different medium. The Van der Waals attraction can induce irreversible flocculation of particles because of the divergence of the interaction potential for  $h \rightarrow 0$ . This often deep potential well is called the primary minimum. The Van der Waals interaction can be screened by dispersing the particles in a medium of similar refractive index. According to Lifschitz theory, the Van der Waals interaction of particles consisting of material A with dielectric permittivity  $\varepsilon_A$ , dispersed in a medium B with dielectric permittivity  $\varepsilon$  is proportional to  $(\varepsilon_A - \varepsilon_B)^2$ . This implies that the Van der Waals interaction vanishes when the particles and medium have similar refractive indices.<sup>2</sup>

The second kind of interactions that plays an important role in many (mostly aqueous) colloidal systems is the electrostatic repulsion due to charge on the surface of the particles. Numerous colloidal systems consist of inorganic oxides or poorly soluble salts, which acquire charge at their surface when dispersed in water. The charge is induced by ions which have an affinity to the surface. If the concentrations of these ions in the bulk is changed, the charge of the surface is changed. These ions are called charge determining ions. The surface charge, together with counter charge in the solvent, constitute the electric double layer around the particle. The electric double layer interaction gives rise to repulsion and is important in these colloidal systems, since it regulates its kinetic stability. The range and strength of this double layer repulsion can be tuned by changing the salt concentration and the concentration of charge determining ions, respectively. DLVO-theory describes colloid stability in terms of a combination of the Van der Waals attraction and the electrostatic repulsion.<sup>3</sup>

The surface of a colloidal particle can be modified by covering it with different kinds of compounds. For example, these can be low molecular organic compounds or polymers. Such a modification may yield steric repulsion. Modifying the surface of the particles with an aliphatic compound and dispersing them in an organic solvent may eliminate

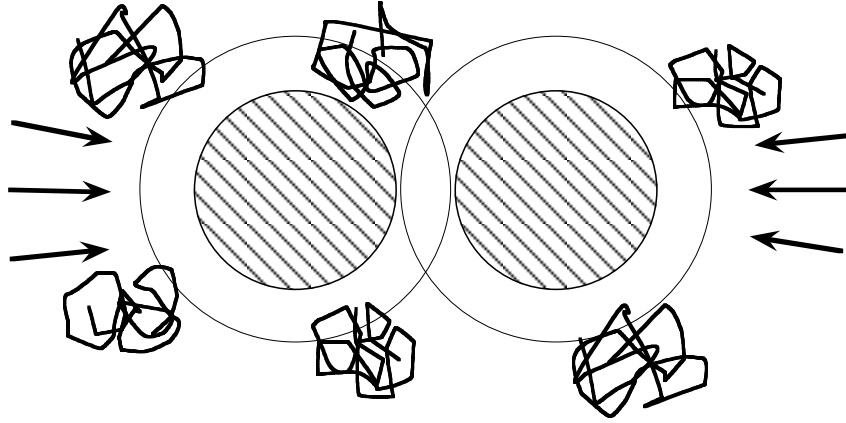


FIGURE 1.1. Polymer in a dispersion of colloidal particles. Imbalance of the polymer osmotic pressure pushes the particles together.

the electrostatic repulsion. If uncharged particles are dispersed in a medium of similar refractive index, the Van der Waals interaction is negligible and the particles can be regarded as simple hard spheres.

Another important type of interaction is depletion interaction. It is well known that addition of non-adsorbing polymer to a colloidal suspension of hard particles leads to an attractive contribution to the pair potential of the particles.<sup>4, 5</sup> For entropic reasons the center of a polymer coil is excluded from a zone around a colloidal particle. Such a zone is called 'depletion zone' or 'depletion layer'. In that zone the polymer segment concentration is lower than in the bulk. When the depletion zones of two particles overlap, there will be an imbalance of the osmotic pressure exerted by the polymers on the particles, since there can be no polymer between the two particles. This imbalance will push the particles together, leading to an effective attraction between the particles, see figure 1.1. This attraction is called depletion interaction. Depletion interaction for flat plates was first described by Asakura and Oosawa<sup>4</sup> and for hard spheres by Vrij.<sup>5</sup> The range of this interaction depends on the size of a polymer coil (as long as the polymer concentration is sufficiently low), so we can tune the range of this depletion attraction by varying the molar mass of the polymer. The strength depends on the osmotic pressure, so we can tune the strength by varying the concentration of the polymer. If the concentrations of both polymer and colloid are high enough, this attraction will induce a flocculation on a macroscopic phase separation.

Since colloidal systems have a rather constant volume, we consider the Helmholtz free energy, further denoted as free energy and indicated by  $G$ , in this section. In general the free energy of the depletion interaction is given by the osmotic pressure,  $\Pi_b$ , of the polymer multiplied by the overlap volume of the depletion zones:

$$G_{dep} = -\Pi_b V_{overlap} \quad (1.1)$$

In the simplest model for describing depletion interaction the polymer solution is regarded to be ideal. This implies that (i) the osmotic pressure is assumed to be given by the law of Van't Hoff, (ii) swelling of polymer because of intrachain excluded volume interactions is ignored, and (iii) the range of the depletion interaction is assumed to be independent of solvent quality and polymer concentration. Furthermore, the polymer-substrate interaction is regarded as a hard sphere interaction. According to equation (1.1) and these four assumptions, the interaction free energy per unit area for two flat plates,  $G_a(h)$  as a function of the separation distance  $h$  for two flat plates can be expressed as

$$G_a(h) = \begin{cases} -\Pi_b(2\delta_0 - h) & 0 < h \leq 2\delta_0 \\ 0 & h \geq 2\delta_0 \end{cases} \quad (1.2)$$

where  $\delta_0$  is the depletion layer thickness at infinite dilution, which is in turn given by  $\delta_0 = 2R_g/\sqrt{\pi}$ , with  $R_g$  the radius of gyration of the polymer.<sup>4</sup>

Vrij gave an expression for the depletion interaction between spherical particles according to the ideal polymer model. Let us consider a solvent in which colloidal particles with diameter  $\sigma$  are dispersed and polymer with a diameter  $\sigma_0$  is dissolved. The colloidal particle-particle interaction and the particle-polymer interaction are assumed to be hard sphere interactions and the polymer-polymer interaction is assumed to be zero (the polymer coils can fully interpenetrate). In many respects, the three component system of particles, polymer and solvent can be regarded as a one component system of particles in a homogeneous medium. According to equation (1.1) the depletion interaction free energy,  $G_{dep}(r)$ , for two spheres can be described as:

$$G_{dep}(r) = \begin{cases} \infty & (r < \sigma) \\ -\Pi_b \frac{4}{3} \pi \bar{\sigma}^3 \left[ 1 - \frac{3}{4} \left( \frac{r}{\bar{\sigma}} \right) + \frac{1}{16} \left( \frac{r}{\bar{\sigma}} \right)^3 \right] & (\sigma < r < 2\bar{\sigma}) \\ 0 & (r > 2\bar{\sigma}) \end{cases} \quad (1.3)$$

Here  $\bar{\sigma} = \frac{1}{2}(\sigma + \sigma_0)$  and  $r$  is the center to center distance of two colloidal particles. In figure 1.2  $G_{dep}(r)$  according to equation (1.3) is plotted as a function of  $r$ .

In real systems polymers rarely behave ideally, and it has been shown that predictions for the phase behaviour do not agree with experimental results.<sup>6-8</sup> Theories on depletion interaction for non-ideal systems are reviewed in chapter 2. The main conclusion of these theories is that for more concentrated systems in a good solvent the non-ideal behaviour of the polymers yields a higher osmotic pressure. This higher osmotic pressure leads to a stronger depletion interaction than in ideal polymer solutions. On the other hand, the range of the depletion interaction decreases for polymer concentrations above the overlap concentration.<sup>9-12</sup> The overlap concentration is the concentration where the center to center distance of individual polymer coils become equal to the

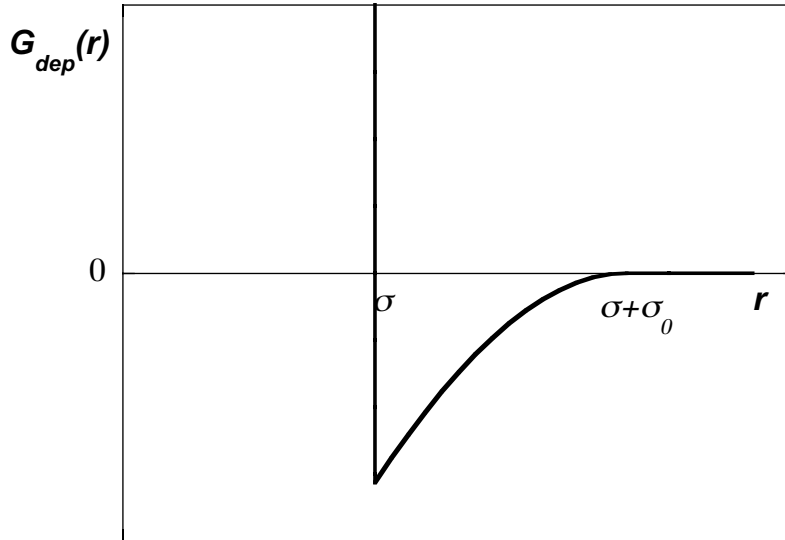


FIGURE 1.2. Depletion interaction free energy as a function of the center to center distance of two spheres according to the ideal polymer model.

radius of gyration.

### 1.3. Phase behaviour of colloid-polymer mixtures

A colloidal dispersion can assume different states: dilute disordered, condensed disordered, and solid disordered states, and an ordered solid state, analogously to respectively gas, liquid, glass, and crystal states in molecular systems. Accordingly, a dilute disordered dispersion is often called *colloidal gas*, a concentrated disordered fluid system *colloidal liquid* and a concentrated ordered one *colloidal crystal*. A solid disordered colloidal dispersion may be called colloidal glass

Under certain conditions, two phases can coexist; the system is phase separated. Generally, phase separation occurs when the free energy of two coexisting phases in the system is lower than that of one homogeneous phase. In figure 1.3 we present a schematic plot of the free energy  $F(V, T, N)$  as a function of the number concentration  $\rho$  ( $= V/N$ ) for a certain temperature for an arbitrary canonical system;  $V$  is the volume,  $T$  the temperature, and  $N$  the number of particles. When the overall composition  $\rho$  of the system satisfies  $\rho_A < \rho < \rho_B$  the system will lower its free energy by separating into two phases **A** and **B**. The points **A** and **B** have a common tangent, so that  $(\frac{\partial F(A)}{\partial \rho_A})_{V,T} = (\frac{\partial F(B)}{\partial \rho_B})_{V,T}$ . Since the volume of the system is constant it can be concluded that the chemical potential  $\mu$  of both phases must be equal,  $\mu_A = \mu_B$  ( $\mu = (\frac{\partial F}{\partial N})_{V,T}$ ). The points **A** and **B** are called binodal points. These can correspond to the gas, liquid, and crystal phases. Plotting the points **A** and **B** for different temperatures yields a phase diagram.

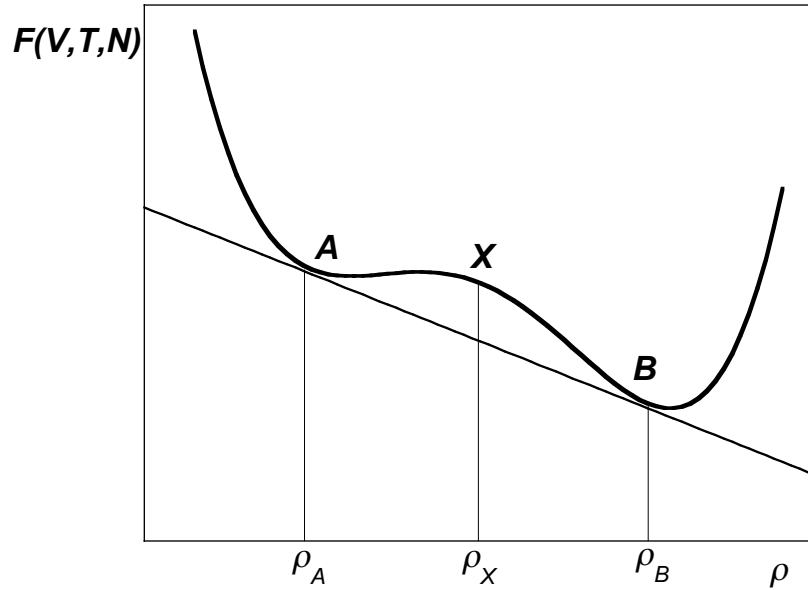


FIGURE 1.3. Free energy  $F(V, T, N)$  as a function of the number concentration. The free energy of the overall composition  $\rho_X$  can be lowered by separating into two phases of composition  $\rho_A$  and  $\rho_B$ . The points **A** and **B** have a common tangent.

A schematic presentation of a phase diagram for a simple monoatomic compound (e.g., argon) is presented in figure 1.4. In systems where a liquid and a gas state exist, there is always a critical temperature  $T_c$ . Above this temperature no phase transition from the gas to the liquid state occurs upon increasing the concentration. This state is called the supercritical fluid state. Below  $T_c$  there is a region in which two fluid states exist: the liquid and the gas states. At very high concentrations a phase transition to a crystal phase occurs. At the triple point (the line labelled 't.p.' in this diagram), the gas, liquid and crystal phase coexist.

In order to obtain a reversible gas-liquid phase separation, two specific properties of the interaction between the particles are required. (i) A short-range repulsive interaction, which prevents irreversible flocculation in the primary minimum; (ii) an attractive interaction which brings the particles together in order to obtain the liquid state. An important condition is that the range of the attraction must be of the same order of magnitude as the radius of the particles. For molecular systems, both the short range repulsion and the long range attraction are given with the molecular species and can therefore not be tuned. As mentioned in the previous section, for colloidal systems we can tune the interaction between particles by adding non-adsorbing polymer. In that case, the phase behaviour can easily be regulated.

In molecular systems the temperature is often the field variable which controls the phase behaviour. In colloid-polymer mixtures, it is the polymer chemical potential  $\mu_p$  which regulates the phase behaviour.<sup>1, 6, 13, 14</sup> The polymer chemical potential is determined

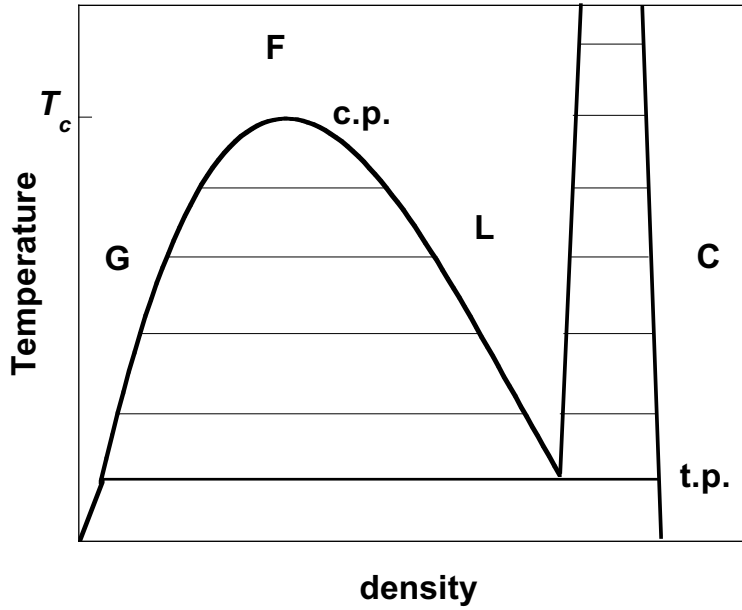


FIGURE 1.4. Schematic presentation of a phase diagram for a one atomic compound. The gas, liquid, fluid, and crystal phases are labelled **G**, **L**, **F**, and **C**, respectively. The critical point and the triple point are indicated by **c.p.** and **t.p.**, respectively.

by the polymer concentration. For a colloid-polymer mixture the semi-grand potential  $\Omega(V, T, N_c, \mu_p)$  plays a role similar to the free energy  $F(V, T, N)$  for a one component system, with  $N_c$  the number of colloidal particles, and  $\mu_p$  the polymer chemical potential. The colloids are treated canonically, whereas the polymers are treated grand canonically, see figure 1.5.

Lekkerkerker *et al.* developed the free volume theory to calculate phase diagrams.<sup>6</sup> In these phase diagrams the polymer concentration is plotted versus the colloid concentration. In literature on depletion interactions and on colloidal phase behaviour several measures for the polymer concentrations are used. The polymer concentration is often expressed as the polymer segment volume fraction,  $\varphi_b$ :

$$\varphi_b = \frac{N_p v_s N}{V} \quad (1.4)$$

Here  $N_p$  is the number of polymers in a phase occupying a volume  $V$ ,  $v_s$  is the volume of one segment, and  $N$  is the number of segments per polymer chain. This quantity will be used in chapter 2. In phase diagrams the polymer packing fraction,  $\varphi_p$  is often used, which is defined by

$$\varphi_p = \frac{N_p v_p}{V} = \frac{N_p \frac{4}{3} \pi R_g^3}{V} \quad (1.5)$$

where  $v_p$  is the volume, and  $R_g$  the radius of gyration of an entire polymer coil. Note that  $\varphi_p$  can only be determined if  $R_g$  is known and that  $R_g$  is not trivially related to the molar mass, particularly for polydisperse polymers. The polymer packing fraction

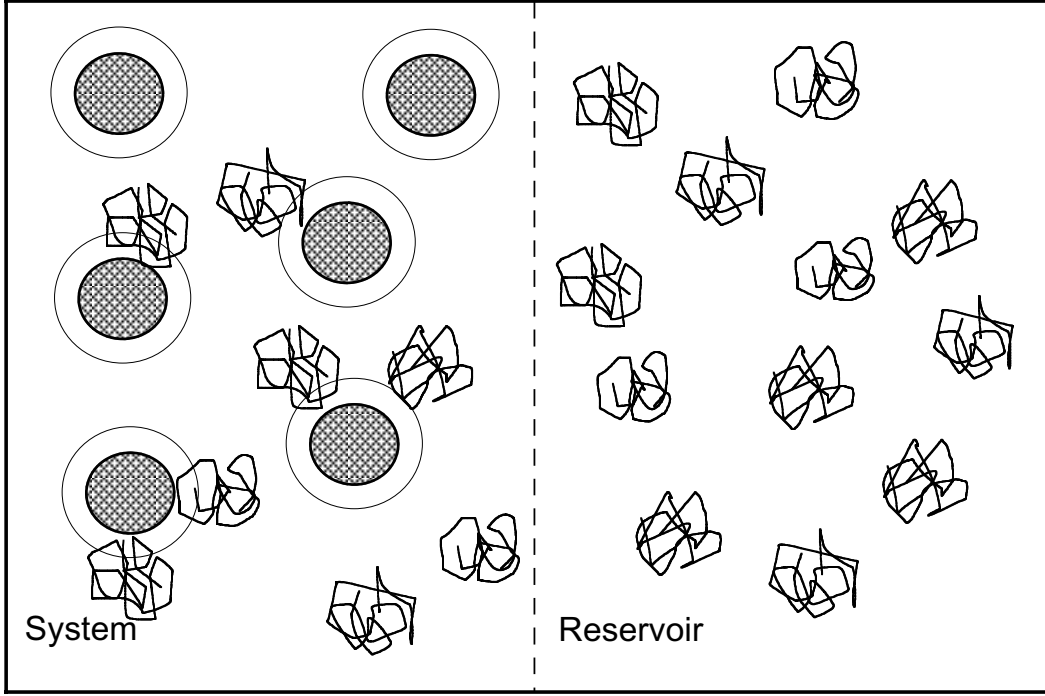


FIGURE 1.5. Schematic representation of a colloid-polymer mixture according to the semi-grand canonical system. The system is in equilibrium with the reservoir by means of a semi-permeable membrane. Only polymers can pass the membrane. In the system  $V$ ,  $T$ ,  $N_c$ , and  $\mu_p$  are constant and described by  $\Omega(V, T, N_c, \mu_p)$

is often one or two orders of magnitude larger than  $\varphi_b$  and by definition unity at the overlap concentration. In experimental phase diagrams of colloidal systems,  $\varphi_p$  is often plotted versus the colloid volume fraction,  $\varphi_c$ . An example of such a calculated phase diagram is presented in figure 1.6. In a phase-separated colloidal system  $\varphi_p$  is different in the two coexisting phases; the tielines are tilted. In the context of the semi-grand canonical system in figure 1.5, one can define a polymer reservoir concentration,  $\varphi_p^r$ . This quantity can be regarded as the polymer concentration in the free volume,  $V_{free}$ . This is the volume not occupied by the colloidal particles with their depletion zones.  $\varphi_p^r$  is directly related to the chemical potential and the osmotic pressure. Since  $\mu_p$  in both phases must be the same, it can be concluded that  $\varphi_p^r$  is equal in both phases.<sup>6, 13</sup>  $\varphi_p^r$  can be expressed as

$$\varphi_p^r = \frac{N_p \frac{4}{3} \pi R_g^3}{V_{free}} = \frac{N_p \frac{4}{3} \pi R_g^3}{\alpha V} = \frac{\varphi_p}{\alpha} \quad (1.6)$$

Here  $\alpha$  is the fraction of  $V_{free}$  of the total volume,  $V$  ( $\alpha = V_{free}/V$ ). It is important to note that  $\varphi_p$  is a density variable whereas  $\varphi_p^r$  is a field variable.



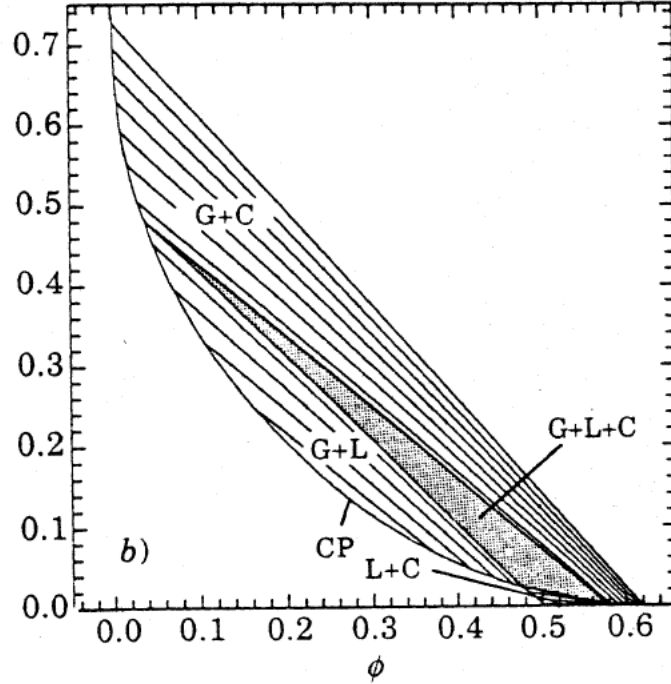


FIGURE 1.6. Phase diagram for colloid-polymer mixture for polymer-colloid size ratio  $q = 0.57$  in the  $\varphi_p$  versus  $\varphi_c$  representation. The symbols G, L, and C refer to the colloidal gas, liquid and gas phases respectively and the critical point is denoted by CP.<sup>6</sup>

For ideal polymers, the relation between the polymer chemical potential and the polymer reservoir concentration is:<sup>6</sup>

$$\mu_p = \mu_p^0 + k_B T \ln \frac{\rho_p}{\alpha} = \mu_p^0 + k_B T \ln \rho_p^r \quad (1.7)$$

Here,  $\mu_p^0$  is a reference chemical potential and  $\rho_p$  and  $\rho_p^r$  are the number concentration of polymer, and the reservoir number concentration of polymer, respectively.

At very low colloid volume fractions ( $\varphi_c < 0.01$ ) and for ideal polymers  $\alpha$  can be estimated by  $\alpha = 1 - \varphi_c(1 + q)^3$ , with  $q$  the polymer-colloid size ratio. An expression for  $\alpha$ , (still for ideal polymers) which leads to a better approximation, can be obtained by using scaled particle theory.<sup>1, 6, 15</sup> This results in

$$\alpha = (1 - \varphi_c) \exp[-(A\gamma + B\gamma^2 + C\gamma^3)] \quad (1.8)$$

where  $A = 3q + 3q^2 + q^3$ ,  $B = \frac{9}{2}q^2 + 3q^2$ , and  $C = 3q^3$  and  $\gamma = \varphi_c/(1 - \varphi_c)$ . A phase diagram for the same system as in figure 1.6 is presented in the  $\varphi_p^r$  versus  $\varphi_c$  representation in figure 1.7. Now the tielines are horizontal. Above the critical  $\varphi_p^r$  there is a region where colloidal liquid and colloidal gas coexist and below it there is no phase transition between a colloidal liquid and a colloidal gas phase, but only one fluid phase. If we compare figure 1.4 with figure 1.7 we see that the polymer reservoir

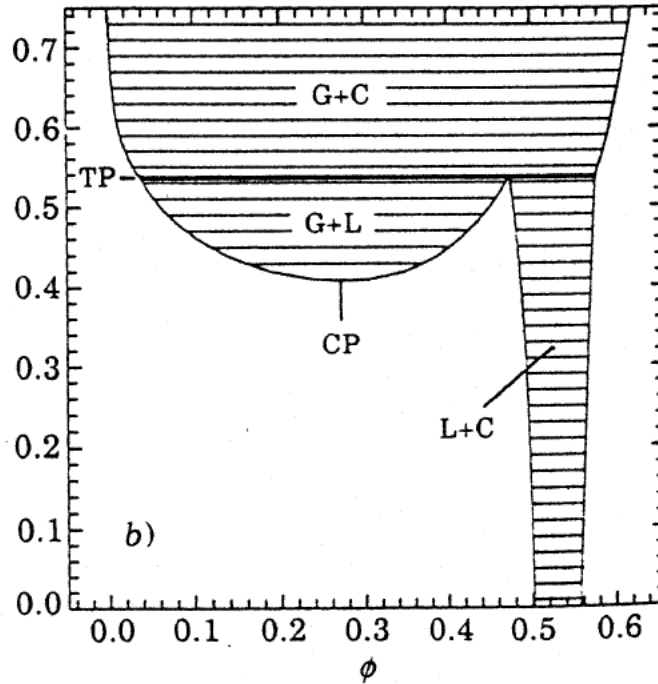


FIGURE 1.7. Phase diagram for colloid-polymer mixture for polymer-colloid size ratio  $q = 0.57$  in the  $\varphi_p^r$  versus  $\varphi_c$  representation. The symbols G, L, and C refer to the colloidal gas, liquid and gas phases respectively. The critical point and the triple point are indicated by CP and TP, respectively.<sup>6</sup>

volume fraction in colloidal systems plays a role similar to the inverse temperature in molecular systems.

It is found that the polymer-colloid size ratio  $q$  plays an important role in the phase behaviour of depletion interaction driven systems.<sup>1, 6, 13, 14</sup> If  $q < 0.3$  the system can separate into one colloidal fluid and a colloidal crystal phase. If  $q > 0.3$  two colloidal fluid phases may occur, the colloidal liquid and gas phases. From this it is concluded that for the existence of a liquid state indeed a long range attraction is required.

The phase behaviour for several colloid-polymer systems has been investigated, both experimentally and theoretically.<sup>1, 6, 13, 14</sup> However, theoretical calculations of phase diagrams do not agree with experimental observations. In experimental systems liquid-gas coexistence occurs often at higher polymer volume fractions than predicted by theory.<sup>7, 8, 16, 17</sup> One important reason for this may be that in the free volume theory the polymers are assumed to be ideal.

Recently, Aarts *et al.*,<sup>8</sup> using the free volume theory, calculated phase diagrams in which excluded volume effects between polymer chains are taken into account. These authors calculated the depletion layer thickness from the negative adsorption of polymer around a sphere using the correlation length and the osmotic pressure as determined from renormalization group theory.<sup>18</sup> They found that for small polymer-colloid size

ratios the difference from ideal behaviour is small, whereas for larger size ratios the two-phase coexistence region shifts to higher polymer concentrations. Furthermore, the liquid-crystal coexistence region becomes more extended. The gas-liquid and the gas-liquid-crystal regions become less extended. Their features lead to a better agreement with experiments.

As shown in the present and the previous section, the phase behaviour of colloid-polymer mixtures can be controlled, because the interactions can be controlled. A true liquid-like phase can exist, and various regions around the liquid-gas critical point can be explored. This is our motivation to use these systems for wetting studies.

## 1.4. Wetting

Wetting is an important phenomenon in every day life. When studying wetting phenomena, one investigates systems where three phases coexist. These might be two liquids, which are in equilibrium with their common gas phase, or a solid substrate in equilibrium with two fluid phases. In many model studies the latter case is studied. In practical cases it is often desirable to regulate the wetting properties. For instance, by means of paint on a surface. An unpainted piece of wood is wetted well by water. However, water will damage the wood, because it allows microorganisms to invade and chemically attack the wood macromolecules. The wettability of wood can be controlled by means of paint. If the wood is painted, the water wets the surface less well: the wood is protected by the layer of paint. On the other hand, in order to obtain a good layer of paint on the wood it is important that the fresh paint wets the wood well. Some other practical situations where wetting properties play an important role are wax on cars to protect the metal against corrosion, and goretex coats, which must breath (water vapour must pass the coat), but not transport the liquid water. In order to understand the wetting behaviour it is important to investigate the interactions which determine the wetting behaviour on a microscopic level. The past 25 years have seen a revival of the study of fundamental aspects of wetting phenomena in general and wetting transitions in particular.<sup>19-24</sup>

The wetting state is determined by the contact angle  $\theta$ . The contact angle is defined as the angle of the substrate with the gas-liquid interface, measured through the most dense fluid phase, see figure 1.8. In figure 1.8 a liquid drop is shown. Because  $0^\circ < \theta < 180^\circ$  this is a case of partial wetting.<sup>19</sup> If  $\theta = 0^\circ$  the substrate is said to be completely wet, a liquid film intervenes between the gas phase and the substrate. In that case no solid-gas interface exists. If  $\theta = 180^\circ$ , the substrate is completely 'dry'; it is completely wet by the gas phase. Here, a gas film intervenes between the liquid phase and the substrate and no solid-liquid interface exists. Complete drying does never occur in real molecular systems, because the Van der Waals attractions between condensed phases is always stronger than that between a condensed phase and a gas phase. However, in

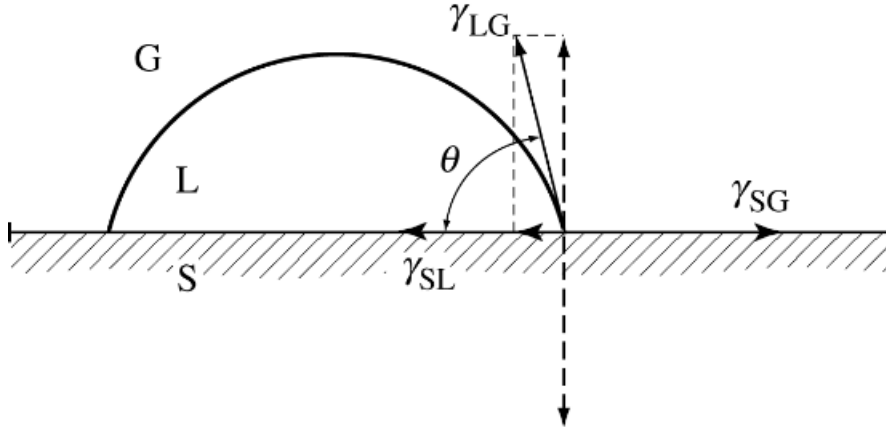


FIGURE 1.8. Liquid drop in equilibrium with its gas phase on a solid substrate.

a colloidal system this is possible. The contact angle is determined by the interfacial tensions of the three interfaces as expressed by Young's law:<sup>25</sup>

$$\cos \theta = \frac{\gamma_{SG} - \gamma_{SL}}{\gamma_{LG}} \quad (1.9)$$

Here  $\gamma_{SG}$  is the interfacial tension of the solid-gas interface,  $\gamma_{SL}$  is the interfacial tension of the solid-liquid interface, and  $\gamma_{LG}$  that of the liquid-gas interface. The interfacial tension is directly related to the free energy  $F$  of the surface, because  $F = \gamma A$ , with  $A$  the area of the surface. Equation (1.9) can be interpreted as a force balance for the three-phase contact line.

Another way to describe the wetting state is in terms of the spreading coefficient,  $S$ :

$$S = \gamma_{SG} - (\gamma_{SL} + \gamma_{LG}) = \gamma_{LG}(\cos \theta - 1) \quad (1.10)$$

If  $S < 0$  the substrate is partially wet, because it is favorable to create a gas-solid interface. If  $S = 0$  the system is completely wet. In that case equation (1.9) and (1.10) are equal because  $\cos \theta = 1$ . For a solid-gas interface, it is unfavorable to exist. It is replaced by two interfaces (liquid-gas and solid-liquid): a liquid film occurs. The free energy can be lowered by creating a film bounded by two interfaces. Positive values of  $S$  correspond to non-equilibrium situations.

The interfacial tensions for a certain system change with temperature. This results in a change of the contact angle. If the wetting state changes from partial to complete or reverse, the system is said to be at the wetting transition temperature. An important aspect of this wetting transition is predicted by Cahn.<sup>20</sup> The argument of Cahn runs as follows: Close to the critical point a solid substrate is always completely wet by one of the fluid phases. At a certain temperature,  $T_W$ , below the critical point  $T_c$ , there may be a transition where the wetting state changes from complete to partial.<sup>20</sup> This can be explained as follows. Because  $-1 \leq \cos \theta \leq 1$  according to Young's law (see equation

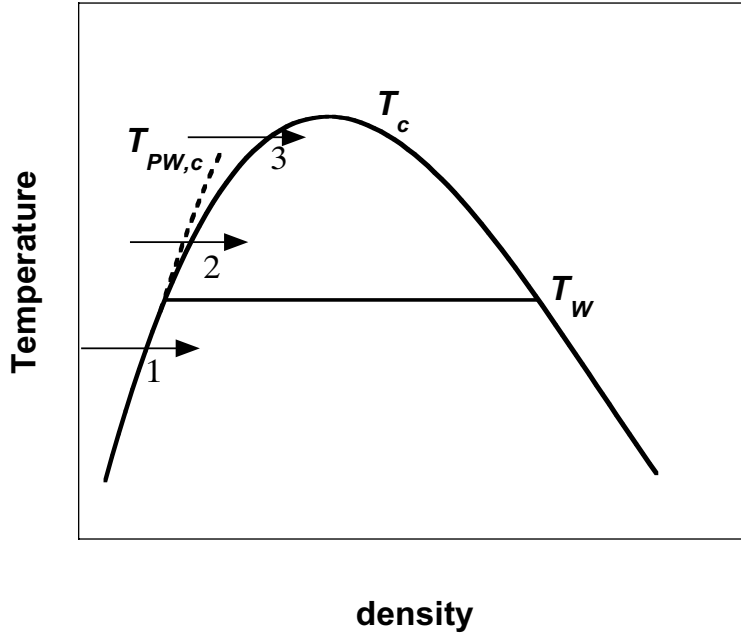


FIGURE 1.9. Phase diagram of a simple system near a surface. The wetting transition temperature is indicated by  $T_W$ , the critical point by  $T_c$  and the prewetting critical point by  $T_{PW,c}$ . The dashed line is the prewetting line.

(1.9)):

$$\gamma_{SG} - \gamma_{SL} \leq \gamma_{LG} \quad (1.11)$$

In the case of partial wetting  $\gamma_{SG} - \gamma_{SL} < \gamma_{LG}$ , upon approach of the transition to complete wetting  $\gamma_{SG} - \gamma_{SL}$  increases until it becomes equal to  $\gamma_{LG}$  at the wetting transition. Near the critical point  $\gamma_{LG}$  approaches zero according to  $\gamma_{LG} \propto (\frac{T-T_c}{T_c})^{1.3}$ . Cahn argued that  $\gamma_{SG} - \gamma_{SL}$  approaches zero according to  $\gamma_{SG} - \gamma_{SL} \propto (\frac{T-T_c}{T_c})^{0.313}$ , because the dependence of  $\gamma_{SG}$  and  $\gamma_{SL}$  should reflect the dependence of the densities of the liquid and gas phases on the temperature. Close to the critical point, this yields the exponent 0.313.<sup>26</sup> The fact that  $0.313 < 1.3$  implies that the inequality in equation (1.11) will turn to an equality, so that a transition from partial to complete wetting should always occur. Although later work has shown that  $\gamma_{SG} - \gamma_{SL}$  goes to zero as  $T \rightarrow T_c$  by a different exponent,<sup>21, 27, 28</sup> the general conclusion that a wetting transition occurs for  $T \rightarrow T_c$  has been proven fairly robust.<sup>23</sup> In figure 1.9 a wetting transition  $T_W$  is indicated in the liquid-gas coexistence region.

A wetting transition is called first order if the derivative of the free energy is discontinuous in the transition point. The wetting transition is called second order if the derivative of the free energy is continuous in the transition point. This second order transition is also called a critical transition. Ross *et al.* studied the wetting behaviour in liquid mixtures of methanol and the  $n$ -alkanes experimentally and observed a crossover of the wetting transition between first order and second order for alkanes with 9, 10

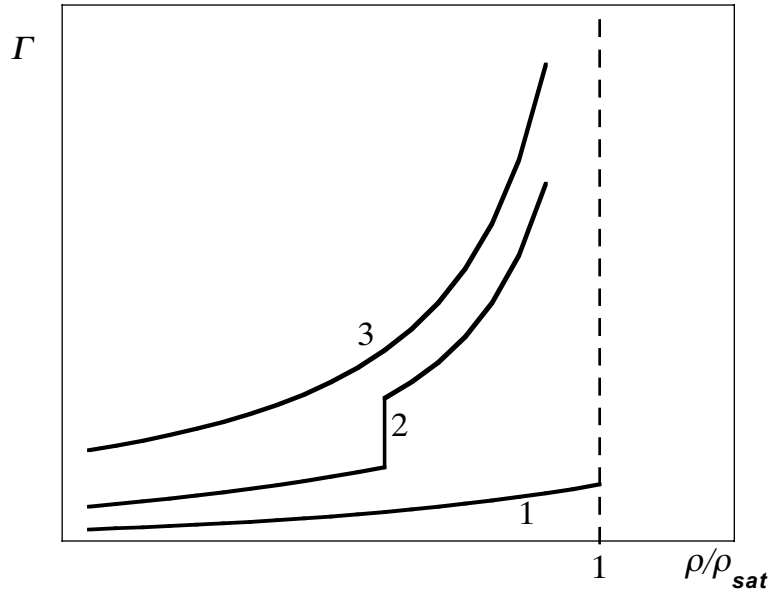


FIGURE 1.10. Adsorption isotherms for  $T < T_W$  (1),  $T_W < T < T_{PW,c}$  (2) and  $T_{PW,c} < T < T_c$  (3). The numbers 1, 2, and 3 correspond to the arrows in figure 1.9.

or 11 carbon atoms.<sup>24</sup> They observed a tricritical wetting point at an effective carbon number situated between 9.6 and 10.

In the complete wetting regime, *prewetting* may occur. At the substrate a liquid film exists below the bulk condensation pressure (or the density). A prewetting line is presented in figure 1.9. The prewetting line ends at the critical prewetting point  $T_{PW,c}$ . Since the wetting state is related to the preference of a liquid to be at a substrate, it can be described in terms of adsorption. In general, the adsorption,  $\Gamma$ , or excess density is given by:

$$\Gamma = \int_0^\infty dr(\rho(z) - \rho_\infty) \quad (1.12)$$

where  $\rho(z)$  is the number concentration at distance  $z$  from the surface and  $\rho_\infty$  the number concentration in the bulk. In figure 1.10 the adsorption is plotted as a function of  $\rho$  for three different temperatures corresponding to the arrows in figure 1.9. The concentration is scaled to the bulk saturation concentration  $\rho_{sat}$ . Isotherm 1, for a temperature below the wetting transition temperature, reaches a finite value if the pressure approaches the bulk saturation pressure; the substrate is partially wet. The isotherm belonging to arrow 2, in between the wetting transition temperature and the critical prewetting temperature, has a discontinuity: a thin film may coexist with a thick (but not macroscopic) film. The meta stable states of the loop yields a discontinuity in the adsorption isotherm. Near the bulk saturation concentration the thickness diverges to macroscopic values (or infinite) at  $\rho = \rho_{sat}$ . Above the critical prewetting temperature

(curve 3), the isotherm continuously approaches macroscopic values if the pressure approaches the saturation pressure.

## 1.5. Outline of this thesis

The central system of this thesis consist of stearylated silica particles dispersed in cyclohexane. Polydimethylsiloxane (PDMS) is added to these systems to obtain a depletion interaction.

Chapter 2 deals with direct measurements of the depletion interaction force by means of colloidal probe atomic force microscopy. The depletion interaction is measured for a series of different molecular weights and concentrations. Furthermore, in this chapter Scheutjens-Fleer Self Consistent Field calculations on depletion interactions are reported where the interaction between a polymer segment and the surface is varied.

In chapter 3 investigations on the wetting behaviour of gas-liquid phase separated colloid-polymer mixtures near a hard wall are briefly reported. The properties of the wall and the colloidal particles are very similar, because the wall is also coated with stearyl alcohol. The proximity to the critical point is varied by varying the polymer concentration. Upon approach to the critical point we investigated whether there is a wetting transition according to the Cahn prediction.

Results on the wetting behaviour of gas-liquid phase separated colloid-polymer mixtures near a hard wall are resumed in chapter 4. In this chapter the data of chapter 3 are compared to a further set of data for a soft wall.

In the last chapter the results of chapter 2, 3 and 4 are summarized.

## References

- [1] Poon, W. C. K.; Pusey, P. N.; Lekkerkerker, H. N. W. *Physics World* **1996**, *9*, 27-32.
- [2] Lyklema, J. *Fundamentals of Interface and Colloid Science I*; Academic Press, London: 1991.
- [3] Verwey, E. J. W.; Overbeek, J. T. G. *Theory of the stability of lyophobic colloids*; Elsevier: 1948.
- [4] Asakura, S.; Oosawa, F. *J. Chem. Phys.* **1954**, *22*, 1255.
- [5] Vrij, A. *Pure Appl. Chem.* **1976**, *48*, 471.
- [6] Lekkerkerker, H. N. W.; Poon, W. C. K.; Pusey, P. N.; Stroobants, A.; Warren, P. B. *Europhys. Letters* **1992**, *20*, 559-564.
- [7] de Hoog, E. H. A.; Lekkerkerker, H. N. W. *J. Phys. Chem. B* **1999**, *103*, 5274-5279.
- [8] Aarts, D. G. A. L.; Tuinier, R.; Lekkerkerker, H. N. W. *J. Phys.: Condens. Matter* **2002**, *14*, 7551-7561.
- [9] Tuinier, R.; Aarts, D. G. A. L.; Wensink, H. H.; Lekkerkerker, H. N. W. *Phys. Chem. Chem. Phys.* **2003**, *5*, 3707-3715.
- [10] Louis, A. A.; Bolhuis, P.; Meijer, E. J.; Hansen, J. P. *J. Chem. Phys.* **2002**, *117*, 1893.
- [11] Bolhuis, P.; Louis, A. A.; Hansen, J. P.; Meijer, E. J. *J. Chem. Phys.* **2001**, *114*, 4296.
- [12] Fleer, G. J.; Scheutjens, J. M. H. M.; Vincent, B. *ACS Symposia* **1984**, 245.
- [13] Ilett, S. M.; Poon, W. C. K.; Pusey, P. N. *Phys. Rev. E* **1995**, *51*, 1344-1352.

- [14] Vincent, B.; Edwards, J.; Emmet, S.; Croot, R. *Colloids Surf.* **1988**, *31*, 267-298.
- [15] Reiss, H.; Frisch, H. L.; Lebowitz, J. L. *J. Chem. Phys.* **1959**, *31*, 1959.
- [16] Wijting, W. K.; Besseling, N. A. M.; Cohen Stuart, M. A. *J. Phys. Chem. B* **2003**, *107*, 10565.
- [17] Bodnár, I.; Oosterbaan, W. D. *J. Chem. Phys.* **1997**, *106*, 7777-7780.
- [18] Schäfer, L. *Excluded Volume Effects in Polymer Solutions*; Springer Verlag, Berlin: 1999.
- [19] Dietrich, S. *Phase Transitions and critical Phenomena*; Academic Press, London: 1988.
- [20] Cahn, J. W. *J. Chem. Phys.* **1977**, *66*, 3667.
- [21] Schick, M. *Introduction to wetting phenomena*; Elsevier Science Publishers B.V.: 1990.
- [22] de Gennes, P. G. *Rev. Mod. Phys.* **1985**, *57*, 827.
- [23] Bonn, D.; Ross, D. *Reports on Progress in Physics* **2001**, *64*, 1085.
- [24] Ross, D.; Bonn, D.; Posazhennikova, A. I.; Indekeu, J. O.; Meunier, J. *Phys. Rev. Lett.* **2001**, *87*, 176103.
- [25] Young, T. *Philos. Trans. R. Soc.* **1805**, *95*, 69.
- [26] Chandler, D. *Introduction to modern statistical mechanics*; Oxford University Press, New York Oxford: 1987.
- [27] Indekeu, J. O. *Physica A* **1991**, *177*, 428.
- [28] Indekeu, J. O. *Acta Phys. Pol. B* **1995**, *26*, 1065.



## CHAPTER 2

# Depletion Interaction measured by Colloidal Probe Atomic Force Microscopy

### ABSTRACT

We investigated the depletion interaction between stearylated silica surfaces in cyclohexane in the presence of dissolved polydimethylsiloxane by means of colloidal probe atomic force microscopy. We found that the range of the depletion interaction decreases with increasing concentration. Furthermore the depletion interaction in this system is much weaker than predicted by theories assuming a hard-wall type interaction between polymer segments and surface. We conclude that the interaction between the polymer segments and the surface is not zero, which weakens the depletion interaction.

## 2.1. Introduction

The presence of nonadsorbing polymer in a colloidal suspension leads to an attraction between the particles which is commonly called depletion interaction. Examples of practical systems where this depletion interaction occurs are protein-polysaccharide mixtures in food systems or latex-polymer mixtures in paint.<sup>1, 2</sup> An extensively studied model system consists of stearylated silica spheres and polydimethylsiloxane (PDMS) in cyclohexane.<sup>3-8</sup> Advantages of this system are that electrostatic repulsion is absent and that Van der Waals attractions are screened because the colloidal particles are dispersed in a medium of nearly the same refractive index.<sup>3-5</sup> Bodnár and Verhaegh studied the phase behaviour of this system thoroughly.<sup>3, 4</sup> De Hoog studied interfacial tensions.<sup>5</sup> Wijting *et al.* and Aarts *et al.* studied the wetting behaviour of a phase separated system in the presence of a solid substrate.<sup>6-8</sup> In all these studies it is found systematically that more PDMS is needed in order to obtain phase separation than expected on theoretical grounds. At first, this was ascribed to the fact that non-ideality of the polymer was not yet accounted for in model calculations. However, even in model calculations that take polymer non-ideality into account, it is still predicted that less polymer is needed than is found in the experimental silica/PDMS/cyclohexane systems.<sup>7, 9</sup>

Let us consider a nonadsorbing polymer coil in a solution near a solid surface. This can be a flat surface, but also the surface of a (spherical) colloidal particle. It is entropically very unfavourable for a polymer coil if the distance between the center of the coil and the surface is smaller than the unperturbed radius of gyration,  $R_g$ . Hence, near the surface there is a zone where the polymer concentration is lower than in the bulk. This zone is called the depletion zone. If the depletion zones of two colloidal particles overlap, the polymer concentration between the particles is decreased as compared to the surrounding solution. This causes an imbalance of the osmotic pressure exerted on two particles which pushes the particles together. Hence, the polymer induces a so-called depletion attraction between two colloidal particles. This attraction is of entropic nature and was first analyzed by Asakura and Oosawa and later by Vrij.<sup>10, 11</sup> At high enough concentrations of both polymer and colloids, depletion interaction will lead to a macroscopic phase separation. The phase behaviour of colloidal systems undergoing depletion-induced phase separation is quite similar to that of molecular systems.<sup>12</sup> Therefore, colloid-polymer mixtures have been a good model for molecular systems. The advantage of using colloidal systems over molecular systems is that one can tune the range and strength of the interaction independently by varying the size of the polymer and the concentration, respectively. Several theories describe this depletion interaction quantitatively. A brief review of these theories will be given in the next section. Based on such quantitative theories of the interactions between colloidal particles, theoretical predictions for the phase behaviour have been made.<sup>9, 13</sup>

In this chapter we describe experimental results on depletion interactions. We performed force measurements by means of colloidal probe atomic force microscopy (CP-AFM). In this technique the force-distance relation for the interaction between a spherical probe particle and a flat surface is measured. The experimental setup will be described in section 2.3. In literature, several studies on various types of colloidal interactions have been presented. For instance the range and strength of electric double layer interactions have been measured.<sup>14-17</sup> Furthermore, the interaction between polymer-covered surfaces has been investigated.<sup>18</sup> Milling *et al.* investigated the depletion interaction between silica surfaces by means of CP-AFM in solutions of sodium poly(acrylate) in water.<sup>19</sup> Biggs *et al.* measured the depletion interaction in solutions of sodium poly(styrene sulfonate) in water and investigated the molecular weight dependence.<sup>20</sup> In these aqueous systems not only depletion interactions, but also electric double layer and Van der Waals interactions play an important role. Biggs *et al.* found a secondary minimum in the interaction potential due to the depletion interaction. The depth of this secondary minimum increased as a function of both molecular weight and concentration. Milling and Biggs presented results on depletion interaction for stearylated silica surfaces in cyclohexane.<sup>21</sup> These authors also used polydimethylsiloxane as nonadsorbing polymer but limited their study to only one molecular mass and concentration. We present more detailed results on CP-AFM measurements on the same system, for different molar masses and concentrations of the polymer.

## 2.2. Theories on depletion interaction

Before reviewing some aspects of depletion interaction, we recall that several regimes in the behaviour of polymer solutions should be considered. Distinguishing these regimes is helpful to understand the behaviour of polymer solutions. For polymers in a good solvent we distinguish in the order of increasing concentration a dilute regime, well below the overlap concentration, a semidilute regime, a marginal regime, and a concentrated regime, respectively. In the dilute regime, the correlation length is independent of the concentration. Above the overlap concentration the correlation length decreases with increasing concentration. The crossovers between these regimes occur continuously.<sup>22</sup>

When we have two flat parallel solid plates immersed in a polymer solution, there is an osmotic pressure on both sides of the walls, see figure 2.1. The outside surfaces experience the bulk osmotic pressure,  $\Pi_b$ . For the inside surfaces, the force per unit area may be different by an amount denoted the disjoining pressure  $\Pi_d$ . A negative value of  $\Pi_d$  implies an attraction between the plates; if  $\Pi_d$  is positive the interaction is repulsive. Since the depletion effect leads to a reduced osmotic pressure on the inside surfaces  $\Pi_d < 0$  and the effective interaction is attractive.

Generally, the depletion interaction free energy per unit area  $G_a$  can be calculated

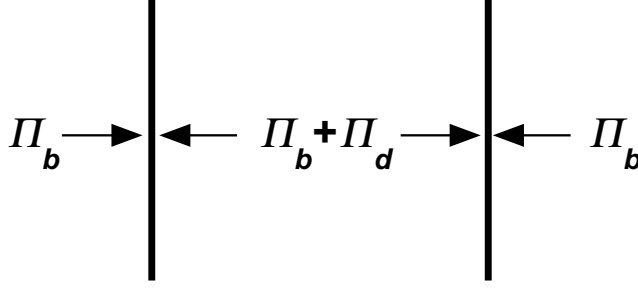


FIGURE 2.1. Osmotic pressure exerted on two flat plates inside and outside a slit.

by means of the adsorption method.<sup>23</sup> In this method the interaction free energy is described by the Gibbs adsorption equation in combination with the Gibbs-Duhem relation  $n_p^{-1}d\Pi_b = d\mu$ . This leads to:

$$G_a(h) = - \int_0^{n_p} dn'_p \frac{1}{n'_p} \left( \frac{\partial \Pi_b}{\partial n'_p} \right) [\Gamma(h) - \Gamma(\infty)] \quad (2.1)$$

Where  $n_p$  is the number concentration of polymer chains in the bulk solution and  $\Gamma(h)$  is the adsorbed amount of polymer per unit area when the plates are separated by a distance  $h$ . For flat plates  $\Gamma(h) - \Gamma(\infty)$  can be expressed as:

$$\Gamma(h) - \Gamma(\infty) = \begin{cases} n_p(2\delta - h) & 0 < h \leq 2\delta \\ 0 & h \geq 2\delta \end{cases} \quad (2.2)$$

With  $\delta$  the depletion layer thickness. This expression implies that the polymer-surface interaction is assumed to behave as a hard sphere interaction for spheres with a radius  $\delta$ . Within the ideal polymer model  $\delta$  is independent of the concentration taking the constant value  $\delta_0$ . Asakura and Oosawa derived that  $\delta_0 = 2R_g/\sqrt{\pi} \approx 1.13R_g$ , with  $R_g$  the radius of gyration of the polymer.<sup>10</sup> The constant  $\delta$  value holds for concentrations well below the overlap value. Another assumption of the ideal polymer model is that the swelling of the polymer because of intrachain excluded volume interactions is ignored. Furthermore the osmotic pressure is assumed to be given by Van't Hoffs law. Inserting equation (2.2) in (2.1) and using that  $\delta$  is independent of  $n_p$  yields the following equation for the interaction free energy per unit area,  $G_a(h)$ :

$$G_a(h) = \begin{cases} -\Pi_b(2\delta_0 - h) & 0 < h \leq 2\delta_0 \\ 0 & h \geq 2\delta_0 \end{cases} \quad (2.3)$$

This is the Asakura Oosawa equation for the interaction free energy.

In the recent past several theories on depletion interaction that account for non-ideality of polymers were developed.<sup>23-25</sup> This means that the concentration dependence of  $\delta$  is taken into account. Tuinier *et al.* used for  $\delta$  the relation  $\delta = 1.071\xi_b$ , where  $\xi_b$  is the bulk correlation length. Renormalization group theory can be used to calculate this  $\xi_b$ .<sup>26</sup> Furthermore, for a good solvent the osmotic pressure is always larger than

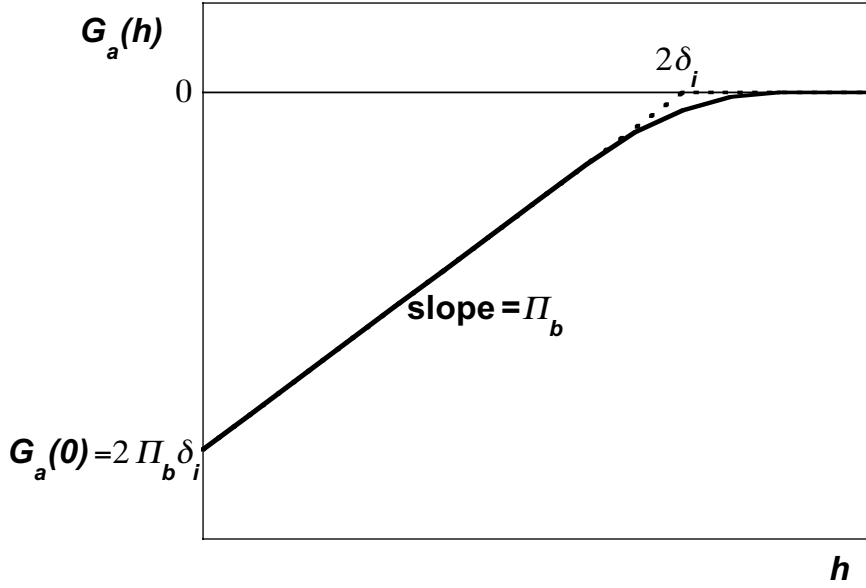


FIGURE 2.2. The solid line represents schematically the depletion interaction free energy  $G_a$  as a function of the separation distance  $h$ , according to Tuinier, Bolhuis and Louis.<sup>23–25</sup> The dashed line represents equation 2.5. The interaction distance  $\delta_i$  is indicated.

the ideal osmotic pressure. Renormalization group theory yields an expression for the osmotic compressibility,  $(\frac{\partial \Pi_b}{\partial n_p})$

$$\left(\frac{\partial \beta \Pi_b}{\partial n_p}\right) = 1 + 2.63 \varphi_p \left(\frac{1 + 3.25 \varphi_p + 4.15 \varphi_p^2}{1 + 1.48 \varphi_p}\right)^{0.309} \quad (2.4)$$

With  $\beta^{-1} = k_B T$  and  $\varphi_p$  the polymer volume fraction scaled to the overlap volume fraction. The term 1 in equation (2.4) corresponds to ideal behaviour. The second term on the right hand side is always positive, so, the osmotic pressure is always larger than the ideal osmotic pressure. Using these ingredients, one can calculate the interaction free energy as a function of the separation distance by numerical integration of equation (2.1). Results of this kind are presented by Tuinier *et al.*<sup>23</sup> This interaction can roughly be described by the regimes (see figure 2.2)

$$G_a(h) = \begin{cases} -\Pi_b(2\delta_i - h) & 0 < h \leq 2\delta_i \\ 0 & h \geq 2\delta_i \end{cases} \quad (2.5)$$

with  $\delta_i$  a quantity which is a measure for the range of the interaction distance, that we will from now on call: *depletion interaction distance*. Of course, in the numerical results of ref.,<sup>23</sup> the two linear regimes of equation (2.5) are not connected around  $h = 2\delta_i$  by a sharp kink, but by a more rounded dependency. The linear part holds well for  $0 < h < \sim 1.6\delta_i$  and for  $h > \sim 2.3\delta_i$  as shown schematically in figure 2.2. The calculations of Tuinier *et al.* agree well with Self Avoiding random Walk (SAW) simulations

by Louis and Bolhuis.<sup>23–25</sup>

In these and many other calculations it is assumed that there is no attraction at all between the polymer segments and the surface. However, in certain cases a small attraction between the polymer segments and the surface might exist. In order for polymer chains to adsorb on a surface, the adsorption energy (an attractive interaction) of a polymer segment and the surface has to exceed a critical value to compensate for the conformational entropy loss. Above this critical value accumulation (positive adsorption) occurs, whereas below this value depletion (negative adsorption) occurs.

The interaction between a polymer segment and the surface may be quantified by the surface interaction parameter  $\chi_S$ , defined as the difference between the polymer-surface interaction energy and the solvent-surface interaction energy in units  $k_B T$ .<sup>22</sup> This interaction parameter is used in lattice models. The critical value, which indicates the crossover between adsorption and depletion is indicated by  $\chi_{S,crit}$  (critical adsorption energy). Usually in theoretical studies on depletion interaction,  $\chi_S$  is taken to be zero. Within a mean field approximation, the depletion interaction free energy can be calculated according to the Scheutjens-Fleer Self Consistent Field (SF-SCF) theory for polymers at interfaces.<sup>22, 27</sup> This theory is a generalization of the Flory-Huggins theory of polymer solutions to inhomogeneous systems. The polymer chains, which consist of  $N$  segments, are placed on a lattice. The Flory-Huggins solvency parameter,  $\chi$ , describes the interaction between a chain and the solvent. For a  $\theta$ -solvent  $\chi = 0.5$ , whereas for good solvents  $\chi$  has a lower value. In calculations published by Scheutjens *et al.*<sup>27</sup> also  $\chi_S$  is chosen to be zero. In this chapter we will present some results from SF-SCF calculations for cases where  $0 \leq \chi_S < \chi_{S,crit}$ .<sup>22</sup>

Fleer *et al.* recently derived a quite simple expression for the depletion layer thickness,  $\delta$ , which is valid for the whole regime between infinite dilution and above the overlap concentration:<sup>28</sup>

$$\frac{1}{\delta^2} = \frac{1}{\delta_0^2} + \frac{1}{\xi_b^2} \quad (2.6)$$

Far beyond the overlap concentration, the depletion layer thickness is described by the correlation length,  $\xi_b$ . Within a mean field approximation, this correlation length can be calculated by an equation of de Gennes in combination with a Flory-Huggins field.<sup>29–31</sup>

$$\frac{l^2}{\xi_b^2} = -3[\ln(1 - \varphi_b) + 2\chi\varphi_b] \quad (2.7)$$

where  $\varphi_b$  is the polymer segment volume fraction in the bulk and  $l$  the segment length. The depletion interaction distance  $\delta_i$  is closely related to the depletion layer thickness  $\delta$ . Fleer *et al.*<sup>28, 30, 31</sup> derived (again within a mean field approximation):

$$\frac{\delta_i}{\delta} = \frac{\frac{1}{N} + \frac{2}{3}v\varphi_b + \frac{1}{2}\varphi_b^2 + \dots}{\frac{1}{N} + \frac{1}{2}v\varphi_b + \frac{1}{3}\varphi_b^2 + \dots} \quad (2.8)$$

with  $N$  the number of segments in a polymer coil and  $v = 1 - 2\chi$ . From equation (2.6) and (2.8), it can be concluded that the range of the depletion interaction at any concentration is always smaller than at infinite dilution. On the other hand the non-ideal behaviour of the osmotic pressure as a function of the concentration leads to a stronger depletion interaction, since the osmotic pressure increases more strongly than linearly with the polymer concentration.

### 2.2.1. Derjaguin approximation

In a colloidal probe AFM experiment, one measures the force between two interfaces, one of which is spherically curved and one is flat. It is justified to convert the force between curved surfaces to the interaction free energy between two flat plates by means of the Derjaguin approximation if the radii of curvature of the interfaces are large as compared to the separation distance,  $h$ .<sup>32</sup> Since  $h$  is of the order of nm and the radius of the probe is  $3 \mu\text{m}$  this approximation is justified for our measurements. According to the Derjaguin approximation the relation between the force  $F_c(h)$  between two spheres and the interaction free energy per unit area,  $G_a(h)$  between flat plates is expressed by

$$F_c(h) = \frac{2\pi a_1 a_2}{a_1 + a_2} G_a(h) \quad (2.9)$$

Where  $a_1$  and  $a_2$  the radii of the two spheres. In the case of a flat plate and a sphere of radius  $R$ ,  $a_1 = \infty$  and  $a_2 = R$ . From this it can be concluded that the interaction free energy per unit area between two plates is related to the force between the colloidal probe and the plate by

$$G_a(h) = \frac{F_c(h)}{2\pi R} \quad (2.10)$$

The interaction free energy for two plates can be calculated from the force between a sphere and a plate by dividing the normalized force,  $F_c(h)/R$  by a factor  $2\pi$ .

## 2.3. Experimental

### 2.3.1. Preparation of spheres and plates

Silica spheres (diameter =  $6 \mu\text{m}$ , gift from Philips Laboratories Eindhoven, the Netherlands) were coated with stearyl alcohol by the method described by Van Helden et al.<sup>33</sup> By sonicating approximately 1 g of spheres in absolute ethanol (Riedel-de Haën, p.A.), a suspension of spheres was prepared. A solution of 5 g stearyl alcohol (Fluka) in ethanol, was added to the suspension, which was heated to  $50 \text{ }^\circ\text{C}$  in an oil bath. A melt of particles in stearyl alcohol was obtained by distillation of the ethanol under a nitrogen atmosphere. Then the temperature of the oil bath was raised to  $180\text{-}200 \text{ }^\circ\text{C}$ . The melt was stirred at this temperature for 6 hours under nitrogen atmosphere. After cooling down, chloroform (Acros) was added to dissolve remaining stearyl alcohol. The

suspension was centrifuged for 30 minutes at 2000 rpm in an Avanti J25-I centrifuge (Beckman Coulter). After removing the solvent, the residue was resuspended in cyclohexane and centrifuged again. After one more washing procedure, we obtained a stable suspension of spheres in cyclohexane. The spheres sediment under gravitation but resuspend easily by shaking. Uncoated spheres aggregate in cyclohexane.

Silicon wafers (WaferNet, Eching, Germany) were heated at 1000 °C for about 100 min. During this heating procedure the silicon surface is oxidized and a SiO<sub>2</sub> layer with a thickness of 80 nm is formed. The plates were cleaned by washing with ethanol and drying with nitrogen. Furthermore, they were cleaned in a plasma cleaner (Harrick PDC-32G) for 2 minutes at high RF level. The contact angle of a droplet of water was less than 10° (nearly complete wetting). Clean plates were immersed overnight in a 180 °C melt of stearyl alcohol. After the heating step, the plates were washed with chloroform and ethanol. A droplet of water on a well-coated plate has a contact angle larger than 90° (partial wetting).

### 2.3.2. Attaching a sphere to an AFM-cantilever

The stearylcoated spheres were attached to a large, narrow legged AFM-cantilever (Digital Instruments Inc. Santa Barbara USA,) with a siliciumnitride tip. The method of Giesbers was used for this purpose.<sup>14</sup> The cantilever was placed on a heating stage which was heated to about 100 °C, because at that temperature the glue (Epikote 1004F, Shell Amsterdam, The Netherlands) melts. Molten glue was attached to the tip of the cantilever by means of a tungsten wire. The wire had been cleaned before by etching it by dipping the wire a few times in a 1 M KOH-solution applying 50 V (A.C.) between the wire and a platinum counter electrode. At 20 °C a spherical particle was picked up from a glass plate by the etched tungsten wire. Then the plateau was heated again to 100 °C and the spherical particle was placed on the glue on the cantilever. After cooling down by taking the cantilever away from the heating stage, the glue solidifies and the sphere is attached firmly to the cantilever.

### 2.3.3. Force measurements

The force measurements were performed using a Digital Instruments Nanoscope III atomic force microscope equipped with a standard liquid cell and a piezo scanner type J. One of the samples was measured with a NanoScope 4 Control Station with a MultiMode AFM equipped with a PicoForce scanner. The cantilever with the spherical particle was placed into a liquid cell. The stearyl-coated substrate was placed on the piezo scanner. The liquid cell was closed by means of a viton O-ring. The liquid cell was filled with pure cyclohexane or a solution of alkyl terminated PDMS (Polymer Source, inc.) in cyclohexane. A schematic drawing of the cell is given in figure 2.3.

The spring constant of one of the the cantilevers was determined using the Nanoscope 4 and applying the method of measuring the thermal noise.<sup>34</sup> The primary data consist of



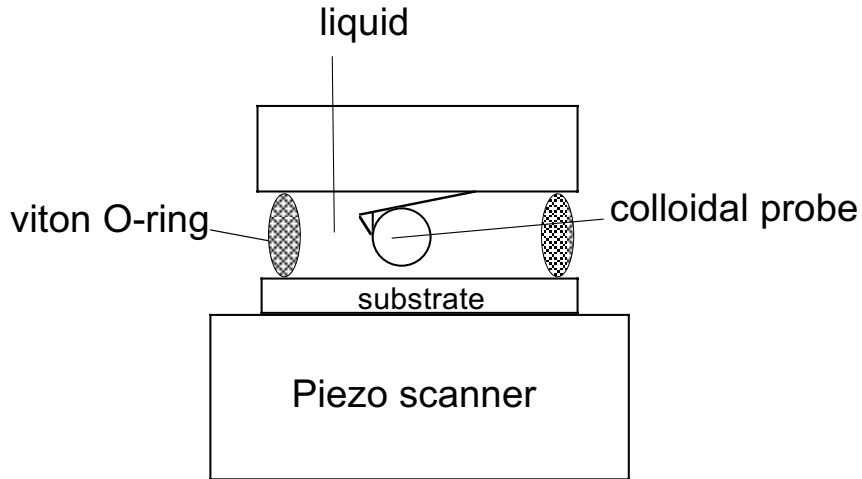


FIGURE 2.3. Schematic representation of the AFM-cell.

a time interval of the deflection signal in contact mode (i.e., with no driving oscillation applied electronically) at thermal equilibrium when the cantilever is free, far away from any solid surface. Brownian motion of surrounding molecules impart random impulses to the cantilever during the sampling. The detected random motion is Fourier transformed to obtain its Power Spectral Density in the frequency domain. Integrating the area under the resonant peak in the spectrum yields the power associated with the resonance frequency. The spring constant can be obtained from the resonance frequency. We measured the force between a sphere and a plate in the presence of different concentrations PDMS for a set of different molecular weights. Properties of the polymers are presented in table 2.1. From now on we will use the code given in the last column to refer to the corresponding molecular weight. The radii of gyration were determined by extrapolation using the experimental data of Verhaegh, Bodnár, and de Hoog<sup>3-5</sup> and the scaling relation for a good solvent  $R_g \propto M_N^{0.6}$ ,<sup>22</sup> with  $M_N$  the number average molecular mass of the polymer. That the latter relation applies for the present polymer/solvent combination is confirmed by the experimental data. Force curves with an unambiguously observable attraction could be obtained within the concentration range indicated in table 2.1. For lower concentrations the attraction became too weak to measure. Above that range the sample is so viscous that it was difficult to handle the solution. Also the overlap concentration,  $\varphi_b^*$ , is mentioned in the table. This overlap concentration is calculated as  $\varphi_b^* = M_N / (\frac{4}{3}\pi R_g^3 N_{Av} \rho)$ , with  $N_{Av}$  Avogadro's number and  $\rho$  the density of the polymer ( $0.98 * 10^{-3} \text{ kg.m}^{-3}$ , independent of the molecular weight of the polymer).

All samples were measured with the Nanoscope III. Only the most concentrated sample of P83 was measured with the Nanoscope 4. The AFM measures the signal of a laser beam deflected by the cantilever as a function of the piezo position. The signal

TABLE 2.1. Properties of the used samples of PDMS.  $M_N$  is the number average molecular mass and  $M_W$  the weight average molecular mass.  $M_W/M_N$  is the polydispersity index. The concentration range is indicated in terms of  $\varphi_b$  and in g/l between the brackets.

$M_N$ [g/mol]	$M_W/M_N$	$R_g$ [nm]	concentration range $\varphi_b$ (g/l)	$\varphi_b^*$	code
14 800	1.14	4.5	0.10-0.12 (99-134)	0.064	P14
31 300	3	8	0.03-0.10 (29-98)	0.035	P31
83 200	1.24	13	0.03-0.12 (33-117)	0.016	P83
118 000	1.16	16	0.01-0.10 (29-98)	0.012	P118

is translated to the deflection of the cantilever. The piezo position is directly related to the separation distance. Each of the deflection vs. piezo position curves contain a base line and a so called constant compliance region. The base line occurs at large separation distances. Because at large distances there is no interaction between the probe and the substrate, the cantilever does not deflect; the force is constant (zero). If there is repulsion or attraction at smaller separation distances, the cantilever will deflect upwards or downwards, respectively. At contact the deflection of the cantilever increases linearly with the piezo position, this is denoted the constant compliance regime. The curves of the cantilever deflection vs. the piezo position were converted into deflection versus separation distance curves by means of the method of Senden.<sup>35</sup> The force can be calculated by multiplying the deflection by the spring constant of the cantilever. The interaction free energy was obtained from the force using the Derjaguin approximation, see equation (2.10). Experiments with P14 and P83 were performed with the same cantilever and sphere. The spring constant for this case was determined at 0.042 N/m. The experiments for P31 and P118 were performed with another cantilever, for which the spring constant was not experimentally determined by us. Here we used the value given by the manual of the Nanoscope<sup>36</sup> for the large narrow legged cantilever (0.06 N/m).

## 2.4. Results and Discussion

### 2.4.1. Force measurements between a hard sphere and a plate

The interaction free energy between a coated sphere and a coated plate in pure solvent as a function of the separation distance,  $h$ , is presented in figure 2.4. This curve is not a perfect hard sphere interaction, because at small separation distances (a few nm), there is some repulsion. This repulsion may be due to surface roughness of both sphere and plate.

Some spheres exhibited a longer ranging repulsive interaction with the flat surface, perhaps due to an imperfect coating. Such spheres were rejected. Only spheres that in

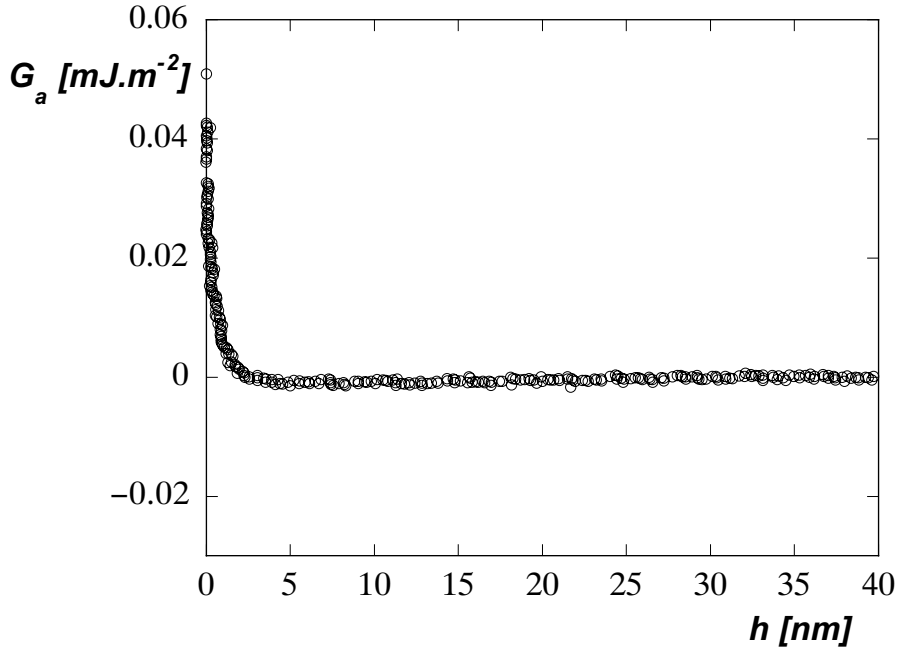


FIGURE 2.4. Interaction free energy as a function of the separation distance for a silica sphere in cyclohexane.

pure solvent exhibited a repulsion with a range smaller than a few nm were used for further measurements.

#### 2.4.2. Force measurements between a sphere and a plate in the presence of a polymer solution

In figures 2.5, 2.6, 2.7 and 2.8 we present examples of curves where the interaction free energy per unit area,  $G_a(h)$ , is plotted as a function of the separation distance. The curves shown are for the highest and lowest concentrations of the PDMS samples, listed in table 2.1. The concentrations and molecular weights are indicated in the captions. These curves consist of both a repulsive part for separation distances very close to contact, as observed in pure solvent, and an attractive part, while at large distances a plateau of zero interaction appears.

In order to obtain quantitative information about the range and strength of the interaction, the part with a positive slope around the inflection point is fitted to a straight line according to figure 2.2. The slope of this curve is the apparent osmotic pressure and the intercept with the ordinate is the depth of the potential well,  $G_a(0)$ . The intercept with the abscissa is twice the depletion interaction thickness,  $\delta_i$ , see equation (2.5). In figure 2.9 we collect data for the depletion interaction thickness as a function of  $\varphi_b$ . We see here that  $\delta_i$  for P83 is lower than for P118 and for P31. It may seem odd that  $\delta_i$  is larger for P31 than for P83, but one should note that only the former sample is highly polydisperse (see table 2.1). The large  $\delta_i$  measured for P31 may be due to the large molecules of the distribution in this sample. As a general trend, the depletion

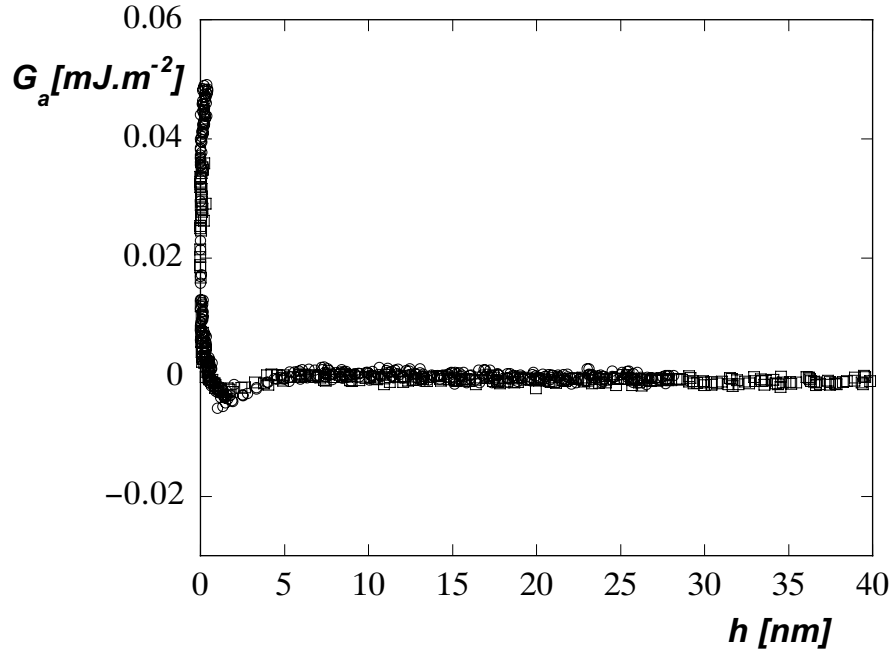


FIGURE 2.5. Interaction free energy as a function of the separation distance for P14 with  $\varphi_b = 0.10$  ( $\square$ ) and  $\varphi_b = 0.12$  ( $\circ$ ).

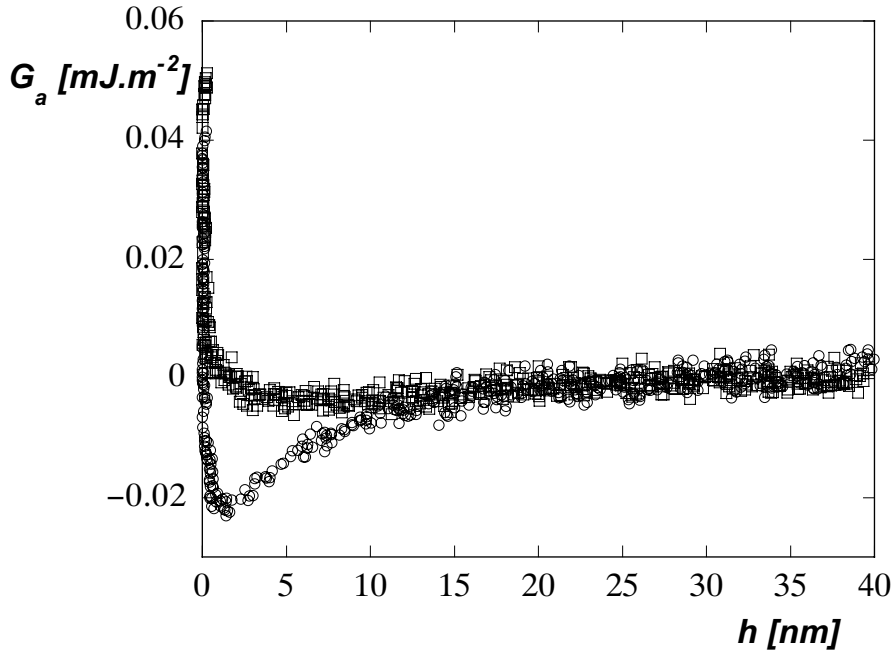


FIGURE 2.6. Interaction free energy as a function of the separation distance for P31 with  $\varphi_b = 0.03$  ( $\square$ ) and  $\varphi_b = 0.10$  ( $\circ$ ).

layer thickness decreases with increasing polymer concentration. The fact that  $\delta_i$  depends both on molecular weight and concentration indicates that the concentrations, for which we could measure an attraction, are in the crossover regime from the dilute to semi-dilute or marginal concentration regimes. For P14 the error in the depletion

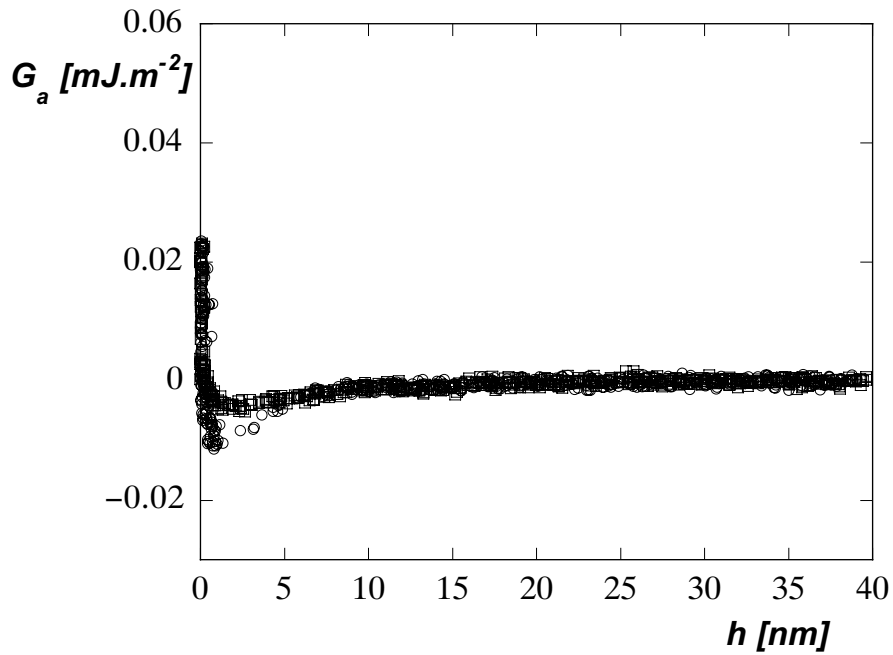


FIGURE 2.7. Interaction free energy as a function of the separation distance for P83 with  $\varphi_b = 0.03$  ( $\square$ ) and  $\varphi_b = 0.12$  ( $\circ$ ).

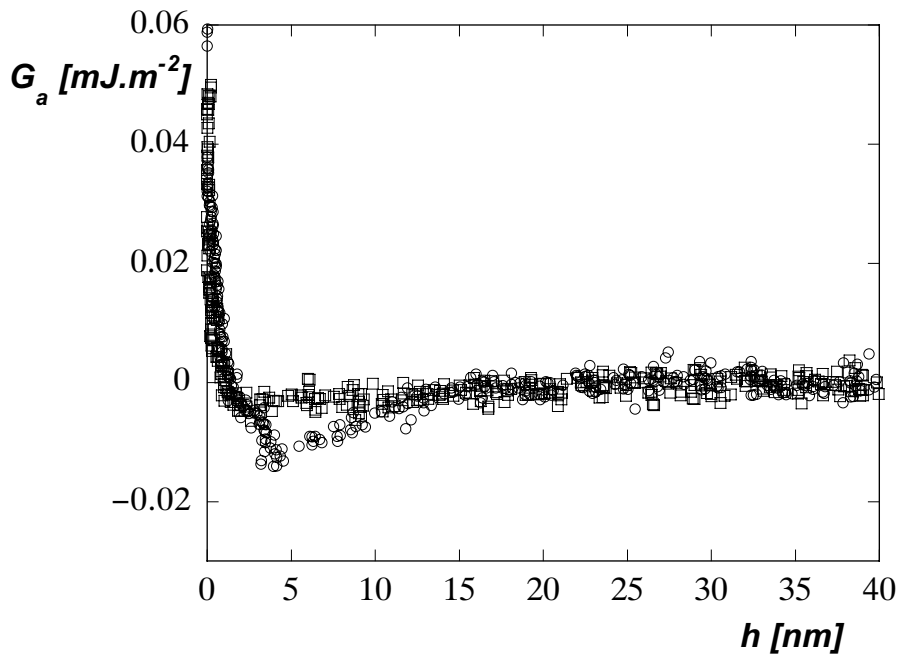


FIGURE 2.8. Interaction free energy as a function of the separation distance for P118 with  $\varphi_b = 0.01$  ( $\square$ ) and  $\varphi_b = 0.10$  ( $\circ$ ).

layer thickness is large, compared to its value, therefore no conclusions can be drawn for this sample.

Let us now consider the curves of P83 and P118 more carefully. These samples are measured for more concentrations than the other ones. As discussed in section 2.2, if

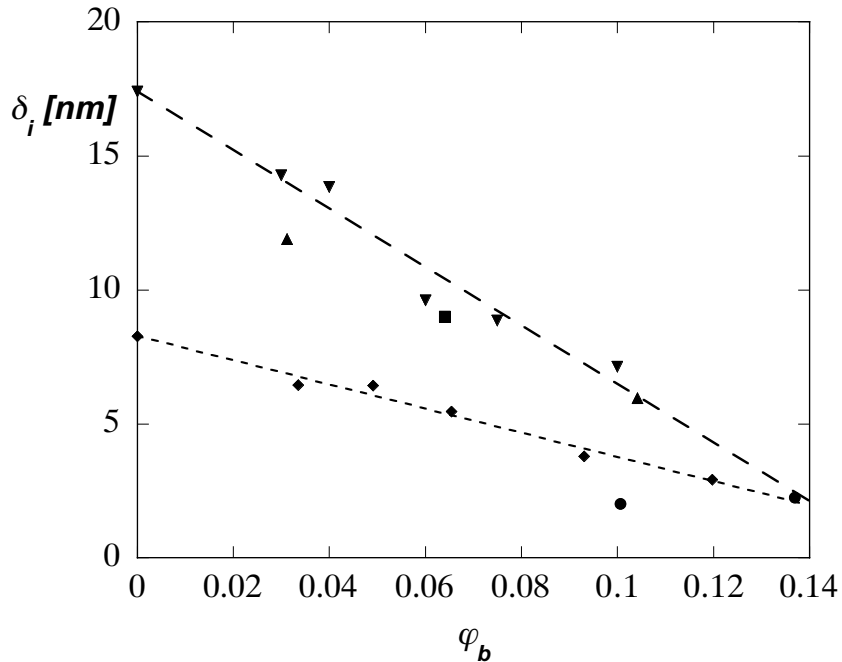


FIGURE 2.9. Depletion interaction thickness as a function of  $\varphi_b$  for P14 (●), P31 (▲), P83 (◆), and P118 (▼). The values at  $\varphi_b = 0$  are extrapolated from a linear fit. The ■ represents the measurement of Milling *et al.*<sup>21</sup> The lines for P83 and P118 are drawn to guide the eye.

the concentration is far beyond the overlap concentration, the depletion layer thickness should not depend on the molecular weight, but only on the concentration (see equation (2.6)). In the dilute regime the depletion interaction thickness is constant and well described by  $\delta_0$ . Extrapolation of our measured values of  $\delta_i$  to zero concentration leads for P83, to a lower value than predicted from the radius of gyration of the sample (measured 9 nm, calculated 13 nm), while for P118 it agrees better (17 nm respectively 16 nm). If we plot  $\log \delta_i$  versus  $\log \varphi_b$  we do not observe linear scaling behaviour, but the slope indicates that we can roughly deduce a scaling behaviour  $\delta_i \propto \varphi_b^{1/2}$ . This scaling behaviour corresponds to the marginal regime. Furthermore, the curves for P83 and P118 in figure 2.9 approach each other upon increasing polymer concentration. This is in agreement with SF-SCF calculations.<sup>22</sup>

According to equation (2.5), both the slope and the intercept of the attractive part of the interaction curve should be proportional to the bulk osmotic pressure. From the fits we obtained values for the apparent osmotic pressure, these are plotted as a function of  $\varphi_b$  in figure 2.10. These are much lower than expected. We find that the measured values are even lower than the ideal osmotic pressure as given by Van't Hoffs law (see the lines plotted in figure 2.10). For polymer solutions in a good solvent, the osmotic pressure should always be larger than the ideal osmotic pressure, especially at higher concentration. For instance the apparent osmotic pressure, obtained from figure 2.10,

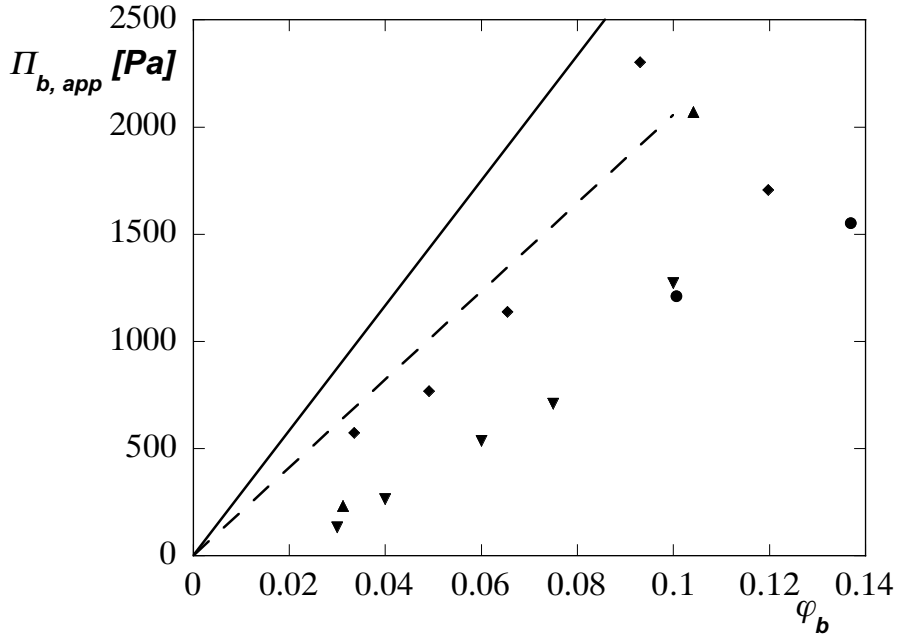


FIGURE 2.10. Apparent osmotic pressure as a function of  $\varphi_b$  for P14 ( $\bullet$ ), P31 ( $\blacktriangle$ ), P83 ( $\blacklozenge$ ), and P118 ( $\blacktriangledown$ ). The solid line represents the ideal osmotic pressure for P83 and dashed line the ideal osmotic pressure for P118.

for  $\varphi_b = 0.09$  of P83 is 2.3 kPa, whereas the ideal osmotic pressure according to Van't Hoff's law for this sample is 2.7 kPa.

A possible explanation for these lower values is that the slope still increases for small separations where our measurements are dominated by the short range repulsion. Due to this short range repulsion we cannot study the depletion interaction at small separation distances. However, according to calculations of Tuinier and SCF calculations the depletion interaction is linear in  $h$  for a range up to about  $1.6\delta_i$ .<sup>23</sup> The short range repulsion ranges in our measurements do not range further than about  $0.6\delta_i$ , so this explanation must be rejected.

The only remaining explanation is that there is some albeit weak attraction between the polymer segments and the surface. In figure 2.11 the depth of the potential well,  $G_a(0)$  (the intercept of the fit) is plotted as a function of the concentration. According to equation (2.5),  $G_a(0) = -2\Pi_b\delta_i$ . The values of  $G_a(0)$  for P31, P83, and P118 do not depend on the molecular weight. If we compare these well depths with those calculated theoretically by Tuinier *et al.*,<sup>23</sup> simulations of Bolhuis<sup>25</sup> and Louis<sup>24</sup> and SF-SCF calculations (figure 2.12, curve for  $\chi_S = 0$ ), it can be concluded that our experimental depths of the potential wells are significantly smaller. These lower values confirm that there must be some attraction between the polymer and the surface, which diminishes the depletion effect. Most likely, it is the segments in the polymer coil which are attracted by the surface, although attraction of the end segments cannot be ruled

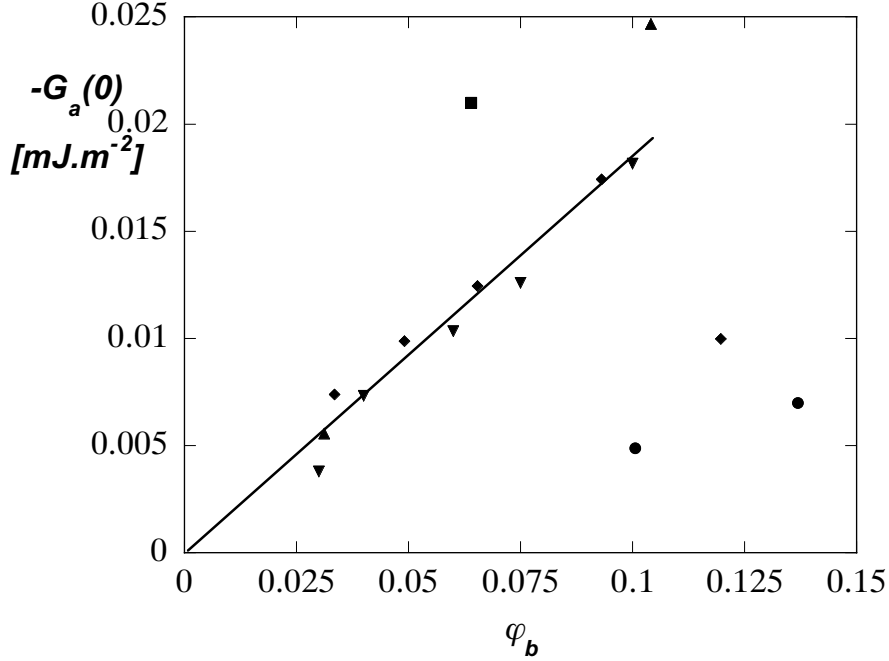


FIGURE 2.11.  $G_a(0)$  as a function of  $\varphi_b$  for P14 (●), P31 (▲), P83 (◆), and P118 (▼).

out. The existence of a polymer-surface attraction implies that the surface interaction parameter,  $\chi_S$  is not zero, but somewhere in the range  $0 < \chi_S < \chi_{S,crit}$ . The result is a weaker depletion interaction. In order to obtain an estimate for the value of  $\chi_S$ , we carried out SF-SCF calculations, for computational details see appendix 2A. For these calculations we used the following parameters: a cubic lattice, number of segments  $N = 1000$ , and solvency interaction parameter,  $\chi = 0.4$ , because this value has been found for PDMS in cyclohexane.<sup>37</sup> We obtained theoretical values for  $G_a(0)$  by calculating the grand potential  $\Omega(h)$  for two flat plates at a separation distance of 100 lattice units ( $\Omega(100)$ ) and at separation distances of 1 and 2 lattice units ( $\Omega(1)$  and  $\Omega(2)$ ) as a function of  $\varphi_b$  for different values of  $\chi_S$ . The separation distance of 100 lattice units is large enough (because  $2R_g = 2\sqrt{\frac{1}{6}1000l} \approx 26l \ll 100l$ ),<sup>22</sup> so that  $\Omega(100)$  is on the plateau of zero interaction. Subtracting the value of  $\Omega(100)$  from that of  $\Omega(1)$  and  $\Omega(2)$  and extrapolating to zero distance yields a value for the depth of the potential well  $G_a(0)$ . In figure 2.12 we plot the depth of the potential well,  $G_a(0)$  as a function of the volume fraction  $\varphi_b$  for different values of  $\chi_S$ . The experimental data (in mJ.m<sup>-2</sup>) were converted to units  $k_B T.l^{-2}$  by choosing  $T = 298$  K, and  $l = 0.56$  nm. Here  $l$  is the length of one polymer segment. Its value was chosen as the size of one solvent molecule, which was obtained from the density of cyclohexane ( $0.774 * 10^3$  kg.m<sup>-3</sup>). For low values of  $\chi_S$  we see that within the calculated concentration range  $G_a(0)$  decreases (becomes more negative) monotonically with increasing concentration. With increasing  $\chi_S$  we see that  $G_a(0)$  decreases less strongly. For  $\chi_S$  values close to



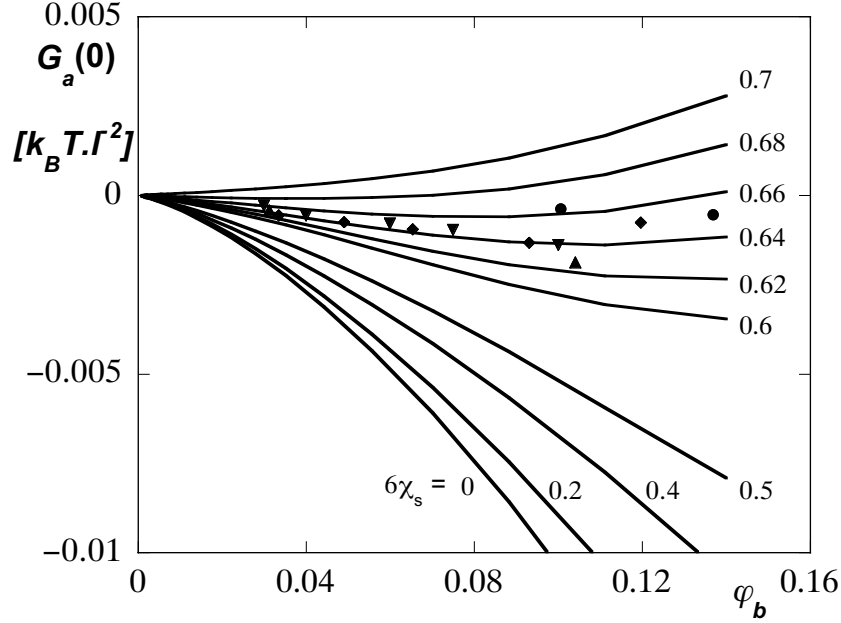


FIGURE 2.12.  $G_a(0)$  as a function of  $\varphi_b$  for different values of  $\chi_S$ , calculated with SF-SCF calculations. Symbols correspond to the experimental data: P14 ( $\bullet$ ), P31 ( $\blacktriangle$ ), P83 ( $\blacklozenge$ ), and P118 ( $\blacktriangledown$ ).

$\chi_{S,crit}$   $G_a(0)$  behaves non-monotonically; it first decreases, passes through a minimum and then increases again. It seems that this non-monotonic concentration behaviour of the well depth is also shown by our experimental data. From figure 2.12 we see that a value  $\chi_S \approx 0.11$  fits our experimental data rather well. Since for a cubic lattice it is seen that  $\chi_{S,crit} = \ln \frac{6}{5} = 0.18$ ,<sup>22</sup> our data roughly correspond to  $(\chi_{S,crit} - \chi_S)/\chi_{S,crit} = 0.41$ . The reduced variable  $(\chi_{S,crit} - \chi_S)/\chi_{S,crit}$  is a measure for the distance to the critical adsorption energy. If  $(\chi_{S,crit} - \chi_S)/\chi_{S,crit} = 1$  the depletion effect is maximal. In figure 2.13 we plot the  $G_a(0)/G_{a,max}$  versus  $(\chi_{S,crit} - \chi_S)/\chi_{S,crit}$  for  $\varphi_b = 0.7$ . For other concentrations the trend of this curve is similar, but we see in figure 2.12 that  $G_a(0)/G_{a,max}$  is even smaller for higher concentrations.  $G_{a,max}$  is the value of  $G_a$  for  $\chi_S = 0$ . From the figure it can be concluded that the depletion interaction is reduced significantly to about  $\frac{1}{6}$  of its maximal value.

Hence, we find that the measured depletion interaction is much lower than the maximal depletion interaction as predicted if one assumes that there is zero interaction between polymer segments and the surface. This result can directly be related to the macroscopic phase behaviour of systems where PDMS is used as nonadsorbing polymer in colloidal suspensions of stearyl-silica in cyclohexane. It is found that more PDMS is needed to reach the colloidal gas-liquid binodal<sup>3-5, 7</sup> than is predicted by the free volume theory for ideal polymers,<sup>13</sup> but also by theories in which excluded volume polymer chains are taken into account.<sup>9</sup> As shown in figure 4.12 the experimental binodal is found at about

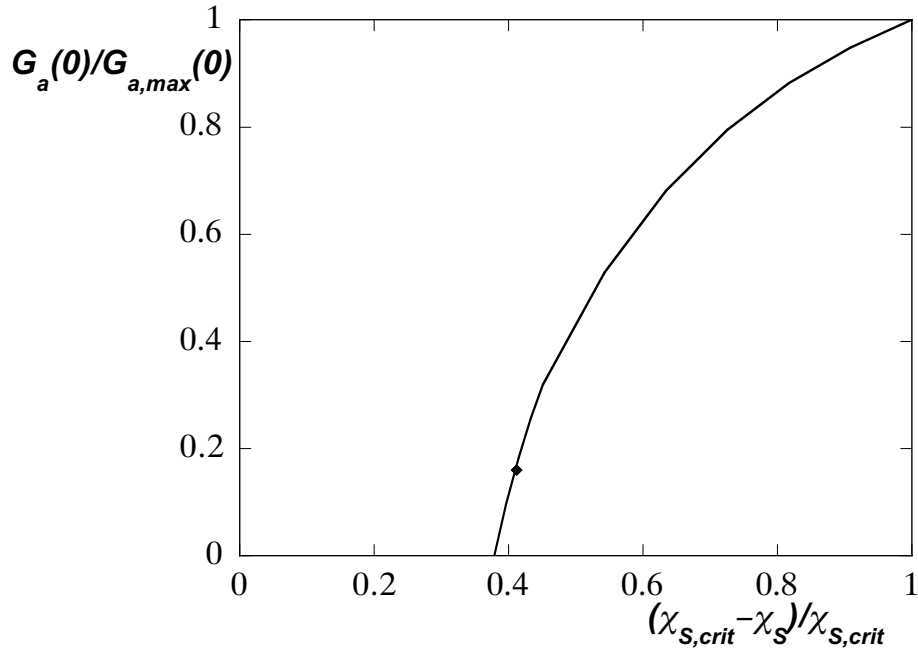


FIGURE 2.13.  $G_a(0)/G_{a,max}(0)$  as a function of  $(\chi_{S,crit} - \chi_S)/\chi_{S,crit}$  for  $\varphi_b = 0.07$ , calculated with SF-SCF calculations. The  $\blacklozenge$  corresponds to  $\chi_S = 0.11$  that fits our measurements.

2 to 3 times higher polymer concentrations than the calculated binodal.

## 2.5. Conclusions

We have investigated the depletion interaction by means of atomic force microscopy. We used a system of a stearylated silica sphere and a stearylated silica surface in the presence of a PDMS solution with different molecular weights and concentrations in cyclohexane. We found that the depletion interaction thickness decreases with increasing concentration polymer, in agreement with theories, discussed in section 2.2.<sup>23-25, 28</sup> However, the measured depth of the potential well is significantly smaller than predicted by these theories. This is explained by the fact that the surface interaction parameter is non-zero. We compared our experimental results with Scheutjens Fler Self Consisted Field calculations and found that the reduced adsorption energy  $(\chi_{S,crit} - \chi_S)/\chi_{S,crit} = 0.41$ . This results in a reduction of the depletion interaction to about  $\frac{1}{6}$  of its maximal value. This smaller magnitude of the depletion interaction is in agreement with the experimental finding on the phase behaviour that more PDMS is needed to reach the colloidal gas-liquid binodal.

## Acknowledgements

We thank Patrick Markus (Veeco) for performing measurements with the picoforce microscope, Frans Leermakers for performing the SF-SCF calculations and Gerard Fler for helpful discussions.

## Appendix 2A. Self-consistent field modelling of homopolymers in a slit

We consider two planar surfaces in the presence of a homopolymer consisting of segments with ranking number  $s = 1, \dots, N_p$  in a monomeric solvent; all chemical potentials are fixed. The characteristic function which determines the free energy of interaction per unit area  $G_a(h)$  is the grand potential  $\Omega$ :

$$G_a(h) = \Omega(h) - \Omega(\infty) \quad (2.11)$$

The grand potential is a function of the scaled distance  $h$  between two plates. Here and below all length scales are normalized by the segment size  $l$ . Self-consistent field (SCF) theory may be used to evaluate the (mean field) grand potential  $\Omega$ . Exact solutions of the SCF equations are only found numerically for which a discretization scheme is needed. We follow the Scheutjens-Fler<sup>38, 39</sup> method in which a lattice is used with lattice spacing  $l$ , i.e. equal to the segment size. Hence the space between the plates has an integer number of lattice layers  $z = 1, \dots, h$ , where  $z = 0$  and  $z = h + 1$  are permanently fully occupied by surface units  $W$ : the volume fractions of the wall units are therefore  $\varphi_W(0) = \varphi_W(h + 1) = 1$ . The lattice sites have a cubic arrangement with a fraction  $\lambda_0 = 4/6$  of the faces connecting to sites within a layer and a fraction of  $\lambda_1 = 1/6$  of the faces pointing to one of the neighbouring layers.

The grand potential may be computed by integration (summation) over the grand potential density  $\omega(z)$ :

$$\Omega(h) = \sum_{z=1}^h \omega(z) \quad (2.12)$$

It can be shown that the grand potential density is a functional of both the segment volume fractions  $\varphi(z)$  and the segment potentials  $u(z)$  of both the polymer ( $P$ ) and the solvent ( $S$ ):<sup>40</sup>

$$\begin{aligned} \omega(z) = & \sum_{i=P,S} \left( -\frac{\varphi_i(z) - \varphi_i^b}{N_i} - u_i(z)\varphi_i(z) \right. \\ & \left. + \frac{1}{2} \sum_{j=P,S} \chi_{ij} \left[ \varphi_i(z) \langle \varphi_j(z) - \varphi_j^b \rangle - \varphi_i^b (\varphi_j(z) - \varphi_j^b) \right] \right) \end{aligned} \quad (2.13)$$

where  $\varphi_i^b$  is the (fixed) bulk volume fraction of component  $i$  and  $\chi_{ij}$  the usual Flory-Huggins interaction parameters between component  $i$  and  $j$ . The angular brackets represent a three-layer average of a spatial dependent argument  $x$ :

$$\langle x(z) \rangle = \lambda_1 x(z-1) + \lambda_0 x(z) + \lambda_1 x(z+1) \approx x(z) + \lambda_1 \frac{\partial^2 x}{\partial z^2} \quad (2.14)$$

The SF-SCF method involves an iterative procedure which results in segment potentials that are consistent with the volume fractions. Their mutual interdependence has been discussed in the literature before.<sup>22</sup> In short the dimensionless segment potentials (in units of  $k_B T$ ) are given by:

$$u_i(z) = u'(z) + \sum_j' \chi_{ij} \langle \varphi_j(z) - \varphi_j^b \rangle \quad (2.15)$$

where the prime indicates that the sum over  $j$  includes the surface, i.e.,  $j = P, S, W$ . This means that in layers  $z = 1$  and  $z = h$  the contribution  $\chi_{PW}$  and  $\chi_{SW}$  are included as, e.g.  $\langle \varphi_W(1) - \varphi_j^b \rangle = \lambda_1$ . Note that only the difference between the affinity of the polymer segments and the solvent molecules for the surface is important for adsorption. This implies that we can set  $\chi_{SW} = 0$  without loss of generality. The Lagrange field  $u'(z)$  is coupled to the incompressibility constraint  $\sum_i \varphi_i(z) = 1$ . The segment potential is used in the Boltzmann weight  $g_i(z) = \exp[-u_i(z)]$ .

The volume fraction of the solvent is just proportional to its Boltzmann weight  $\varphi_S(z) = \varphi_S^b g_S(z)$  whereas the volume fraction of the polymer is given by the composition law

$$\varphi_P(z) = \varphi_P^b \sum_{s=1}^{N_P} \frac{g_P(z, s) g_P(z, N_P - s + 1)}{g_P(z)} \quad (2.16)$$

where we have made use of the inversion symmetry in the polymer chain. The Green's function  $g_P(z, s)$  expresses the statistical weight of a chain fragment of  $s$  segments subject to the restriction that one end is at position  $z$ .  $g_P(z, s)$  is found by the propagator equation

$$g_P(z, s) = g_P(z) \langle g_P(z, s-1) \rangle \quad (2.17)$$

which is started with the free end probability  $g_P(z, 1) = g_P(z)$ . The propagator implements a first-order Markov approximation for the chain statistics. Using equation 2.14 for the angular brackets, and expanding the Boltzmann weight for small line fragments  $s$ , it is easily seen that equation 2.17 is consistent with the (continuous) Edwards<sup>41</sup> equation which is typically used as the starting point for analytical approximations:

$$\frac{\partial g_P(z, s)}{\partial s} = \lambda_1 \frac{\partial^2 g_P(z, s)}{\partial z^2} - u_P(z) g_P(z, s) \quad (2.18)$$

In the continuous (Edwards) approach, the finite surface affinity of the polymer segments, which in the discretized SCF theory is included in the segment potential of equation 2.15, must be replaced by the surface boundary condition  $\partial \ln g / \partial z = -c$ , where  $c$  is the adsorption length introduced by de Gennes.<sup>29</sup>

## References

- [1] Doublier, J.-L.; Garnier, C.; Renard, C.; Sanchez, C. *Curr. Opin. Coll. Int. Sci.* **2000**, *5*, 184.
- [2] Hughes, D. F. K.; Robb, I. D.; Dowsing, P. J. *Langmuir* **1999**, *15*, 5227.
- [3] Verhaegh, N. A. M.; van Duijneveldt, J. S.; Dhont, J. K. G.; Lekkerkerker, H. N. W. *Physica A* **1996**, *230*, 409.
- [4] Bodnár, I.; Oosterbaan, W. D. *J. Chem. Phys.* **1997**, *106*, 7777-7780.
- [5] de Hoog, E. H. A.; Lekkerkerker, H. N. W. *J. Phys. Chem. B* **1999**, *103*, 5274-5279.
- [6] Wijting, W. K.; Besseling, N. A. M.; Cohen Stuart, M. A. *Phys. Rev. Lett.* **2003**, *90*, 196101.
- [7] Wijting, W. K.; Besseling, N. A. M.; Cohen Stuart, M. A. *J. Phys. Chem. B* **2003**, *107*, 10565.
- [8] Aarts, D. G. A. L.; van der Wiel, J. H.; Lekkerkerker, H. N. W. *J. Phys.: Condens. Matter* **2003**, *15*, S245-S250.
- [9] Aarts, D. G. A. L.; Tuinier, R.; Lekkerkerker, H. N. W. *J. Phys.: Condens. Matter* **2002**, *14*, 7551-7561.
- [10] Asakura, S.; Oosawa, F. *J. Chem. Phys.* **1954**, *22*, 1255.
- [11] Vrij, A. *Pure Appl. Chem.* **1976**, *48*, 471.
- [12] Poon, W. C. K.; Pusey, P. N.; Lekkerkerker, H. N. W. *Physics World* **1996**, *9*, 27-32.
- [13] Lekkerkerker, H. N. W.; Poon, W. C. K.; Pusey, P. N.; Stroobants, A.; Warren, P. B. *Europhys. Letters* **1992**, *20*, 559-564.
- [14] Giesbers, M. *Surface Forces studied with colloidal probe Atomic force microscopy, PhD-thesis*; Wageningen University: 2001.
- [15] Giesbers, M.; Kleijn, J. M.; Cohen Stuart, M. A. *J. Colloid Interface Sci.* **2002**, *248*, 88-95.
- [16] Giesbers, M.; Kleijn, J. M.; Cohen Stuart, M. A. *J. Colloid Interface Sci.* **2002**, *252*, 138-148.
- [17] Barten, D.; Kleijn, J. M.; Duval, J.; van Leeuwen, H. P.; Lyklema, J.; Cohen Stuart, M. A. *Langmuir* **2003**, *19*, 1133.
- [18] Giesbers, M.; Kleijn, J. M.; Fler, G. J.; Cohen Stuart, M. A. *Colloids Surf. A* **1998**, *142*, 343.
- [19] Milling, A. J.; Kendall, K. *Langmuir* **2000**, *16*, 5106-5115.
- [20] Biggs, S.; Burns, J. L.; Yan, Y.; Jameson, G. J.; Jenkins, P. *Langmuir* **2000**, *16*, 9242-9248.
- [21] Milling, A. J.; Biggs, S. *J. Colloid Interface Sci.* **1995**, *170*, 604.
- [22] Fler, G. J.; Cohen Stuart, M. A.; Scheutjens, J. M. H. M.; Cosgrove, T.; Vincent, B. *Polymers at Interfaces*; Chapman & Hall, London Glasgow New York Tokyo Melbourne Madras: 1993.
- [23] Tuinier, R.; Aarts, D. G. A. L.; Wensink, H. H.; Lekkerkerker, H. N. W. *Phys. Chem. Chem. Phys.* **2003**, *5*, 3707-3715.
- [24] Louis, A. A.; Bolhuis, P.; Meijer, E. J.; Hansen, J. P. *J. Chem. Phys.* **2002**, *117*, 1893.
- [25] Bolhuis, P.; Louis, A. A.; Hansen, J. P.; Meijer, E. J. *J. Chem. Phys.* **2001**, *114*, 4296.
- [26] Schäfer, L. *Excluded Volume Effects in Polymer Solutions*; Springer Verlag, Berlin: 1999.
- [27] Fler, G. J.; Scheutjens, J. M. H. M.; Vincent, B. *ACS Symposia* **1984**, 245.
- [28] Fler, G. J.; Skvortsov, A. M.; Tuinier, R. *Macromolecules* **2003**, *36*, 7857.
- [29] de Gennes, P. G. *Scaling Concepts in Polymer Physics*; Cornell University Press: Ithaca, NY: 1979.

- [30] Lyklema, J. *Fundamentals of Interface and Colloid Science IV*; Academic Press, London: to be published.
- [31] Fleer, G. J.; Leermakers, F. A. M. *Coagulation and Flocculation, Surfactant Science Series Vol. 47*; Marcel Dekker, Inc. New York, Basel, Hong Kong: to be published 2004.
- [32] Israelachvili, J. *Intermolecular and surface forces, 2nd edition ed.*; London, Academic press: 1992.
- [33] van Helden, A. K.; Jansen, J. W.; Vrij, A. *J. Colloid Interface Sci.* **1981**, *81*, 354.
- [34] Hutter, J. L.; Bechhoefer, J. *Review of Scientific instruments* **1993**, *64*, 1868.
- [35] Senden, T. J. *Current Opinion in Colloid & Interface Science* **2001**, *6*, 95-101.
- [36] "Digital Instruments Nanoscope®III Multimode Scanning Probe Microscope, Instruction Manual version 1.5", 1993.
- [37] Kuwahara, N.; Okazawa, T.; Kaneko, M. *J. Polym. Sci. part C* **1968**, *23*, 543.
- [38] Scheutjens, J. M. H. M.; Fleer, G. J. *J. Phys. Chem.* **1979**, *83*, 1619.
- [39] Scheutjens, J. M. H. M.; Fleer, G. J. *J. Phys. Chem.* **1980**, *84*, 178.
- [40] Evers, O. A.; Scheutjens, J. M. H. M.; Fleer, G. J. *Macromolecules* **1990**, *23*, 5221.
- [41] Edwards, S. F. *Proc. Phys. Soc.* **1965**, *85*, 613.

## CHAPTER 3

# Wetting in a Colloidal Liquid-Gas System\*

### ABSTRACT

We present first observations of wetting phenomena in depletion interaction driven, phase separated colloidal dispersions (coated silica/cyclohexane/PDMS). The contact angle of the colloidal liquid-gas interface at a solid substrate (coated glass) was determined for a series of compositions. Upon approach to the critical point, a transition occurs from partial to complete wetting.

---

\*In slightly modified form published as: Wijting, W. K.; Besseling, N. A. M.; Cohen Stuart, M. A. *Physical Review Letters* **2003**, *90*, 196101.

Colloidal systems make convenient experimental models of simple fluids, as they are composed of particles with interactions that can be tuned in both strength and range. This chapter presents the first observations on wetting (contact angles) and a wetting transition occurring in depletion interaction driven systems.

Wetting phenomena are typical, perhaps even characteristic, for the liquid state. They occur always when three phases coexist, at least one of which is liquid, and not more than one solid. If two fluid phases are in contact with a solid, partial wetting can be characterized by the static contact angle,  $\theta_0$ , which is by Young's law related to the interfacial tensions,  $\gamma$ , between the three phases:<sup>1</sup>

$$\cos \theta_0 = \frac{\gamma_{SG} - \gamma_{SL}}{\gamma_{LG}} \quad (3.1)$$

Here, the subscripts  $S$ ,  $L$ , and  $G$  refer to the solid, the liquid and the gas phase, respectively. If the contact angle is  $0^\circ$ , the substrate is said to be completely wet by the liquid; if  $0^\circ < \theta < 180^\circ$ , the substrate is partially wet.<sup>2</sup> In equation (3.1) the denominator depends only on the interaction between molecules that make up the liquid and the gas. The numerator also depends on the interaction between these molecules and the substrate. Cahn predicted that near the critical point a solid substrate is completely wet by one of the two fluid phases. At a certain temperature below the critical point the wetting behaviour may change from complete to partial. This phenomenon is called the wetting transition and is a true phase transition.<sup>3, 4</sup>

The past 25 years have seen a revival of the study of fundamental aspects of wetting phenomena in general and wetting transitions in particular.<sup>2-7</sup> For further investigations it would be very convenient to control the interactions on a microscopic level. Clearly, with atomic or molecular fluids this is impossible because the interactions are given with the molecular species. As an alternative, colloidal systems make very convenient experimental model systems, because the interactions can be *tuned*, both in *range* and *strength*. Therefore, colloidal systems have played an important role in the experimental verification of theories of condensed matter in general, and of liquids in particular.<sup>8, 9</sup>

The phase behaviour of colloidal dispersions has a strong analogy with that of atomic or molecular systems. Similar to molecular systems, colloidal particles dispersed in a liquid medium can assume various states. A dilute disordered dispersion is called "*colloidal gas*", a concentrated disordered one is called "*colloidal liquid*" and a concentrated ordered dispersion "*colloidal crystal*". Using colloidal model systems, the requirements for the very existence of the liquid state have been clarified, namely, the existence of an attraction with a range that is not too short, compared to the diameter of the repulsive core of the pair potential.

In order to prepare colloids in a liquid state, one proceeds as follows. Since the bare Van der Waals attraction cannot be tuned, one uses colloidal particles for which this



attraction is screened by dispersing them in a medium of similar dielectric permittivity (according to Lifschitz theory<sup>10</sup>). For such a system, the attraction, that causes gas-liquid phase separation, is generated by adding nonadsorbing polymer. This is called depletion interaction and is of entropic nature.<sup>9, 11–18</sup> The interaction free energy of this depletion interaction is given by the product of the overlap volume of two depletion zones and the osmotic pressure due to the polymer. Similarly, there will be depletion attraction between colloidal particles and a macroscopic surface on which polymer does not adsorb. Below the overlap concentration the range of the attraction is twice the radius of gyration of the polymer. Hence, the depletion interaction can be varied by choosing the molar mass and the concentration of the polymer. The advantage of such systems is that the interactions (hard core repulsion/depletion attraction) are known, at least in principle. Depletion interactions between coated silica surfaces in solutions of polydimethylsiloxane (PDMS) can be measured, and have been measured for certain molecular weights and concentrations.<sup>19</sup> The polymer chemical potential plays a role similar to that of the inverse temperature in ordinary atomic or molecular systems.<sup>13, 14, 16, 17</sup> If the concentrations of colloidal particles and polymer are sufficiently high, the depletion interaction will lead to phase separation: A colloid poor phase and a colloid rich phase coexist.

The colloidal system used in the present study consisted of organophilic silica particles (radius,  $R_c = 14$  nm), dispersed in cyclohexane.<sup>20, 21</sup> The dielectric permittivities of silica and cyclohexane are very similar so that, in the absence of polymer, the particles behave as hard spheres.<sup>20, 22</sup> We used PDMS as nonadsorbing polymer. The number average molecular weight was 83 200 g/mole, corresponding to a radius of gyration,  $R_g = 13$  nm, and the heterodispersity index was 1.24. The size ratio  $q = R_g/R_c$  for this system equals 0.93. The liquid-gas phase behaviour of similar silica/PDMS/cyclohexane systems has been studied extensively.<sup>15, 23, 24</sup>

In figure 3.1 the phase diagram of the system is presented. Here the polymer concentration<sup>†</sup>  $\varphi_{pol}$  is plotted versus the colloid volume fraction,  $\varphi_{coll}$ . The phase diagram is constructed according to the method of Bodnár *et al.*<sup>23</sup> The critical point was located by extrapolating the middles of the tielines to the binodal. In the same figure, compositions are indicated at which we performed wetting experiments. These compositions vary with respect to their proximity to the critical point. In order to examine the wetting behaviour, we chose a substrate which has only hard repulsion and depletion attraction with the particles. We used glass coated with the same organophilic groups as the particles (on which PDMS does not adsorb).

---

<sup>†</sup>The polymer concentration is scaled to the overlap concentration,  $\varphi_{pol} = c/c^*$  with  $c$  the weight concentration and  $c^*$  its value at overlap. The overlap concentration is calculated by  $c^* = M_N / (\frac{4}{3}\pi R_g^3 N_{Av})$ , with  $N_{Av}$  Avogadro's number.

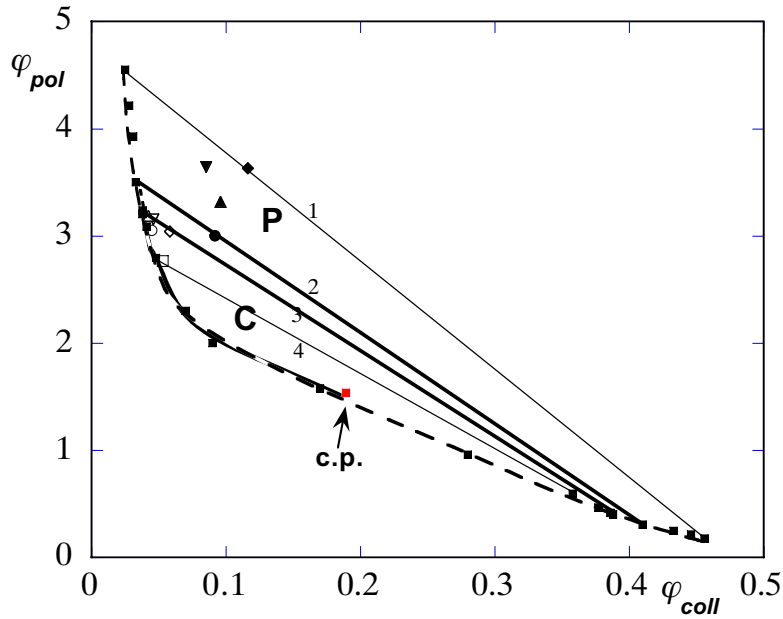


FIGURE 3.1. Phase diagram of the silica/PDMS/cyclohexane system. The polymer concentration,  $\varphi_{pol}$ , is plotted versus the volume fraction colloid  $\varphi_{coll}$ . The binodal points are denoted with solid squares and the critical point is indicated by c.p. The binodal is represented by the dashed curve. At the tielines (solid lines), indicated by 1, 2, 3 and 4, the polymer reservoir concentrations are 5.5, 4.5, 4.3, and 4.1, respectively. The overall compositions of the samples are given by A ( $\blacklozenge$ ), B ( $\blacktriangledown$ ), C ( $\blacktriangle$ ), D ( $\bullet$ ), E ( $\blacklozenge$ ), F ( $\blacktriangledown$ ), G ( $\blacktriangle$ ), H ( $\circ$ ), J ( $\square$ ). Points E and G are on the same tieline (have the same polymer chemical potential). Where complete wetting occurs the binodal is drawn as a fat solid line and in the interval in which the wetting transition occurs as a dotted one. The complete and partial wetting regimes are indicated by C and P, respectively.

In order to make meaningful observations we had to overcome some experimental difficulties. These are due to the low optical contrast between the phases and the small size of the meniscus. Concerning the latter, the capillary length,  $l_c$ , is an important parameter which marks the crossover between a regime where  $\gamma_{LG}$  dominates the shape of a meniscus and another regime where gravity dominates that shape. It is defined by  $l_c = \sqrt{\gamma_{LG}/\Delta\rho g}$ , where  $\Delta\rho$  is the density difference between the two phases and  $g$  is the gravitation constant. Since in colloidal systems  $\gamma_{LG}$  is very low,<sup>24</sup>  $l_c$  is orders of magnitude smaller ( $O$  tens of  $\mu$  m) than in typical molecular systems ( $O$  mm). We studied menisci around vertically suspended fibres of treated glass with a diameter of about 0.2 mm. Pictures of menisci were captured using appropriate viewing optics. We obtained the best results by illuminating the sample with a diffuse parallel light beam through the sample in the direction of objective and CCD Camera. It turned out,

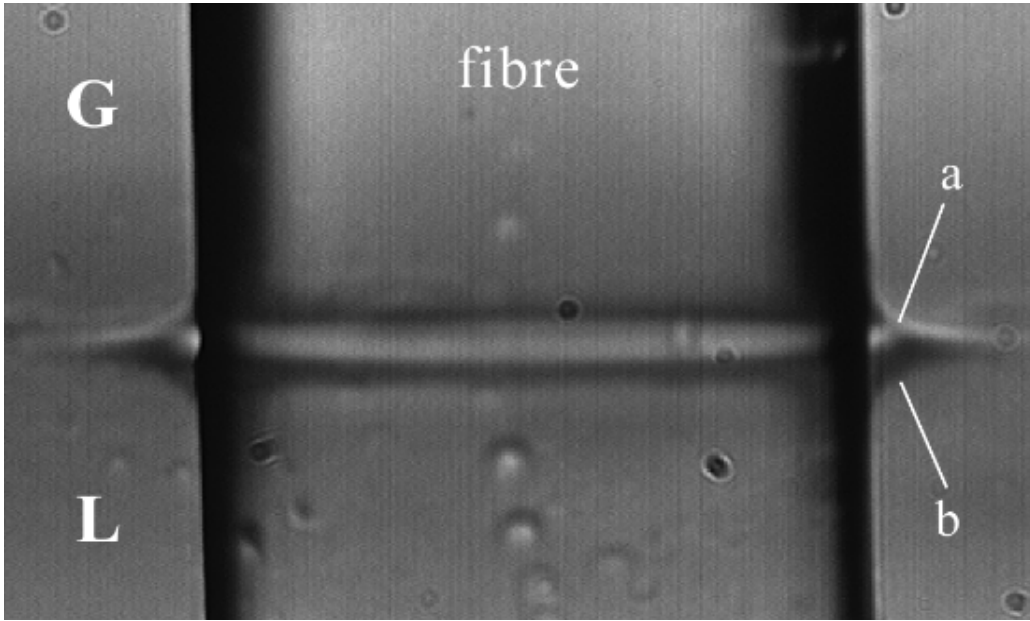


FIGURE 3.2. Image of a meniscus at a fibre suspended in a colloidal liquid-gas system (sample A). The capital **G** and **L** refer to the colloidal gas and colloidal liquid phase, respectively. The meniscus is indicated by **a** and its mirror image by **b**.

however, that both the meniscus and its mirror image were seen, and it could not easily be decided which is which. The technical solution to this problem was to determine dynamic contact angles by moving the fibre up or down by means of an electronically controlled actuator. In this way, unambiguous and more accurate static contact angles could be obtained.

In figure 3.2 we present an image of a meniscus at the fibre of sample A (see figure 3.1). A similar result is presented by Aarts *et al.*<sup>25</sup> The colloidal gas and liquid phases are separated by a horizontal interface; the upper phase is the colloidal gas and the lower phase the colloidal liquid. The flat interface itself cannot be seen, but its position can be deduced by means of the mirror images it produces. Near the fibre we can clearly distinguish the curved part of the meniscus and its mirror image. The true meniscus is distinguished from its mirror image by its response to the downward or upward movement of the fibre in the dynamic experiments. This allowed us to unambiguously conclude that the static meniscus curves upwards. Hence, the contact angle is smaller than  $90^\circ$  but an accurate value cannot easily be determined from a static profile. Therefore we determined the static contact angle,  $\theta_0$  by interpolation from dynamic contact angles measured for a large number of velocities. In figure 3.3 we present, by way of example,  $\cos \theta$  for the samples A (deep in the two phase coexistence region) and J (more close to the critical point) as a function of the velocity. These contact angles were determined by drawing tangents to the liquid-gas interfaces in the three phase

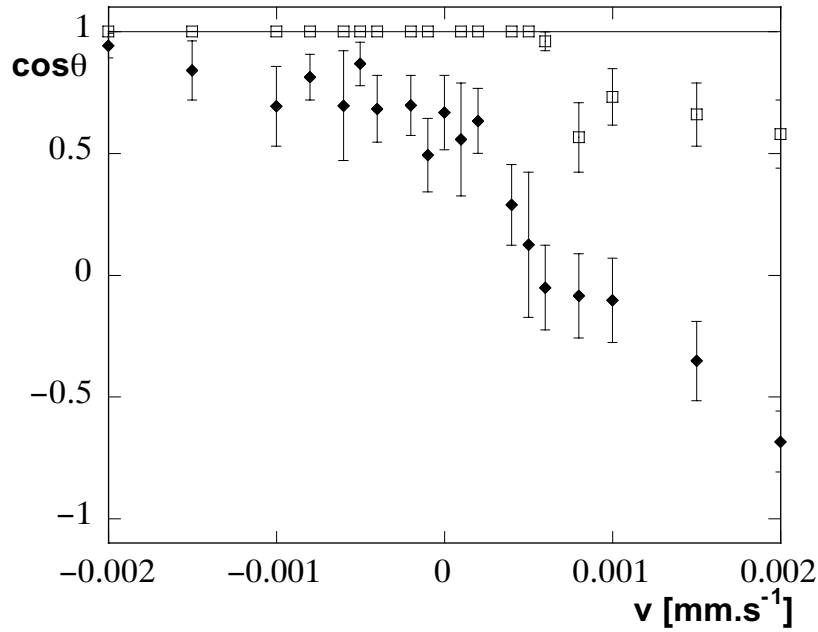


FIGURE 3.3. The cosine of the dynamic contact angle of sample A (◆) and J (□) at the substrate as a function of the velocity of the substrate with respect to the colloidal liquid-gas interface. A positive velocity corresponds to an advancing contact angle and a negative to a receding contact angle.

points. Extrapolation of contact angles to zero velocity from the positive ( $v > 0$ ) side yields the static *advancing* contact angle and from the negative ( $v < 0$ ) side the static *receding* contact angle. Often these two contact angles are different: At zero velocity there is a discontinuity in the contact angle- velocity curve (contact angle hysteresis). In our system however, it seems that there is no discontinuity, within the error of the experiment. This implies that hysteresis, if any, is smaller than the scatter in our data. This justifies our interpolation procedure.

We first conclude that static contact angles for all samples in figure 3.1 are smaller than  $90^\circ$ , which indicates that the substrate prefers the liquid over the gas phase. This can be understood by considering the underlying interactions (particle-particle and particle-substrate). The depletion interaction is proportional to the overlap volume of the depletion zones.<sup>11, 12</sup> Since the radius of curvature of the fibre is much larger than that of a particle, the fibre can be regarded as a flat substrate. The overlap volume between the depletion zones of a spherical particle and a flat substrate is larger than the overlap volume for two spherical particles, at the same distance. Hence, the attraction between a particle and the substrate is stronger than that between two particles. In the colloidal liquid phase, there are many more particles than in the colloidal gas phase, so the substrate attracts the colloidal liquid phase much more strongly than the colloidal gas phase. Therefore a contact angle smaller than  $90^\circ$  is expected.

We see that for sample A the static contact angle has a finite value at zero velocity,

while for sample J this contact angle is  $0^\circ$ . Hence, it can be concluded that sample A is a case of partial wetting, and sample J of complete wetting. So, there must be a transition from partial wetting to complete wetting, upon approaching the critical point. In order to narrow down the range where it occurs, we measured  $\theta_0$  for all samples indicated in figure 3.1. The results appear in figure 3.4 as a plot of  $\cos \theta_0$  versus an appropriate field variable<sup>14</sup> which measures the proximity to the critical point. For this variable there are several options. One option is to use the polymer reservoir concentration,  $\varphi_{pol}^r$ , which is related to the polymer chemical potential. This quantity cannot be directly determined experimentally. It can be estimated by correcting the actual polymer concentration ( $\varphi_{pol}$ ) in the gas phase for the volume of the colloidal particles with their depletion zones by means of scaled particle theory.<sup>13, 14</sup> However, near the critical point the polymer reservoir concentration cannot be determined in this way. As an alternative, the difference in colloid volume fraction between the liquid and the gas phase, ( $\Delta\varphi_{coll} = \varphi_{coll,l} - \varphi_{coll,g}$ ) can be used. This difference vanishes in the critical point. It is known that near the critical point for most three dimensional systems  $\Delta\varphi \sim (X - X_c)^{0.313}$ , where  $X$  is the relevant field variable (often the temperature, but in our case it is related to  $\varphi_{pol}^r$  or the polymer chemical potential) and  $X_c$  its value in the critical point.<sup>26</sup> Therefore we choose in figure 3.4 to use  $(\Delta\varphi_{coll})^{1/0.313}$  as the measure for the distance to the critical point. This is the central result of this chapter.

We see, that at  $0.034 < (\Delta\varphi_{coll})^{1/0.313} < 0.044$  ( $0.35 < \Delta\varphi_{coll} < 0.38$ ) there is a transition between partial and complete wetting:  $\cos \theta_0$  changes there between unity and a smaller value. This corresponds to  $4.3 < \varphi_{pol}^r < 4.5$ . In figure 3.1 this interval is between the thick tielines 2 and 3. The occurrence of this wetting transition is in agreement with the qualitative prediction of Cahn.<sup>3</sup> We can make a more quantitative comparison with predictions of Brader *et al.* and Dijkstra *et al.*, who calculated the location of such a wetting transition for colloid-polymer mixtures by density functional theory and Monte-Carlo simulations, respectively.<sup>16, 17</sup> In the Monte Carlo simulations, it was found that for  $q = 1$  it occurs in the region  $0.011 < (\Delta\varphi_{coll})^{1/0.313} < 0.012$  ( $1.05 < \varphi_{pol}^r < 1.10$ ).<sup>27</sup> For the density functional calculations we have only data for  $q = 0.6$ ; the transition occurs at  $(\Delta\varphi_{coll})^{1/0.313} = 0.015$  ( $\varphi_{pol}^r = 0.595$ ). The values of both  $(\Delta\varphi_{coll})^{1/0.313}$  and  $\varphi_{pol}^r$  at the wetting transition are significantly lower than our experimental result, but also their binodals differ significantly from ours. The differences may be due to the fact that in the simulations and calculations the polymers are taken to be ideal, while in our experiments they are not. Within the ideal polymer model, below overlap the osmotic pressure is overestimated (as it corresponds with a larger number concentration of polymer molecules). Above overlap it neglects the shrinking of the depletion layer thickness and the enhanced (as compared to Van't Hoff's law) increase of the osmotic pressure with increasing polymer concentration. It cannot easily be estimated what the

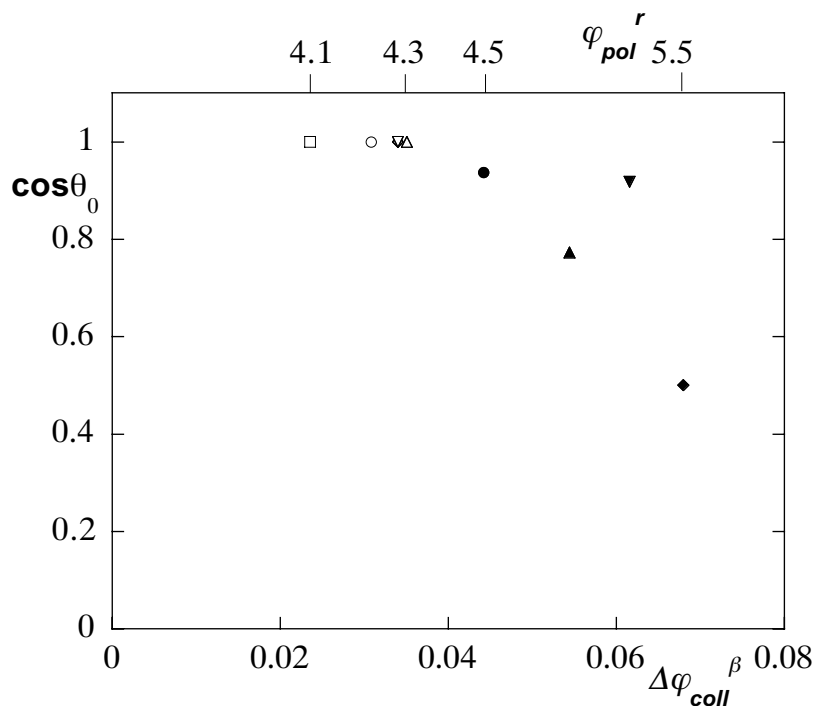


FIGURE 3.4. The cosine of the static contact angle as a function of  $\Delta\varphi_{coll}^\beta$  with  $\beta = 1/0.313$ . The symbols are explained in the capture of figure 1.  $\nabla$  represents two independent measurements.

effects of the ideal polymer approximation will be on the macroscopic (phase) behaviour of a colloidal system. It turns out that it leads to an overestimation of the tendency for phase separation: In real systems the binodal is found at much higher values of  $\varphi_{pol}$  (or  $\varphi_{pol}^r$ ) than is predicted by the ideal polymer model. Recent calculation of the phase diagram taking non-ideality into account lead to better, although not perfect, agreement with experiments.<sup>18</sup> We find predictions based on the fact that the ideal polymer approximation also underestimates for the value of  $\varphi_{pol}^r$  at which the wetting transition occurs, and to a smaller extend of  $\Delta\varphi_{col}$ . The accuracy of our experimental data is not sufficient to decide whether the wetting transition is first or second order. It seems to be either second order or weakly first order.

In conclusion, we have demonstrated that wetting phenomena can be experimentally investigated using colloidal systems exhibiting gas-liquid phase behaviour. The beauty of these systems is that the attractive interaction can be controlled in strength and range. This opens up many perspectives for studying the relation between wetting phenomena and the underlying interactions, e.g. far from the critical point or close to criticality. We were able to locate a Cahn wetting transition upon approaching the critical point at  $0.034 < (\Delta\varphi_{coll})^{1/0.313} < 0.044$ . By this we have tested successfully the well-known Cahn prediction regarding wetting transitions.<sup>3</sup>

## References

- [1] Young, T. *Philos. Trans. R. Soc.* **1805**, 95, 69.
- [2] Dietrich, S. *Phase Transitions and critical Phenomena*; Academic Press, London: 1988.
- [3] Cahn, J. W. *J. Chem. Phys.* **1977**, 66, 3667.
- [4] Schick, M. *Introduction to wetting phenomena*; Elsevier Science Publishers B.V.: 1990.
- [5] de Gennes, P. G. *Rev. Mod. Phys.* **1985**, 57, 827.
- [6] Bonn, D.; Ross, D. *Reports on Progress in Physics* **2001**, 64, 1085.
- [7] Ross, D.; Bonn, D.; Posazhennikova, A. I.; Indekeu, J. O.; Meunier, J. *Phys. Rev. Lett.* **2001**, 87, 176103.
- [8] Hagen, M. H. J.; Meijer, E. J.; Mooij, G. C. A. M.; Frenkel, D.; Lekkerkerker, H. N. W. *Nature* **1993**, 365, 425-426.
- [9] Poon, W. C. K.; Pusey, P. N.; Lekkerkerker, H. N. W. *Physics World* **1996**, 9, 27-32.
- [10] Lyklema, J. *Fundamentals of Interface and Colloid Science I*; Academic Press, London: 1991.
- [11] Asakura, S.; Oosawa, F. *J. Chem. Phys.* **1954**, 22, 1255.
- [12] Vrij, A. *Pure Appl. Chem.* **1976**, 48, 471.
- [13] Lekkerkerker, H. N. W.; Poon, W. C. K.; Pusey, P. N.; Stroobants, A.; Warren, P. B. *Europhys. Letters* **1992**, 20, 559-564.
- [14] Poon, W. C. K.; Ilett, S. M.; Pusey, P. N. *Il Nuovo Cimento Soc. Ital. Fis.* **1994**, 16 D, 1127-1139.
- [15] Verhaegh, N. A. M.; van Duijneveldt, J. S.; Dhont, J. K. G.; Lekkerkerker, H. N. W. *Physica A* **1996**, 230, 409.
- [16] Brader, J.; Evans, R.; Schmidt, M.; Löwen, H. *J. Phys.: Condens. Matter* **2002**, 14, L1-L8.
- [17] Dijkstra, M.; van Roij, R. *Phys. Rev. Lett.* **2002**, 89, 208303-1.
- [18] Aarts, D. G. A. L.; Tuinier, R.; Lekkerkerker, H. N. W. *J. Phys.: Condens. Matter* **2002**, 14, 7551-7561.
- [19] Milling, A. J.; Biggs, S. *J. Colloid Interface Sci.* **1995**, 170, 604.
- [20] van Helden, A. K.; Jansen, J. W.; Vrij, A. *J. Colloid Interface Sci.* **1981**, 81, 354.
- [21] Pathmamanoharan, C.; Philipse, A. P. *J. Colloid Interface Sci.* **1994**, 165, 519-521.
- [22] Kops-Werkhoven, M. M.; Fijnaut, H. M. *J. Chem. Phys.* **1981**, 74, 1618.
- [23] Bodnár, I.; Oosterbaan, W. D. *J. Chem. Phys.* **1997**, 106, 7777-7780.
- [24] de Hoog, E. H. A.; Lekkerkerker, H. N. W. *J. Phys. Chem. B* **1999**, 103, 5274-5279.
- [25] Aarts, D. G. A. L.; van der Wiel, J. H.; Lekkerkerker, H. N. W. *J. Phys.: Condens. Matter* **2003**, 15, S245-S250.
- [26] Chandler, D. *Introduction to modern statistical mechanics*; Oxford University Press, New York Oxford: 1987.
- [27] Dijkstra, M. 2002 personal communications.





## CHAPTER 4

# Wetting Behaviour in Colloid-Polymer Mixtures at Different Substrates\*

### ABSTRACT

We present experimental observations on wetting phenomena in depletion interaction driven, phase separated colloidal dispersions. The contact angle of the colloidal liquid-gas interface at a solid substrate was determined for a series of compositions. Upon approach to the critical point, a transition occurs from partial to complete wetting. The interaction with the substrate was manipulated by modifying the substrate with a polymer. In that case a transition from partial to complete drying is observed upon approach to the critical point.

---

\*In modified form published as: Wijting, W. K.; Besseling, N. A. M.; Cohen Stuart, M. A. *Journal of Physical Chemistry B* **2003**, *107*, 10565-10570.

## 4.1. Introduction

Colloidal systems have played an important role as experimental model systems to study generic properties of fluid and solid matter in general.<sup>1</sup> In colloidal systems, time and length scales are larger than in molecular systems, so colloidal systems are in some respects more convenient in experimental studies. Another advantage of colloidal systems as compared to molecular systems is that we can tune the properties, such as particle size and the range and strength of the interactions, on a continuous scale. This motivates our use of colloidal systems as an experimental model system to investigate wetting phenomena.

The phase behaviour in colloidal systems can be controlled by nonadsorbing polymer. Nonadsorbing polymer in a colloidal suspension of hard spherical particles yields an attractive contribution to the interaction between the particles, which is called depletion interaction.<sup>1-10</sup> The free energy of this depletion interaction is equal to the overlap volume of two depletion zones times the osmotic pressure because of the polymer. Below the polymer overlap concentration the range of the attraction is twice the radius of gyration of the polymer. So the interaction can be tuned in both range and strength by varying the molecular mass and the concentration of polymer, respectively. If the concentrations of colloidal particles and polymer are sufficiently high, the depletion interaction will lead to phase separation: a colloid poor phase which is called *colloidal gas*, and a colloid rich phase, which is called *colloidal liquid*, coexist. Also a *colloidal crystal* may occur. Structure and phase behaviour of colloidal systems is quite similar to that of systems consisting of noble gas atoms or simple isometric molecules. For several colloidal systems the phase behaviour has been investigated both experimentally and theoretically.<sup>1, 4-7, 11</sup>

In the theories of Poon and Lekkerkerker<sup>5, 6</sup> the polymers are assumed to be ideal. This implies that (i) swelling of polymer because of interchain excluded volume interactions is ignored, (ii) the range of the depletion interaction is assumed independent of solvent quality and polymer concentration, and (iii) the polymer osmotic pressure is assumed to be given by the law of Van't Hoff. In experimental studies, the polymers are rarely ideal and the polymer concentration often exceeds the overlap concentration. Furthermore, in several older theories<sup>1, 4-6</sup> the interaction between two colloidal particles is taken to be pair wise additive. However, three and more body interactions are usually not negligible. Brader and others accounted for this non-pair wise additivity.<sup>8, 9, 11</sup> Aarts *et al.* made theoretical calculations in which excluded-volume polymer chains are explicitly considered.<sup>11</sup> In that paper also the variation of the thickness of the depletion layer as a function of the curvature of the colloidal particles and of the concentration of polymer are taken into account.

The size ratio of the polymer coils and the colloidal particles ( $q = R_g/R_c$ , with  $R_g$

the radius of gyration of the polymer and  $R_c$  the radius of the colloidal particles) has to be  $q > 0.3$  in order to make the existence of a colloidal liquid state possible.<sup>1, 5, 6</sup> Generally, for a liquid phase to be possible an attraction with a range of the order of magnitude of the particles is required.

In this chapter we describe wetting experiments on phase separated colloid-polymer systems. We consider a solid substrate in equilibrium with two fluid phases (colloidal liquid and colloidal gas). In this situation the equilibrium wetting state can be described by the static contact angle,  $\theta_0$ . Through Young's law the contact angle is related to the interfacial tensions,  $\gamma$ <sup>12</sup>

$$\cos \theta_0 = \frac{\gamma_{SG} - \gamma_{SL}}{\gamma_{LG}} \quad (4.1)$$

Here the subscripts  $S$ ,  $L$ , and  $G$  refer to the solid substrate, the (colloidal) liquid, and the (colloidal) gas phases respectively. If  $0^\circ < \theta_0 < 180^\circ$  the substrate is said to be partially wet. Complete wetting corresponds with  $\theta_0 = 0^\circ$ . In this case there can be no substrate-gas interface at coexistence of liquid and gas because a liquid film intervenes between the substrate and the gas phase. If  $\theta_0 = 180^\circ$  we speak of complete drying: at liquid-gas coexistence, a gas film will intervene between the liquid and the substrate.<sup>13</sup>  $\gamma_{LG}$  only depends on the interactions between the particles that make up the liquid and the gas phases, whereas  $\gamma_{SG}$  and  $\gamma_{SL}$  also depend on the interactions between these particles and the substrate.

Cahn predicted that, always when two coexisting fluid phases exist in the presence of a third phase (substrate), near the critical point a substrate is completely wet by one of the two coexisting fluid phases. At a certain temperature below the critical point, wetting may change from complete to partial. This phenomenon is called the wetting transition and is a true phase transition.<sup>14</sup> If the derivative of a free energy-temperature curve (or a contact angle-temperature curve) is discontinuous at the wetting transition, a wetting transition is first order. If that derivative is continuous in the transition point, the transition is second order or critical.<sup>15-17</sup> First order wetting transitions occur usually far from the critical point, whereas second order wetting transitions occur more close to the critical point.<sup>16</sup>

In non-equilibrium situations, the three phase contact line may move with respect to the substrate. Usually, the contact angle depends on the velocity with which the substrate and the contact line move with respect to each other. A liquid can advance over the substrate, or it can recede from the substrate, leading to advancing and receding contact angles, respectively. Extrapolation to zero velocity yields the static advancing and the static receding contact angle, respectively. For many systems the static receding contact angle is smaller than the static advancing contact angle. So, at zero velocity there is a discontinuity in a contact angle-velocity curve (contact angle hysteresis). This hysteresis occurs because of chemical inhomogeneity and/or roughness on the scale of

molecules.<sup>18</sup>

The past 25 years have seen a revival of the study of fundamental aspects of wetting phenomena in general and wetting transitions in particular.<sup>13–19</sup> To investigate the relations between macroscopic wetting behaviour and the underlying microscopic interactions, it would be convenient to have an experimental system in which these microscopic interactions can be tuned. With atomic or molecular systems this is not possible. However, using colloidal systems we can independently tune the interactions between the particle and that between a particle and the substrate and investigate the consequences for wetting behaviour. Recently we published a letter on our first observations of a wetting transition in a phase separated colloid polymer mixture.<sup>10</sup> Furthermore Aarts *et al.* reported observations on menisci of the colloidal liquid-gas interface at a hard substrate.<sup>20</sup> In the present chapter we give a more elaborate account of wetting transitions in colloidal systems. We will vary the composition of colloid-polymer mixtures and study the wetting behaviour as a function of the proximity to the critical point and investigate whether there is a wetting transition as predicted by Cahn.<sup>15</sup> We will also vary the interaction of the particles with the substrate by modifying the substrate. Although we will use dynamical experiments to determine contact angles, in the present study we will focus on static wetting behaviour.

## 4.2. Experimental

### 4.2.1. Colloidal system

We prepared colloidal particles by modifying commercially available silica particles (Ludox HS40, Aldrich) with stearylalcohol (pA quality, Aldrich) using the method of Van Helden and Pathmamanoharan.<sup>21, 22</sup> The radius of these particles, dispersed in cyclohexane (pA quality, Aldrich), is  $R_c = 14$  nm (determined by dynamic light scattering). The density of these particles is determined at  $1.63 * 10^3$  kg.m<sup>-3</sup> by weighing 5 ml dispersion, drying the dispersion and weighing the dried particles. The refractive indices of silica and cyclohexane are very similar (1.4588 and 1.4266 respectively), so the Van der Waals attraction between the particles is negligibly small and, in the absence of polymer, the particles behave as hard spheres.<sup>21, 23, 24</sup> Because of the low refractive index differences and the small size of the particles even concentrated suspensions are transparent.

As nonadsorbing polymer, we used polydimethylsiloxane (PDMS, Polymer Sources, inc.) with a number average molecular weight,  $M_N$ , of 83 200 g/mole, corresponding to a radius of gyration,  $R_g = 13$  nm. The heterodispersity index ( $M_W/M_N$  with  $M_W$  the weight average molecular mass) was 1.24. The radius of gyration was determined by extrapolation using the experimental data of Verhaegh, Bodnár, and de Hoog<sup>25–27</sup> and the scaling relation for polymers in a good solvent  $R_g \propto M_N^{0.6}$ .<sup>28</sup> That the latter relation applies for the present polymer solvent combination is confirmed by the experimental

data.

The size ratio for our system  $q = 0.93$ . This is slightly lower than that of Verhaegh, de Hoog and Aarts.<sup>20, 25, 27</sup> The liquid-gas phase behaviour of similar silica/PDMS/cyclohexane systems has been studied extensively.<sup>25-27</sup>

We determined the phase diagram for our system by using the method of Bodnár and Oosterbaan, which requires the phase volumes along at least three different dilution lines (i.e. lines with a constant polymer-colloid concentration ratio) to be measured.<sup>26, 27</sup> Using the mass balance the phase diagram can be constructed. We used four dilution lines to get a higher accuracy.

#### 4.2.2. Wetting experiments

Contact angle measurements on the chosen colloidal liquid-gas system bring their own specific difficulties. One of the reasons is that the capillary length,  $l_c$ , is very small. The capillary length is defined by  $l_c = \sqrt{\gamma_{LG}/\Delta\rho g}$  (where  $\Delta\rho$  is the density difference between the two fluid phases and  $g$  the gravitation constant). It determines the crossover between the regime where gravity dominates the shape of a meniscus and the regime where the interfacial tension dominates that shape. Here  $l_c$  is small ( $O$  tens of  $\mu\text{m}$ ) because  $\gamma_{LG}$  in colloidal systems is very low ( $O \mu\text{N.m}^{-1}$ ), whereas there is still an appreciable density difference. So, the menisci are very small. In typical molecular systems (far from the critical point)  $l_c \sim O$  mm. We observed menisci at fibres with a diameter of about 0.2 mm, which were vertically suspended through the colloidal liquid-gas interface. The other difficulty is that the optical contrast between the two colloidal phases is low, which makes observations with a microscope rather difficult. We performed the wetting experiments using home built viewing optics. The best results were obtained by illuminating the sample with a diffuse parallel light beam through the sample in the direction of objective and CCD Camera (Pulnix). The light beam was made parallel with the help of a negative lens ( $f = -5.0$  mm,  $\emptyset = 5.0$  mm) and a positive lens ( $f = 70.0$  mm,  $\emptyset = 60$  mm). A diffuse filter and a diaphragm were placed between the positive lens and the sample. The objective (Melles Griot) has a long working distance and a magnification of 15.75.

To determine dynamic contact angles, the fibre was moved through the interface at different velocities by means of an electronically controlled actuator (Newport). This actuator can move a plastic spring to which the fibre is attached. By moving the fibre downwards the liquid advances over the substrate and by moving the fibre upwards the liquid recedes from the substrate. The fibre was moved into or out of the interface with velocities in the range of 0 to 15  $\mu\text{m.s}^{-1}$ . For each velocity, an image was captured 25 seconds after the beginning of the movement. At this time a steady state was reached. After each experiment we waited until the system was completely relaxed before starting a next measurement at another velocity. From the response of the meniscus to the

movement of the fibre we could distinguish the meniscus from its mirror image. Static contact angles were determined by interpolating the cosine of the contact angle to zero velocity. That such an interpolation is justified will be explained in the results section.

### 4.2.3. Substrates

In this subsection the preparation of the substrates is described. We examined two distinctly different substrates. One might be denoted *hard* substrate and the other *soft* substrate. The surface of a stearylated glass fibre should be similar to that of the colloidal particles and has only hard repulsion and depletion attraction with the particles. These are the hard fibres.

In order to prepare these, glass fibres were cleaned by ultrasonating them for 30 min in ethanol (96%) and putting them in a plasma cleaner (Harrick PDC-32G) for 10 min at high RF level. The fibres were then stored for at least 24 h in clean ethanol (96%). This was done because we have indications that siloxane groups on the surface have to rehydrolyse after the plasma treatment. The fibres were coated with stearyl alcohol by heating them for four hours in a melt of stearyl alcohol at 180°C. After the heating procedure, the excess stearyl alcohol was removed from the fibres by storing the samples in chloroform. After at least 24 hours the fibres were stored in clean chloroform, before using them in experiments.

A second series of fibres were modified by grafting with PDMS (Aldrich  $M_N = 31300$  and  $M_W/M_N = 3.0$ ). To this end, they were heated, after the cleaning step, for 30 min at 70°C in a melt of PDMS. After the heating procedure excess PDMS was removed by storing the fibres in cyclohexane. After 24 hours the fibres were stored in clean cyclohexane. These fibres are denoted as *soft fibres*. That PDMS is attached to the glass can be deduced from the observations that the contact angle of water is significantly larger on a PDMS treated surface than on unmodified glass. It is likely that grafted PDMS forms a fluffy polymer layer in cyclohexane with a distribution of loops and tails, but the structure is presently unknown. So far the properties of PDMS treated glass have not been characterized in detail.

## 4.3. Results and discussion

In figure 4.1, the phase diagram of our silica/PDMS/cyclohexane system as described in section 4.2.1 is presented. Here the polymer packing fraction,  $\varphi_{pol}$  is plotted versus the colloid volume fraction,  $\varphi_{coll}$ . The polymer packing fraction is scaled to the overlap concentration,  $\varphi_{pol} = c/c^*$  with  $c$  the weight concentration and  $c^*$  its value at overlap. The overlap concentration is calculated by  $c^* = M_N / (\frac{4}{3}\pi R_g^3 N_{Av})$ , with  $N_{Av}$  Avogadro's number. Some tielines connecting coexisting binodal points are drawn. The critical point is determined by extrapolating the middles of the tielines to the binodal. Our

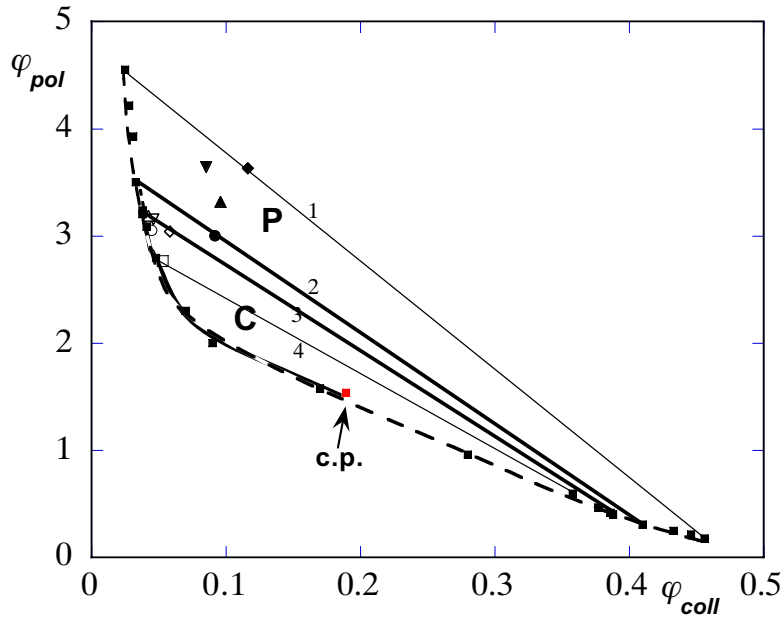


FIGURE 4.1. Phase diagram of the silica/PDMS/cyclohexane system. The polymer concentration,  $\varphi_{pol}$  is plotted versus the volume fraction colloid  $\varphi_{coll}$ . The binodal points are denoted with solid squares and the critical point is indicated with c.p. The binodal is represented by the dashed curve. At the tielines (solid lines), indicated by 1, 2, 3 and 4, the polymer reservoir concentrations are 5.5, 4.5, 4.3, and 4.1, respectively. The overall compositions of the samples, used in the wetting experiments, are given by A ( $\blacklozenge$ ), B ( $\blacktriangledown$ ), C ( $\blacktriangle$ ), D ( $\bullet$ ), E ( $\diamond$ ), F ( $\nabla$ ), G ( $\triangle$ ), H ( $\circ$ ), J ( $\square$ ). Points E and G are on the same tieline (have the same polymer chemical potential). The complete and partial wetting regimes are indicated by C and P, respectively.

phase diagram is very similar to that of de Hoog *et al.* who used a slightly larger polymer.<sup>27</sup> The binodal is only slightly tilted compared to that of de Hoog. In the phase diagram we plotted also the compositions of the samples (A-J) that were used in the wetting experiments.

In figures 4.2 and 4.3 we present some typical images of menisci at the hard and soft fibre for a colloid-polymer composition relatively far from the critical point (sample A, see figure 4.1). Similar menisci are also observed by Aarts *et al.* for a planar surface.<sup>20</sup> In both pictures the colloidal gas and liquid phases are separated by a horizontal interface; the upper phase is the colloidal gas and the lower phase the colloidal liquid. The flat interface itself cannot be seen in these images, but its position can be deduced by means of the mirror images it produces. However, with the naked eye the interface between the colloidal liquid and gas phase is well visible and very sharp. Near the fibre we can clearly distinguish the curved part of the meniscus as well as its mirror image. The meniscus can be distinguished from its mirror image by the response to downward

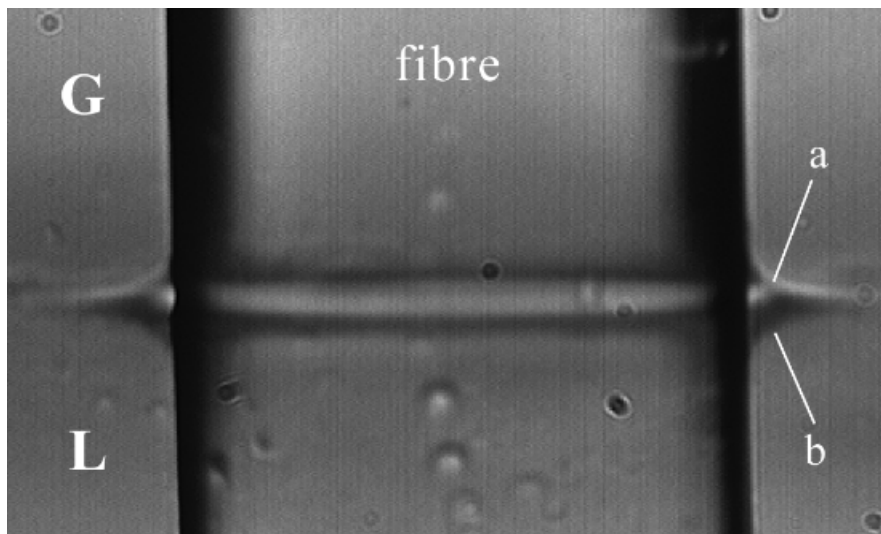


FIGURE 4.2. Image of a meniscus at a hard fibre suspended in a colloidal liquid-gas system (sample A). The capital **G** and **L** represent the colloidal liquid and the colloidal gas phase respectively. The meniscus and its mirror image are indicated by **a** and **b**, respectively.

or upward movements of the fibre in dynamic experiments. More detailed observation of the meniscus shows that there is a bright edge at the meniscus which is not visible at the mirror image. At the hard fibre the meniscus curves upward for all cases that were examined, while at the soft fibre it curves downward. This implies that the static contact angle is smaller than  $90^\circ$  at the hard fibre and larger than  $90^\circ$  at the soft fibre. This holds for all compositions indicated in figure 4.1.

The fact that the static contact angles at the hard fibre are all smaller than  $90^\circ$  implies that the substrate prefers the liquid phase over the gas phase, whereas at the soft fibres the opposite is true. These qualitative observations can be understood by comparing the interactions between two particles with that between a particle and the substrate. Because the radius of curvature of the fibre is much larger than that of a particle, the fibre can be regarded as a flat substrate. The depletion interaction free energy is proportional to the overlap volume of the depletion zones.<sup>2,3</sup> The overlap volume of the depletion zones of a spherical particle and a flat hard substrate is larger than that of two spherical particles at the same distance, see figure 4.4. Hence, the attraction between a particle and the substrate is stronger than that between two particles. In the colloidal liquid phase there are many more particles than in the colloidal gas phase, so the substrate attracts the colloidal liquid phase much more strongly than the colloidal gas phase. Therefore, a contact angle smaller than  $90^\circ$  is expected at a hard substrate, in agreement with our measurements.

If we attach a fluffy polymer layer at the surface, the depletion attraction is counteracted by a repulsive steric contribution. Such moderated depletion interaction involving



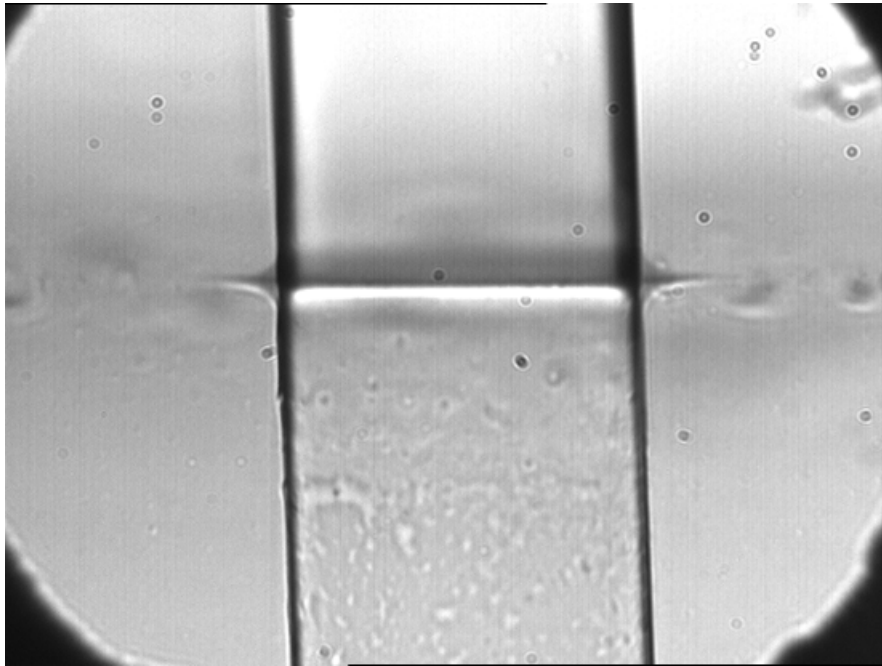


FIGURE 4.3. Image of a meniscus at a soft fibre suspended in a colloidal liquid-gas system (sample A).

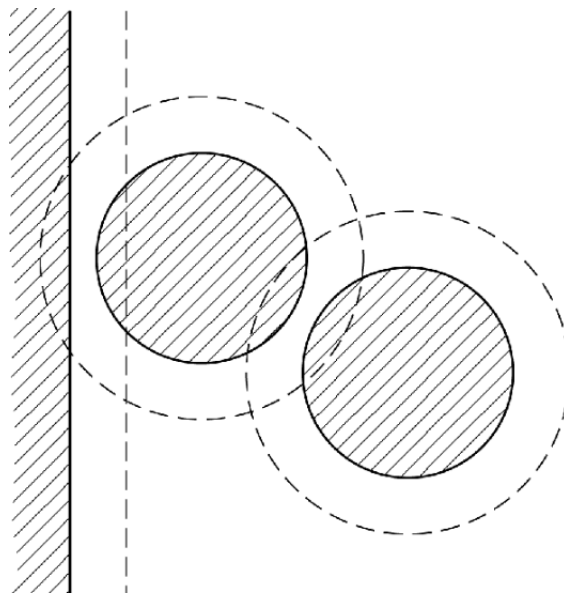


FIGURE 4.4. Overlap of depletion zones of 2 particles and of a particle and a wall.

a polymer coated surface is called soft depletion.<sup>29-32</sup> It is expected that it will lead to a larger contact angle. We find that the contact angle at the soft fibre is larger than  $90^\circ$  for all colloid-polymer compositions that were examined (figure 4.1). The substrate prefers the gas phase over the liquid phase.

Let us now consider the images of sample A (deep in the two phase coexistence region) and J (closer to the critical point) at the hard fibre more carefully. These images are

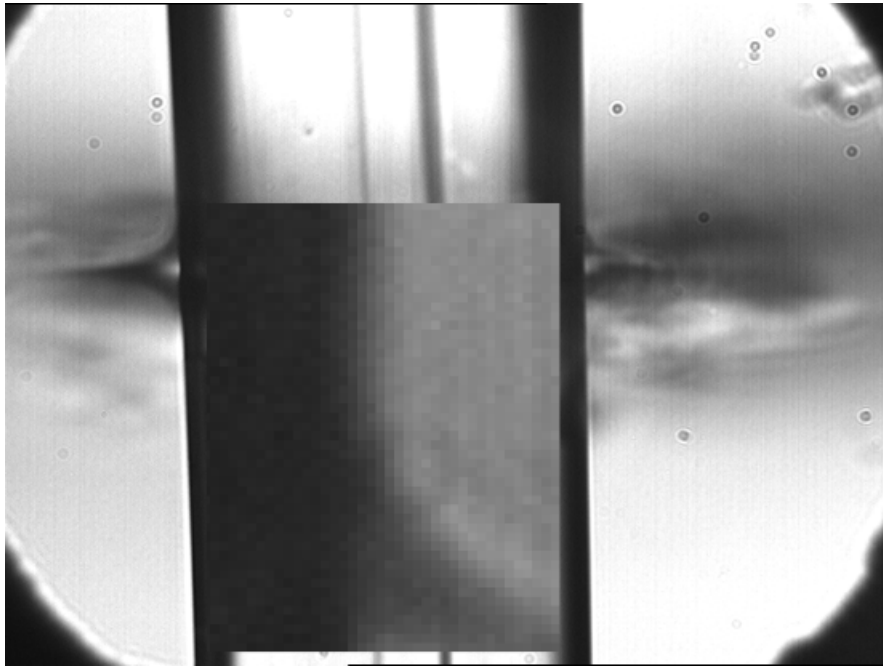


FIGURE 4.5. Image of a static meniscus at a hard fibre suspended in a colloidal liquid-gas system (sample J). The inset represents the profile very close to the fibre.

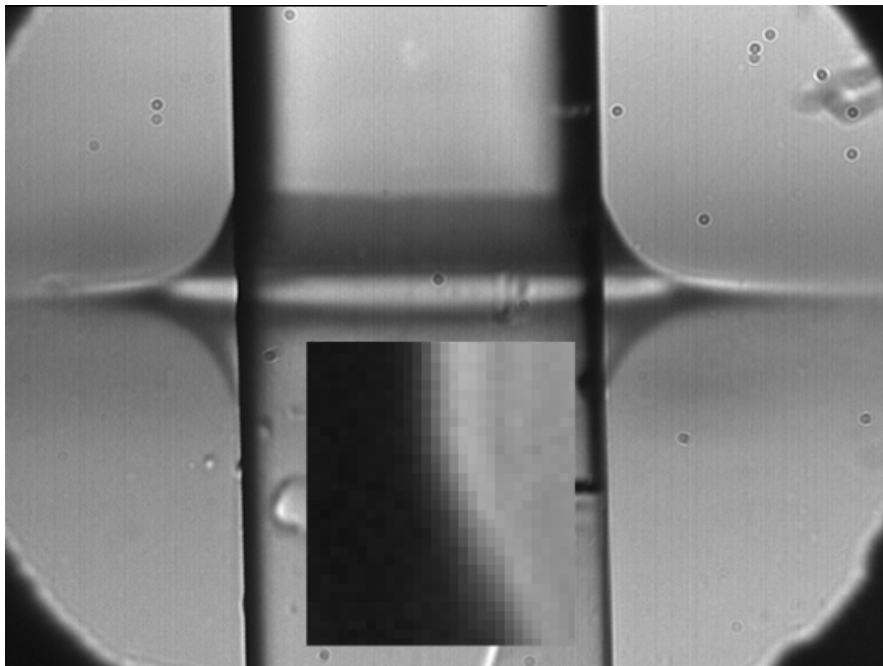


FIGURE 4.6. Image of a steady state meniscus at an upward moving hard fibre suspended in a colloidal liquid-gas system  $v = 2.5 \mu\text{m}\cdot\text{s}^{-1}$  (sample A). The inset represents the profile very close to the fibre.

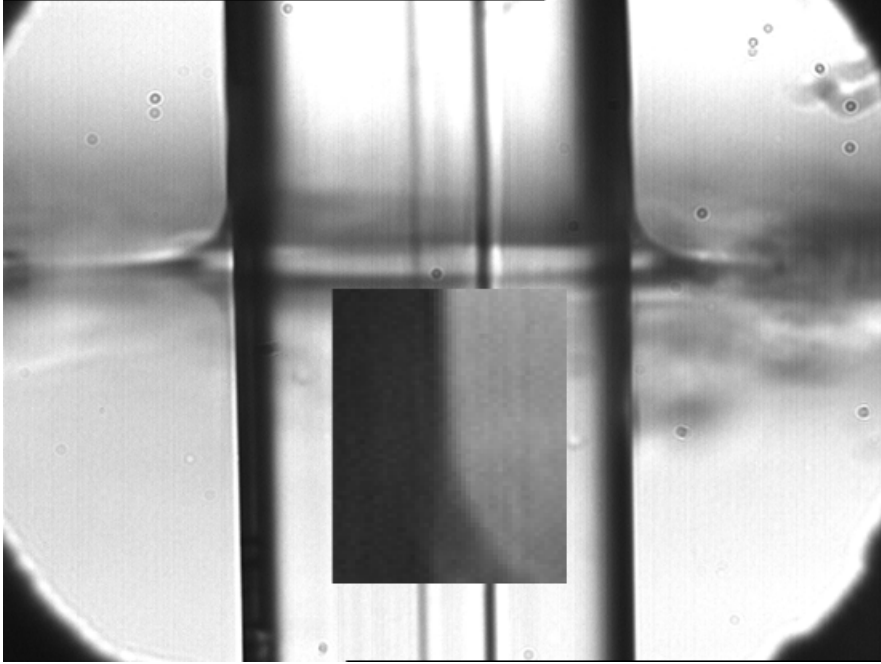


FIGURE 4.7. Image of a steady state meniscus at an upward moving hard fibre suspended in a colloidal liquid-gas system  $v = 2.5 \mu\text{m.s}^{-1}$  (sample J). The inset represents the profile very close to the fibre.

presented in figures 4.2 and 4.5, respectively. It is hard to distinguish the differences between the profiles because the contours are somewhat fuzzy. For this reason it was not possible to fit the contour to a solution of the Laplace equation in combination with hydrostatics.<sup>33</sup> In the inset of figure 4.5 the magnified part of the meniscus very near to the fibre is shown. We see that the meniscus approaches the fibre smoothly, this suggests that this is a case of complete wetting. For figure 4.2 it is hard to study the profile close to the fibre because of fuzziness. If we observe the steady state pictures of these samples at an upward speed of the fibre of  $2.5 \mu\text{m.s}^{-1}$ , we see that the menisci are enlarged. These menisci are presented in figures 4.6 and 4.7. The contour is because of the enlargement sharper and better visible. This large change of the meniscus upon movement of the fibre indicates that hydrodynamic forces influences not only the dynamic contact angle, but also the whole profile of the meniscus. Therefore these contours cannot be fitted to the Laplace equation. In the insets we see that the meniscus of sample A (figure 4.6) approaches the fibre with a finite (non-zero) contact angle, whereas the meniscus of sample J approaches the fibre smoothly. These observations indicate that sample A is a case of partial wetting, whereas sample J is a case of complete wetting. Furthermore, in figure 4.6 we see clearly an edge at the three phase contact line, which is not present at figure 4.7. This confirms the fact that sample A is a case of partial wetting and sample J a case of complete wetting.

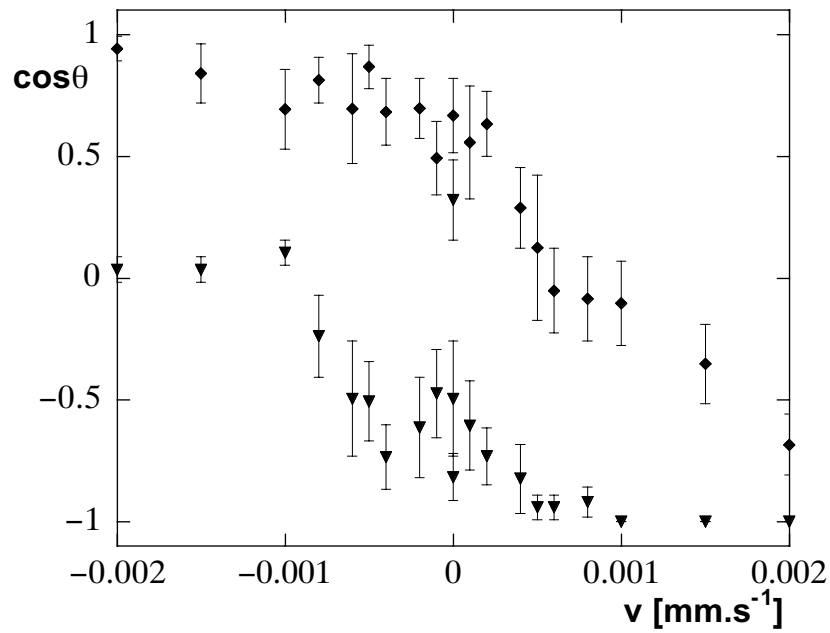


FIGURE 4.8. Cosine of the dynamic contact angle of sample A at the substrates as a function of the velocity of the substrate with respect to the colloidal liquid-gas interface. The  $\blacklozenge$  are at the hard substrate and  $\blacktriangledown$  at the soft substrate. A positive velocity corresponds to an advancing contact angle and a negative to a receding contact angle.

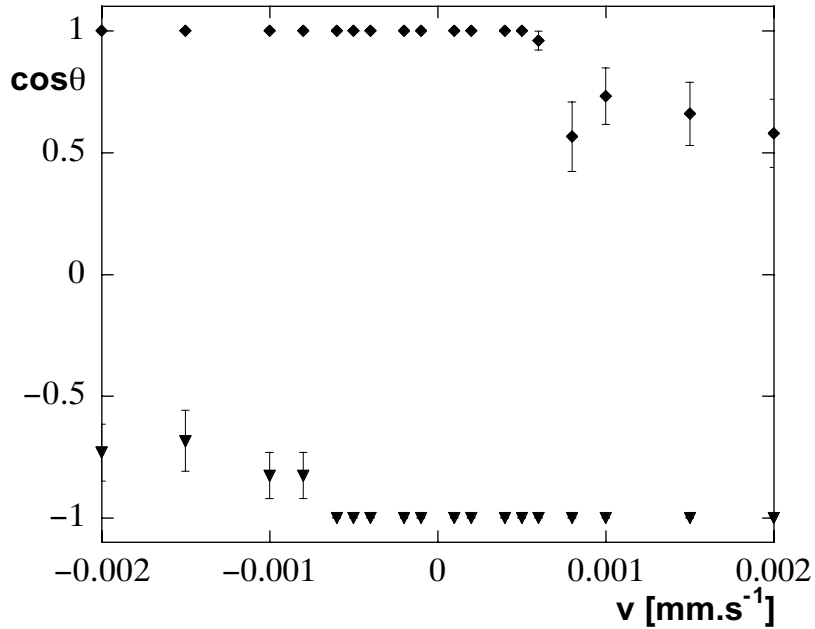


FIGURE 4.9. Cosine of the dynamic contact angle of sample J at the substrate as a function of the velocity of the substrate with respect to the colloidal liquid-gas interface. The  $\blacklozenge$  are at the hard substrate and  $\blacktriangledown$  at the soft substrate.

Given the limited accuracy of single static images the static contact angle was determined by interpolation from dynamic contact angles. In figure 4.8  $\cos \theta$  is plotted as a function of the velocity for sample A for both substrates. For sample J similar data are plotted in figure 4.9. All contact angles were determined by drawing tangents to the liquid-gas interfaces in the three phase points. This leads to an error of about  $10^\circ$  in the data (see error bars). From the plots it appears that the static advancing and the static receding contact angles are the same, within the error of the experiment. This implies that hysteresis, if any, is smaller than the scatter in the data. The apparent absence of hysteresis may be explained by the fact that colloidal particles are presumably large compared to the typical length scale of the roughness or heterogeneity of the surface. Therefore, such roughness seems to play a minor role in colloidal systems in contrast to what is usually seen for molecular systems. Because of the absence of notable hysteresis, it is justified to determine the static contact angle by interpolation between positive and negative velocities. Also in these  $\cos \theta$  versus velocity curves, we see for sample A that the static contact angle has a finite value at zero velocity, whereas for sample J this contact angle is  $0^\circ$  ( $\cos \theta_0 = 1$ ). This confirms our qualitative conclusion from the images that, for the hard fibre, sample A is a case of partial wetting, and sample J of complete wetting. At the soft fibre we observe for sample J complete drying and for sample A partial wetting (figures 4.8 and 4.9). So, between these compositions, there must be a transition between partial and complete wetting at the hard fibre and a transition between partial wetting and complete drying at the soft fibre. Static contact angles are measured as described above for all samples A-J indicated in figure 4.1. In this way we were able to narrow down the interval at which the wetting transition occurs. For the samples A-D we see partial wetting at both substrates. For the samples E-J we observed complete wetting for the hard substrate and complete drying for the soft substrate. In figure 4.1 the complete wetting regime was indicated by the capital C, whereas the capital P corresponds to the partial wetting regime. The wetting transitions occur in between the thick tielines, indicated by 2 and 3, in figure 4.1. The observation of these wetting transitions is the central result of this chapter. In view of the Cahn argument we want to present these data as a function of a (reduced) field variable which measures the proximity to the critical point. In ordinary molecular systems the temperature is the field variable which affects the phase behaviour. In colloid-polymer mixtures the polymer reservoir packing fraction,  $\varphi_{pol}^r$ , is related to the relevant field variable. This quantity plays a role similar to the inverse temperature in molecular systems.<sup>1, 4-6, 8, 9</sup> In theoretical and simulation studies the phase behaviour of colloid-polymer mixtures is often presented in terms of  $\varphi_{pol}^r$ . However, this quantity is not experimentally accessible. In order to be able to make some comparison with theoretical predictions,<sup>8, 9, 11</sup> we have estimated  $\varphi_{pol}^r$  by correcting the actual polymer packing fraction ( $\varphi_{pol}$ ) in the gas phase for the volume of the colloidal particles with

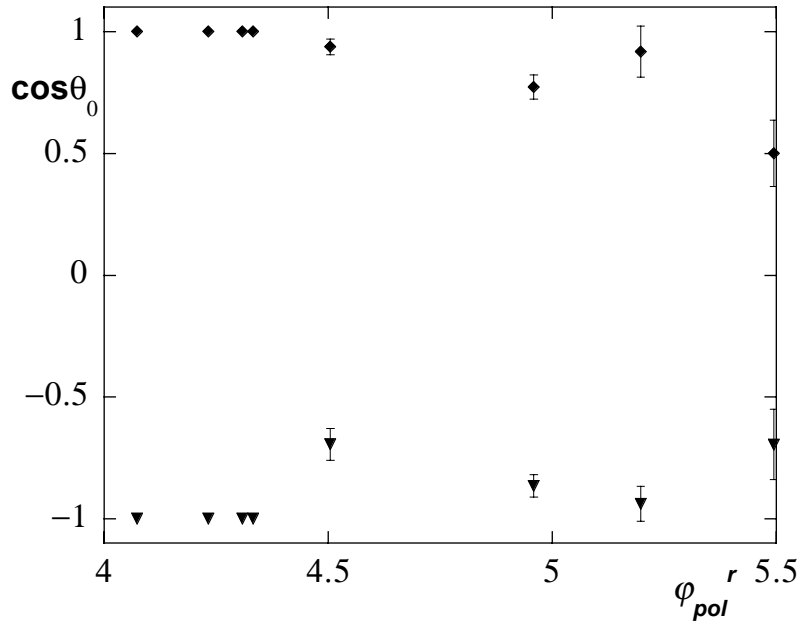


FIGURE 4.10. Cosine of the static contact angle as a function of  $\varphi_{pol}^r$  at the hard substrate ( $\blacklozenge$ ) and at the soft substrate ( $\blacktriangledown$ ).

their depletion zones by means of scaled particle theory.<sup>5, 6</sup> In this estimation, variation of the depletion zone thickness with polymer concentration and particle radius is neglected. A plot of  $\cos \theta_0$  as a function of  $\varphi_{pol}^r$ , estimated in this way, is shown in figure 4.10. The error in  $\cos \theta_0$  was estimated by taking the root of the average of the squared deviations from the  $\cos \theta$ -velocity plots. From figure 4.10 it can be concluded that upon approaching the critical point for both substrates wetting transitions occur in the range  $4.3 < \varphi_{pol}^r < 4.5$ . However, near the critical point the polymer reservoir concentration cannot be calculated neither by scaled particle theory nor by other theories. So, for our experimental results  $\varphi_{pol}^r$  cannot be used as a measure for the proximity to the critical point. Furthermore, this way to determine the polymer reservoir packing fraction is based on several assumptions.

As an alternative we will use the difference in colloid volume fraction between the liquid and the gas phase ( $\Delta\varphi_{coll} = \varphi_{coll,l} - \varphi_{coll,g}$ ) to quantify the proximity to the critical point. This quantity can be unambiguously calculated from the experimental data for each composition within the two-phase region, since the tielines are known. Moreover, we know that  $\Delta\varphi_{coll}$  vanishes in the critical point. It is known that near the critical point for most simple molecular systems  $\Delta\varphi \sim (T - T_c)^{0.313}$ , where  $T$  is the temperature and  $T_c$  its value in the critical point.<sup>34</sup> If we assume that this critical exponent is also valid for all samples in our system, then  $(\Delta\varphi_{coll})^{1/0.313}$  would be a quantity proportional to the relevant field variable, at least close to the critical point, and is a suitable measure for the distance to the critical point. In figure 4.11 we plot the data accordingly and see that in the interval  $0.034 < (\Delta\varphi_{coll})^{1/0.313} < 0.044$  ( $0.35 < \Delta\varphi_{coll} < 0.38$ )  $\cos \theta_0$

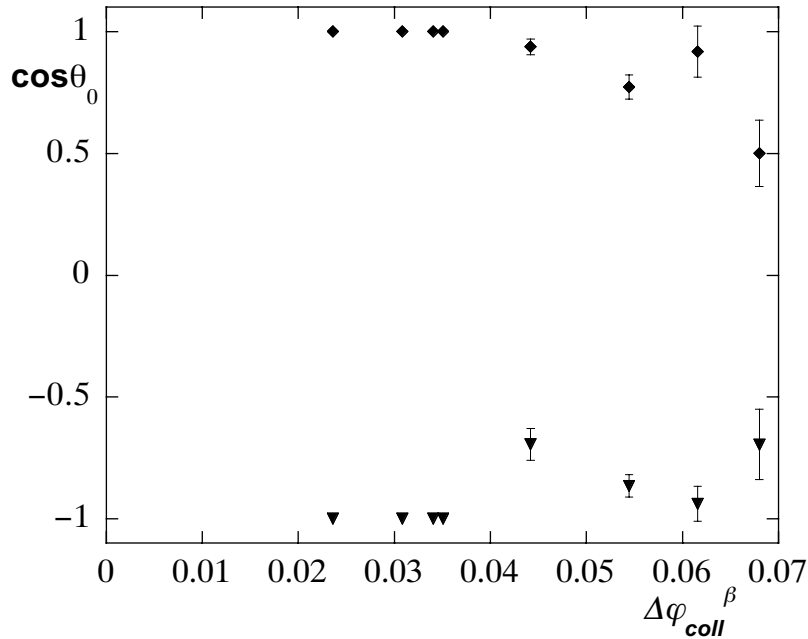


FIGURE 4.11. Cosine of the static contact angle as a function of  $\Delta\varphi_{coll}^\beta$  with  $\beta = 1/0.313$  at the hard substrate ( $\blacklozenge$ ) and at the soft substrate ( $\blacktriangledown$ ).

changes between plus unity and a smaller value at the hard fibre, and between minus unity and a higher value at the soft fibre. In other words, both the transition from partial to complete wetting at the hard fibre, and that from partial wetting to complete drying at the soft fibre occur in this interval. The occurrence of these wetting transitions is in agreement with the qualitative prediction by Cahn.<sup>15</sup> Between the critical point and the wetting transition point, the hard fibre is completely wet by the colloidal liquid phase, whereas the soft fibre is completely wet by the colloidal gas phase. The fact that both wetting transitions occur in the same range of  $\Delta\varphi_{coll}$  is probably a coincidence. The position of the wetting transition must depend on surface properties, like the PDMS grafting density. So far, this has not been systematically investigated. The scatter in  $\cos\theta_0$  at the soft fibre is larger than at the hard fibre. This is probably due to the fact that the treatment of the surface with PDMS is not as reproducible as that is with stearyl alcohol. The accuracy of our experimental data is not sufficient to decide whether the wetting transition is first or second order. It seems to be either second order or weakly first order.

We can compare our results quantitatively with predictions from Monte Carlo simulations and density functional theory calculations for similar systems by Dijkstra *et al.* and Brader *et al.*, respectively.<sup>8,9</sup> In these papers the location of a wetting transition is calculated for a hard wall and  $q = 1$  and  $q = 0.6$ , respectively. In figure 4.12 the phase diagram and the wetting transitions from the Monte Carlo simulations, from

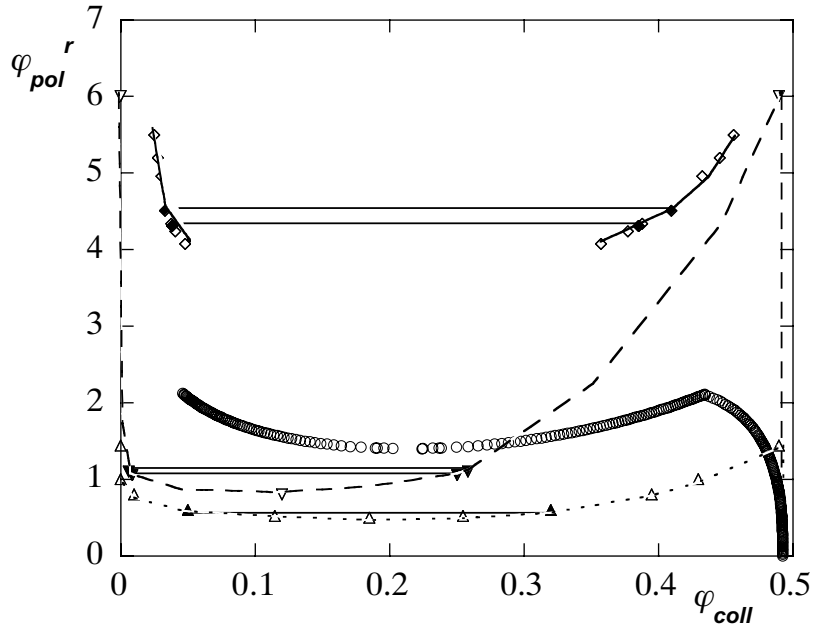


FIGURE 4.12. Wetting transitions in the phase diagram for Monte Carlo simulations ( $\nabla$ , dashed curve<sup>8</sup>), density functional calculations ( $\triangle$ , dotted curve<sup>9</sup>), and our experiments ( $\diamond$ , solid curve). The locations of the wetting transitions are represented by the solid symbols. The calculations of Aarts are given by  $\circ$ .<sup>11</sup> Parameters and conditions for each set of data are discussed in the text.

the density functional theory calculations and our experimental results (for which  $\varphi_{pol}^r$ -values were calculated as described above) are plotted together. The liquid-gas binodals are plotted in the  $\varphi_{pol}^r - \varphi_{coll}$ -representation. The simulated and calculated two phase coexistence regions are at significantly lower  $\varphi_{pol}^r$  values than our experimental one. These differences may be due to the fact that in the simulations and calculations the polymers are taken to be ideal, whereas in our system the polymers are swollen and do not behave ideally. For real polymers, around the overlap concentration, the range of the depletion interaction starts to decrease with increasing concentration of polymer. On the other hand, the osmotic pressure, which determines the strength of the attractive force, increases more strongly with concentration than predicted by Van't Hoff's law. It turns out that neglecting these effects leads to an over-estimation of the tendency for phase separation: in real systems the binodal is found at much higher values of  $\varphi_{pol}$  (or  $\varphi_{pol}^r$ ) than is predicted by the ideal polymer model. Recent calculations by Aarts *et al.*, taking non-ideality into account, lead to better, although not perfect, agreement with experiments.<sup>11</sup> This binodal is also plotted in figure 4.12. The fact that the experimental binodal is found at higher polymer concentrations than predicted by Aarts *et al.* is explained by the fact that the segment-substrate interaction is non zero for our system, see chapter 2 of this thesis. It is not meaningful to compare the  $\varphi_{pol}^r$ -values at which the wetting transitions occur, because the binodals are



significantly different. It was found that the wetting transition occurs somewhere in the regime  $0.011 < (\Delta\varphi_{coll})^{1/0.313} < 0.012$  and at  $(\Delta\varphi_{coll})^{1/0.313} = 0.015$  for the simulations and the calculations, respectively. These values are also significantly lower than our results. Brader and Dijkstra observed three layering transitions in the partial wetting regime prior to the transition to complete wetting. These layering transitions cannot be determined experimentally by our method.

#### 4.4. Conclusions

We have demonstrated that wetting phenomena can be experimentally investigated in colloidal systems exhibiting gas-liquid phase behaviour, by independently manipulating the particle-particle interaction and the particle-substrate interaction. The beauty of these systems is that one can effectively eliminate Van der Waals forces and replace them with weak attractive interaction of controllable range and strength. This opens up many perspectives for studying the relation between wetting phenomena and the underlying interactions. We observed menisci at fibres far from the critical point and close to criticality, and observed the well known Cahn transition.<sup>15</sup> The adjustment of particle-substrate interactions, being an essential element in such studies, was shown to be possible by means of polymer chains grafted to the substrate. Again, such interactions can be tuned by a judicious choice of chain length and grafting density of the polymer, for which adequate methods are available.<sup>29-32</sup> We have shown that Cahn wetting transitions are present at both a hard and a soft substrate. At the hard substrate, we see a transition from partial to complete wetting. At the soft substrate, we see a transition from partial wetting to complete drying.

## References

- [1] Poon, W. C. K.; Pusey, P. N.; Lekkerkerker, H. N. W. *Physics World* **1996**, *9*, 27-32.
- [2] Asakura, S.; Oosawa, F. *J. Chem. Phys.* **1954**, *22*, 1255.
- [3] Vrij, A. *Pure Appl. Chem.* **1976**, *48*, 471.
- [4] Vincent, B.; Edwards, J.; Emmet, S.; Croot, R. *Colloids Surf.* **1988**, *31*, 267-298.
- [5] Ilett, S. M.; Poon, W. C. K.; Pusey, P. N. *Phys. Rev. E* **1995**, *51*, 1344-1352.
- [6] Lekkerkerker, H. N. W.; Poon, W. C. K.; Pusey, P. N.; Stroobants, A.; Warren, P. B. *Europhys. Letters* **1992**, *20*, 559-564.
- [7] Poon, W. C. K. *J. Phys.: Condens. Matter* **2002**, *14*, R859-R880.
- [8] Dijkstra, M.; van Roij, R. *Phys. Rev. Lett.* **2002**, *89*, 208303-1.
- [9] Brader, J.; Evans, R.; Schmidt, M.; Löwen, H. *J. Phys.: Condens. Matter* **2002**, *14*, L1-L8.
- [10] Wijting, W. K.; Besseling, N. A. M.; Cohen Stuart, M. A. *Phys. Rev. Lett.* **2003**, *90*, 196101.
- [11] Aarts, D. G. A. L.; Tuinier, R.; Lekkerkerker, H. N. W. *J. Phys.: Condens. Matter* **2002**, *14*, 7551-7561.
- [12] Young, T. *Philos. Trans. R. Soc.* **1805**, *95*, 69.
- [13] Dietrich, S. *Phase Transitions and critical Phenomena*; Academic Press, London: 1988.

- [14] Schick, M. *Introduction to wetting phenomena*; Elsevier Science Publishers B.V.: 1990.
- [15] Cahn, J. W. *J. Chem. Phys.* **1977**, *66*, 3667.
- [16] Bonn, D.; Ross, D. *Reports on Progress in Physics* **2001**, *64*, 1085.
- [17] Ross, D.; Bonn, D.; Posazhennikova, A. I.; Indekeu, J. O.; Meunier, J. *Phys. Rev. Lett.* **2001**, *87*, 176103.
- [18] de Gennes, P. G. *Rev. Mod. Phys.* **1985**, *57*, 827.
- [19] Bonn, D.; Bertrand, E.; Shahidzadeh, N.; Ragil, K.; Posazhennikova, A. I.; Broseta, D.; Meunier, J.; Indekeu, J. O. *J. Phys.: Condens. Matter* **2001**, *13*, 4903-4914.
- [20] Aarts, D. G. A. L.; van der Wiel, J. H.; Lekkerkerker, H. N. W. *J. Phys.: Condens. Matter* **2003**, *15*, S245-S250.
- [21] van Helden, A. K.; Jansen, J. W.; Vrij, A. *J. Colloid Interface Sci.* **1981**, *81*, 354.
- [22] Pathmamanoharan, C.; Philipse, A. P. *J. Colloid Interface Sci.* **1994**, *165*, 519-521.
- [23] Lyklema, J. *Fundamentals of Interface and Colloid Science I*; Academic Press, London: 1991.
- [24] Kops-Werkhoven, M. M.; Fijnaut, H. M. *J. Chem. Phys.* **1981**, *74*, 1618.
- [25] Verhaegh, N. A. M.; van Duijneveldt, J. S.; Dhont, J. K. G.; Lekkerkerker, H. N. W. *Physica A* **1996**, *230*, 409.
- [26] Bodnár, I.; Oosterbaan, W. D. *J. Chem. Phys.* **1997**, *106*, 7777-7780.
- [27] de Hoog, E. H. A.; Lekkerkerker, H. N. W. *J. Phys. Chem. B* **1999**, *103*, 5274-5279.
- [28] Fleer, G. J.; Cohen Stuart, M. A.; Scheutjens, J. M. H. M.; Cosgrove, T.; Vincent, B. *Polymers at Interfaces*; Chapman & Hall, London Glasgow New York Tokyo Melbourne Madras: 1993.
- [29] van Lent, B.; Israels, R.; Scheutjens, J. M. H. M.; Fleer, G. J. *J. Colloid Interface Sci.* **1990**, *137*, 380.
- [30] Cosgrove, T.; Heath, T.; van Lent, B.; Leermakers, F. A. M.; Scheutjens, J. M. H. M. *Macromolecules* **1987**, *20*, 1697.
- [31] Vincent, B.; Edwards, J.; Emmet, S.; Jones, A. A. *Colloids Surf.* **1986**, *18*, 261.
- [32] Jones, A.; Vincent, B. *Colloids Surf.* **1989**, *42*, 113.
- [33] Hartland, S.; Hartley, R. W. *Axisymmetric fluid-liquid interfaces*; Elsevier Amsterdam Oxford New York: 1976.
- [34] Chandler, D. *Introduction to modern statistical mechanics*; Oxford University Press, New York Oxford: 1987.

# Summary and Outlook

## Summary

In this last chapter I will review and integrate the findings of the previous chapters and give suggestions for further research on this topic.

In chapter 2 measurements of depletion interactions by means of colloidal probe atomic force microscopy (CP-AFM) are described. We found that the behaviour of the range of the depletion interaction is roughly in agreement with predictions of Flerer *et al.*<sup>1</sup> The strength of the depletion interaction is not in agreement with predictions of Tuinier *et al.*<sup>2</sup> and Louis<sup>3</sup> and Bolhuis.<sup>4</sup> It is much smaller. We explain this by the fact that the segment-surface interaction for polydimethylsiloxane (PDMS) and a stearylated silica surface is non zero. Comparison of our experimental values with values obtained by Scheutjens Flerer Self Consistent Field theory for different values of  $\chi_S$  leads to a reduced segment surface interaction parameter of 0.41. This corresponds to a decrease to about one order of magnitude of the maximal depletion interaction (see figure 2.13). This strong weakening is in agreement with experimental findings that significantly more PDMS is needed to reach the colloidal liquid-gas binodal than predicted, even if non ideality of the polymers is taken into account.<sup>5, 6</sup>

In chapter 3 we present observations of wetting phenomena in depletion interaction driven, phase-separated colloidal dispersions. These dispersions consist of stearyl coated silica spheres in cyclohexane with PDMS as non-adsorbing polymer. The dynamic contact angle was determined by moving a thin fibre upward or downward through the colloidal liquid gas interface and drawing tangents to the meniscus at the fibre in the three phase contact line. The dynamic contact angle was measured as a function of the velocity of the fibre. From these dynamic contact angles the static contact angle was determined by interpolation to zero velocity. We observed no noticeable hysteresis. The contact angle of the colloidal liquid-gas interface at a solid substrate (coated glass) was determined for a series of compositions. We were able to locate a Cahn wetting transition<sup>7</sup> from partial to complete wetting upon approaching the critical point. By this we have tested successfully the well known Cahn prediction regarding wetting transitions for colloid-polymer mixtures.

In the same way we determined the contact angle of the colloidal liquid-gas interface at a soft solid substrate for a series of compositions. A soft solid substrate was obtained by heating a glass fibre in a melt of PDMS. In this way we manipulated the colloidal particle-substrate interaction. Upon approach to the critical point, a transition occurs

from partial to complete drying. The region where the wetting transition occurs was compared with that of density functional calculations of Brader *et al.* and Monte Carlo simulations of Dijkstra *et al.*<sup>8,9</sup>

## Outlook

In our experiments it was very hard to determine the contour of the meniscus because the optical contrast between the colloidal liquid and gas phase is very low. For further investigations it would be preferable that this optical contrast will be optimized. An option is to use fluorescent labelled particles. The advantage of using fluorescent particles is that these particles will be highlighted by confocal scanning laser microscopy. Since in the colloidal liquid phase there are many more particles than in the colloidal gas phase, the liquid phase is highlighted, whereas the gas phase is dark. The contrast between the highlighted phase and the dark phase is so sharp that the meniscus is well defined. Aarts *et al.* studied the wetting behaviour of a system of fluorescent labelled polymethylmethacrylate (PMMA) particles dispersed in decaline with polystyrene as non-adsorbing polymer.

The use of a vertically suspended fibre is very nice, because if in focus, one is sure that the plane of observation is perpendicular to the fibre. If one uses a flat plate it would be probable that the plate is tilted a little. In that case the plane of observation is not perpendicular to the plate.

We determined the static contact angle near a vertically suspended fibre by means of an interpolation of dynamic contact angles. From these contact angle versus velocity curves we concluded that hysteresis is negligible. The data obtained from the measurements of the contact angle as a function of the velocity were accurate enough to determine a static contact angle but not to investigate the dynamic wetting behaviour. It would be preferable to investigate the dynamic wetting behaviour with a higher accuracy.

We investigated the depletion interaction by means of a standard atomic force microscope. It would be preferable to measure the same samples by means of a picroforce apparatus. Furthermore the depletion interaction between a silica coated sphere and a PDMS-coated surface in the presence of PDMS dissolved in cyclohexane is an interesting system to investigate. Analogously to the wetting behaviour, reported in chapter 4, we expect that the depletion effect vanishes because of the polymer coating.

Our results indicate that the depletion effect is not maximal for the investigated system. As mentioned in chapter 2 the segment-surface interaction is non-zero. It would be probable that this interaction is tunable by changing the solvent properties. If a co-solvent or displacer is added to the solvent the polymer may be displaced by the co-solvent. This results in a weaker segment-surface interaction and hence, in a stronger depletion

interaction. Suitable displacers for PDMS in cyclohexane may be dimethylpentane or tetramethylsilane. These molecules might have a higher affinity to the stearylated surface than PDMS because of a high number of methyl groups.

If the depletion interaction is stronger than in the measured system, it would be probable that the wetting behaviour is different. A stronger particle-wall interaction may result in a wetting transition at higher polymer reservoir concentrations. It would be possible that the wetting transition vanishes and that there is only a complete wetting regime.

## References

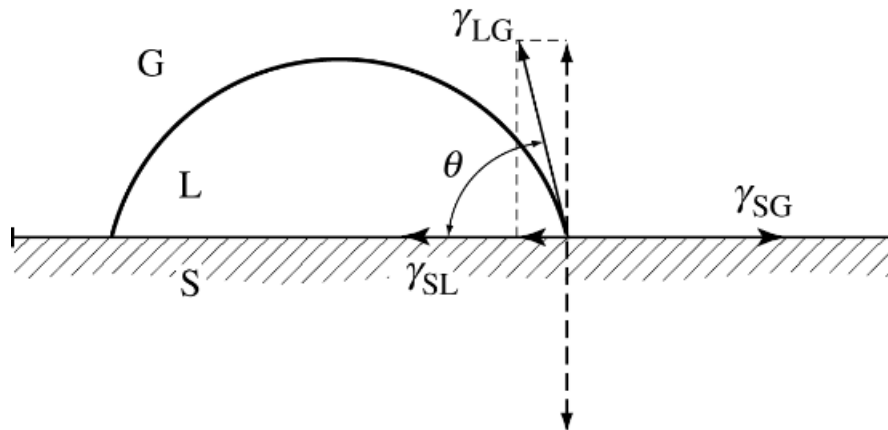
- [1] Fleer, G. J.; Skvortsov, A. M.; Tuinier, R. *Macromolecules* **2003**, *36*, 7857.
- [2] Tuinier, R.; Aarts, D. G. A. L.; Wensink, H. H.; Lekkerkerker, H. N. W. *Phys. Chem. Chem. Phys.* **2003**, *5*, 3707-3715.
- [3] Louis, A. A.; Bolhuis, P.; Meijer, E. J.; Hansen, J. P. *J. Chem. Phys.* **2002**, *117*, 1893.
- [4] Bolhuis, P.; Louis, A. A.; Hansen, J. P.; Meijer, E. J. *J. Chem. Phys.* **2001**, *114*, 4296.
- [5] Aarts, D. G. A. L.; Tuinier, R.; Lekkerkerker, H. N. W. *J. Phys.: Condens. Matter* **2002**, *14*, 7551-7561.
- [6] Wijting, W. K.; Besseling, N. A. M.; Cohen Stuart, M. A. *J. Phys. Chem. B* **2003**, *107*, 10565.
- [7] Cahn, J. W. *J. Chem. Phys.* **1977**, *66*, 3667.
- [8] Brader, J.; Evans, R.; Schmidt, M.; Löwen, H. *J. Phys.: Condens. Matter* **2002**, *14*, L1-L8.
- [9] Dijkstra, M.; van Roij, R. *Phys. Rev. Lett.* **2002**, *89*, 208303-1.



## Samenvatting voor niet-vakgenoten

De titel van dit proefschrift luidt in gewoon Nederlands: Bevochtigingsverschijnselen en Interacties in Fasengescheiden Colloïd-Polymeermengsels. Ik denk dat in deze titel een aantal woorden voorkomen waarvan veel mensen niet precies weten wat ze betekenen. Als we bevochtigingsverschijnselen bestuderen, dan kijken we naar verschijnselen waar drie fasen (bijvoorbeeld gas, vloeistof en een vaste stof of twee vloeistoffen en vaste stof of twee vloeistoffen en een gas) met elkaar in evenwicht zijn. Bijvoorbeeld een druppel water die in evenwicht is met de lucht en op een tafel ligt. Colloïden zijn deeltjes met een afmeting tussen ongeveer een miljoenste en een duizendste van een millimeter, ze zijn groter dan gewone moleculen. Deze deeltjes bevinden zich in een medium. We zeggen dat ze in dat medium gedispergeerd zijn. Vaak zijn vaste of vloeibare deeltjes gedispergeerd in een vloeistof. Dit soort colloïdale systemen komen ook in het dagelijks leven voor, denk aan verf, inkt, melk, bloed en witbier. Voorbeelden waar een vaste stof of een vloeistof gedispergeerd is in een gas zijn rook en mist. Behalve dat colloïdale systemen praktische toepassingen hebben, zijn ze ook van belang als modelsysteem voor de wetenschap. Polymeren zijn moleculen die uit ketens van bijvoorbeeld honderd of duizend atomen bestaan. In de praktijk komen polymeren voor in bijvoorbeeld kunststoffen. Fasengescheiden betekent dat minimaal twee fasen waarneembaar zijn; in dit proefschrift twee vloeibare fasen. Deze fasen zijn gescheiden door een grensvlak. Interacties zijn de wisselwerkingen die colloïden of moleculen met elkaar of met een oppervlak kunnen hebben als ze ver van elkaar zijn of als ze dichtbij elkaar zijn. Deze wisselwerkingen kunnen ook gezien worden als de krachten die deeltjes op elkaar uitoefenen.

Bevochtigingsverschijnselen zijn belangrijk in het dagelijks leven. En niet alleen dat, we willen ze ook kunnen sturen. Water bevochtigt onbewerkt hout bijvoorbeeld heel erg goed. Zodanig dat het water helemaal in het hout kan trekken en vervolgens ervoor zorgt dat het hout gaat rotten. Brengen we nu een laag verf op het hout aan, dan wordt het hout veel slechter bevochtigd. Aan de andere kant is het wenselijk dat vloeibare verf makkelijk op het hout wordt aangebracht, de verf moet het hout goed bevochtigen. Nog een voorbeeld is een goretex jas. Als het regent willen we graag droog blijven; water moet buiten de jas blijven. Aan de andere kant willen we graag dat water aan de binnenkant van de jas is, ontstaan door zweet, makkelijk naar buiten kan. Daarom bestaat zo'n jas uit kleine vezels waar doorheen waterdamp (gasvormig water) wel naar



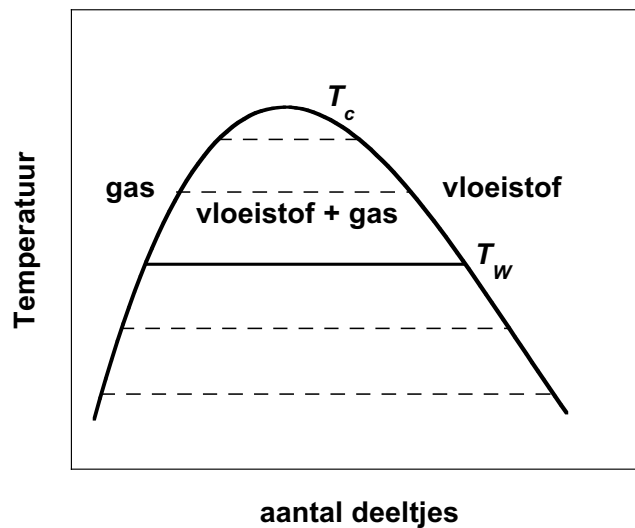
FIGUUR 1. Druppel in evenwicht met zijn gasfase op een vast oppervlak.

buiten kan. Deze vezels worden op hun beurt weer slecht bevochtigd door vloeibaar water zodat het regenwater niet naar binnen kan.

Hoe kunnen we nu vaststellen of een oppervlak door een bepaalde vloeistof goed of slecht bevochtigd wordt? Dat kan door de randhoek. In figuur 1 zien we een druppel op een vaste stof liggen. De druppel wordt aangeduid door L (van het engelse woord liquid), de lucht door G (van het engelse woord gas) en de vaste stof door S (engelse woord solid). De randhoek wordt aangeduid met de griekse letter  $\theta$ . Hoe kleiner deze hoek, hoe beter het oppervlak bevochtigd wordt. We hebben afgesproken dat als de randhoek  $0^\circ$  is, dan spreken we van volledige bevochtiging. We zien dan geen druppel(s) op het oppervlak liggen, maar er ligt een hele film op het oppervlak. Is de randhoek tussen  $0^\circ$  en  $180^\circ$  dan spreken we van partiële bevochtiging. Is de randhoek  $180^\circ$  dan spreken we van volledige droging. Dat laatste kan echter in vloeistof-gas systemen aan een vast oppervlak niet voorkomen.

Nu ga ik iets over vloeistof-gas gebieden in een fasendiagram vertellen en dat relateren aan bevochtigingsgedrag. In figuur 2 is een fasendiagram weergegeven. In de figuur is een zogenaamd kritisch punt aangegeven met  $T_c$ . Bij een temperatuur boven dit kritische punt vindt er geen gas-vloeistof overgang meer plaats als we het deeltjes aantal laten toenemen. Beneden deze temperatuur vinden we drie gebieden: een gasgebied, een vloeistof+gasgebied en een vloeistofgebied. De kromme dikke lijn die deze gebieden scheidt, noemen we de binodaal. In een gasfase zitten minder deeltjes dan in een vloeistoffase, daarom staat de gasfase links en de vloeistoffase rechts. Hebben we nu bij een gegeven temperatuur een systeem met een algehele samenstelling in het vloeistof+gas gebied dan zal het systeem fasenscheiden in een gasfase en een vloeistoffase met samenstellingen die precies aan weerszijden van een stippellijn op de binodaal





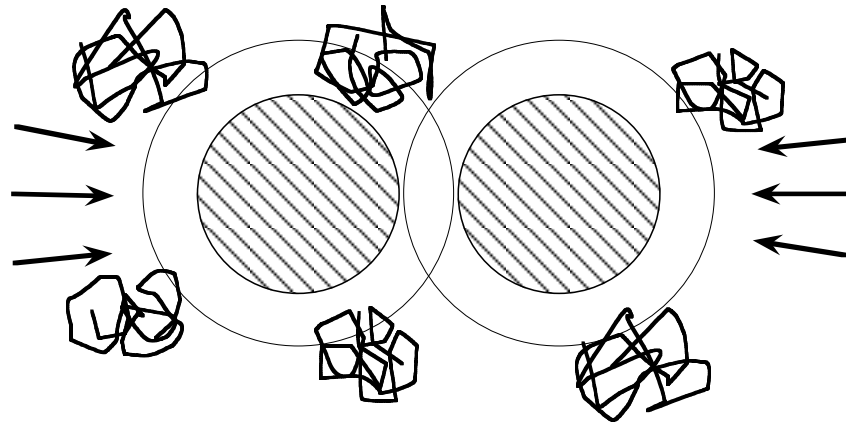
FIGUUR 2. Fasendiagram.

liggen. Er zijn vier stippelijnen getekend, maar eigenlijk moeten we bij elke temperatuur zo'n stippelijne denken. Zitten we meer naar rechts op de stippelijne, dan is er meer vloeistof, zitten we meer naar links dan hebben we meer gas. Vlakbij het kritisch punt zijn de samenstellingen van de gas- en vloeistoffase bijna hetzelfde.

In het vloeistof+gasgebied is ook een doorgetrokken lijn weergegeven met daarbij  $T_w$ . Bij deze temperatuur is iets bijzonders aan de hand ten aanzien van het bevochtigingsgedrag. Als we een oppervlak in het gas-vloeistof grensvlak aanbrengen, dan vindt boven deze temperatuur altijd volledige bevochtiging plaats en daaronder partiële. Echter niet in alle systemen hoeft per se partiële bevochtiging voor te komen. Het feit dat zo'n overgang van volledige naar partiële bevochtiging plaatsvindt noemen we een *bevochtigingsovergang*. Het subscript  $W$  slaat op de engelse term wetting transition.

De randhoek kan dus veranderen met de temperatuur. De grootte van de randhoek wordt bepaald door de grensvlakspanningen, aangeduid met  $\gamma$ , die bij de gas-vloeistof, vloeistof-vast en gas-vast-grensvlakken horen. Daarom staan die pijlen in figuur 1. De idee achter het bestaan van de grensvlakspanning zit hem in het feit dat moleculen liever diep in de fase zitten (in de bulk) dan in het grensvlak, het is een soort energiebarrière. We zouden dus het bevochtigingsgedrag kunnen veranderen door de grensvlakspanning te veranderen. De grensvlakspanning hangt op zijn beurt weer af van de interacties die moleculen in een fase met elkaar hebben, maar ook van de interacties die moleculen met het oppervlak hebben. En dit is het centrale thema van dit proefschrift. Ik heb gekeken naar de verandering van het bevochtigingsgedrag als we deze interacties veranderen of manipuleren.

Als we gewone moleculen zouden gebruiken dan kunnen we de interacties helaas niet zomaar zonder meer manipuleren. We kunnen alleen de temperatuur veranderen om



FIGUUR 3. Depletieinteractie. Door polymeer toe te voegen aan een colloïdale dispersie worden deeltjes naar elkaar toegedrukt.

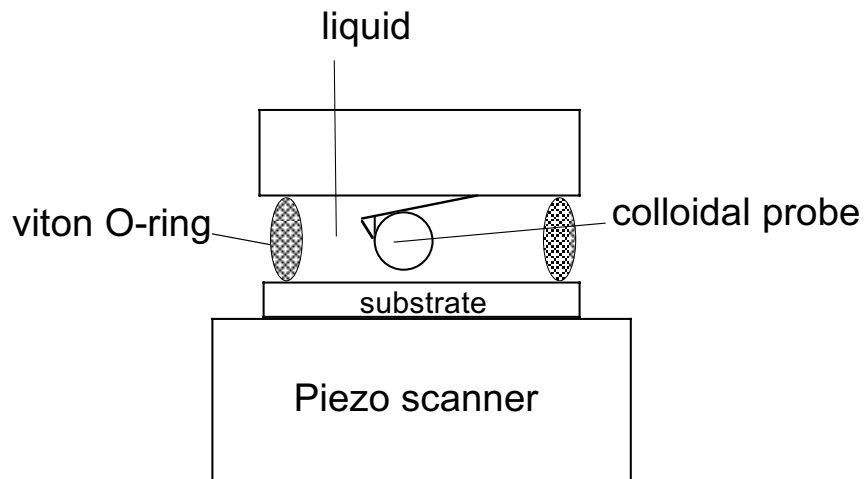
de interacties te veranderen. Gebruiken we colloïden, dan kunnen we wel de interacties zo manipuleren als we zelf willen.

Een belangrijke ontdekking ten aanzien van het bestaan van een vloeistoffase uit het verleden is dat moleculen, of in ons geval colloïden, elkaar aan moeten trekken. Deze aantrekkende kracht moet dan ook nog eens werken over een afstand die ongeveer even groot is als het molecuul (of colloïd) zelf. Voor bucky balls, dat zijn moleculen met de structuur van een voetbal, bestaat de vloeistofoestand niet omdat voor deze moleculen die aantrekkende kracht over een veel te kleine afstand werkt.

We kunnen bolvormige colloïden in een oplosmiddel zodanig maken dat ze zich gedragen als harde bollen. Dat wil zeggen dat als de middelpuntsafstand tussen deze bollen groter is dan de diameter dat ze elkaars aanwezigheid niet merken, de kracht (of interactie) die ze op elkaar uitoefenen is dan 0. Een afstand kleiner dan de diameter is niet mogelijk; de kracht is oneindig groot.

Voegen we nu polymeren toe aan deze harde bollen colloïden dan gebeurt er iets heel speciaals, de bollen gaan elkaar aantrekken, vandaar de term colloïd-polymer mixtures in de titel. Deze aantrekking werkt over een afstand die ongeveer even groot is als het polymeer zelf. Verder is de sterkte van deze aantrekking afhankelijk van de concentratie van de polymeren. We kunnen de aantrekking dus zelf sturen door de grootte van het polymeer en de concentratie te variëren.

Hoe kunnen we nu verklaren dat colloïden elkaar aantrekken als we er polymeer aan toevoegen? In figuur 3 zien we polymeren (zes stuks) in de buurt van twee colloïden of deeltjes. Het middelpunt van een polymeerkluwen kan niet dichtbij een deeltje komen dan weergegeven met de dunne cirkel. Hierdoor is de concentratie polymeer bij de wand van het deeltje plaatselijk lager dan verder weg in de oplossing. De laag binnen de dunne cirkel noemen we depletiezone (depletie betekent uitsluiting). De polymeren oefenen een osmotische druk uit op de colloïden. Als een enkel colloïd vrij in de oplossing is,



FIGUUR 4. Schematische weergave van een atomic force microscope.

dan is op elke plaats op het colloïd de osmotische druk hetzelfde. Echter, overlappen de depletiezones van 2 deeltjes elkaar, dan is de osmotische druk over beide deeltjes niet overal hetzelfde, maar in het overlapgebied tussen de deeltjes ontstaat een onderdruk. Hierdoor worden de colloïden naar elkaar toegedrukt, weergegeven door de pijlen. Effectief ontstaat hierdoor een aantrekking tussen de deeltjes die depletieinteractie wordt genoemd. Een belangrijke voorwaarde voor het optreden van depletieinteractie is dat de polymeren niet aan het oppervlak van een colloïd vast willen plakken, ze mogen niet of heel slecht adsorberen. Als heel veel colloïden naar elkaar toegedrukt worden, dan zal het systeem fasenscheiden in twee fasen. Een fase waar veel polymeren en weinig colloïden zijn, en een fase waarin weinig polymeren en veel colloïden zijn. Omdat we meer naar de colloïden kijken dan naar de polymeren noemen we de fase met weinig deeltjes *colloïdaal gas* en de fase met veel deeltjes *colloïdale vloeistof*. Voor de duidelijkheid, als we de fasen in bijvoorbeeld een reageerbuis bekijken, dan zien we van boven naar beneden: gasvormig lucht, vloeibaar colloïdaal gas en vloeibaar colloïdale vloeistof. Het fasengedrag van deze systemen is tamelijk analoog aan eenvoudige moleculaire systemen. Alleen wordt dit gedrag nu niet bepaald door de temperatuur, maar door de polymeerconcentratie.

In hoofdstuk 2 staan metingen van de depletieinteractie beschreven. De metingen zijn gedaan met een atomic force microscope. In figuur 4 staat een deel van dit apparaat schematisch weergegeven. Het bestaat uit een heel klein veertje met een hele kleine naald (het driehoekje links naast de colloidal probe) eraan, zo dun, dat in de punt van de naald slechts een paar atomen zitten. Deze naald kunnen we door middel van een piezo scanner op verschillende afstanden van een vast oppervlak (substrate) houden. Omdat de naald zo klein is kunnen we krachten meten die op atomaire schaal tussen

het naaldje en het oppervlak plaatsvinden. Deze krachten kunnen we meten doordat de veer doorbuigt bij een bepaalde kracht op een bepaalde afstand. We richten een laserbundel op de bovenkant van de veer. Deze wordt gereflecteerd op een (niet weergegeven) detector. Als de veer doorbuigt valt het laserlicht anders op de detector dan wanneer deze niet doorbuigt. De punt van de naald echter is tamelijk slecht gedefinieerd. Een bolletje is veel beter gedefinieerd. Daarom hebben we een bolletje (een colloïdal probe) aan de veer geplakt. Als we nu het veertje met bol bij een oppervlak brengen in een polymeeroplossing, dan kunnen we de depletiekracht meten. Een belangrijk resultaat van mijn metingen is dat de depletiekracht voor het gemeten systeem zwakker is dan voorspeld is door theorieën. Dat komt doordat niet geheel aan de voorwaarde wordt voldaan dat de polymeren niet aan het oppervlak blijven plakken.

Brengen we nu een vast oppervlak aan in het grensvlak tussen de colloïdale gas- en vloeistoffasen, dan kunnen we het bevochtigingsgedrag bestuderen. Dit staat beschreven in hoofdstuk 3 en 4. In deze hoofdstukken hebben we niet naar een druppel op een plaat gekeken, omdat druppels van colloïdale vloeistoffen in colloïdaal gas niet makkelijk te maken zijn. Daarom is het bevochtigingsgedrag bestudeerd door naar de meniscus aan een verticale glazen fiber te kijken en zo de randhoek te meten. Een meniscus is het kromme oppervlak dat een vloeistof-gas grensvlak maakt aan een vast oppervlak. Er is gevonden dat ook in een colloïd-polymeer systeem een bevochtigingsovergang plaatsvindt. Als we aan een harde wand het kritisch punt naderen vindt een overgang van partiële naar volledige bevochtiging plaats. Door polymeren aan de glazen fiber chemisch te verankeren krijgen we een zachte fiber. Naderen we aan een zachte fiber het kritisch punt, dan vinden we een overgang van partiële bevochtiging naar volledige droging. Voor colloïdale systemen bestaat volledige droging dus wel.

## List of publications

- Wijting, W. K.; Besseling, N. A. M.; Cohen Stuart, M. A. Wetting in a Colloidal Liquid-Gas System *Physical Review Letters* **2003**, *90*, 196101. (chapter 3)
- Wijting, W. K.; Besseling, N. A. M.; Cohen Stuart, M. A. Wetting Behaviour in Colloid-Polymer Mixtures at Different Substrates *Journal of Physical Chemistry B* **2003**, *107*, 10565-10570. (chapter 4)
- Wijting, W. K.; Knoben, W; Besseling, N. A. M.; Leermakers, F.A.M.; Cohen Stuart, M. A., Depletion Interaction Measured by Colloidal Probe Atomic Force Microscopy *submitted to Physical Chemistry Chemical Physics*. (chapter 2)



# Dankwoord

Bij het schrijven van dit proefschrift zijn meerdere mensen betrokken geweest, die ik bij deze wil bedanken. In de eerste plaats is dat mijn promotor Martien. Ik had wat meer aandacht nodig dan de gemiddelde promovendus en ik ben blij dat ik die van je heb kunnen krijgen. Dat gebeurde veelal in de vorm van gesprekken of suggesties op experimenteel vlak, maar ook ten aanzien van de teksten. Je bijdrage heeft beslist geleid tot een verbetering van alles wat in dit proefschrift staat beschreven.

Dan is er mijn copromotor Klaas die altijd voor me klaar stond. We hebben de afgelopen vijf jaar heel wat meegemaakt. En ik heb heel veel van je geleerd. Jouw bijdrage is zonder meer de belangrijkste. Al jouw suggesties hebben zeker geleid tot een beter resultaat, zowel op wetenschappelijk gebied als op tekstueel gebied.

Daarnaast wil ik een aantal andere mensen van de vakgroep bedanken. Ten eerste Wout Knoben die me de kneepjes van het vak van bolletjes plakken heeft geleerd en belangrijke metingen voor hoofdstuk 2 heeft verricht. Deze metingen waren aanvankelijk bedoeld als 'testmetingen' voor een onderdeel van je afstudeervak dat je uitvoerde in het kader van het promotie-onderzoek van Jasper van der Gucht, maar hebben, gecombineerd met aanvullende experimenten, geleid tot een waardevolle bijdrage ten aanzien van het begrip van depletie-interactie. Ten tweede was er de inbreng van Remco Fokkink. Zonder zijn bijdrage bij het optimaliseren van de randhoekmeter konden belangrijke experimenten voor de hoofdstukken 3 en 4 niet worden uitgevoerd. Daarbij was de ook technische hulp van Ronald Wegh onmisbaar. Vervolgens wil ik Frans Leermakers bedanken voor de SCF-berekeningen die we samen hebben uitgevoerd. Verder heb ik ook met plezier twee jaar in je kolloidchemieteam meegedraaid. Verder kwam een aantal andere inhoudelijke bijdragen van Gerard Fleeer, Maarten Biesheuvel (jammer dat we je saaie berekeningen niet hebben kunnen gebruiken) en Mieke Kleijn. Van Ben Spee zal me altijd bij blijven dat hij, altijd direct apparatuur, glaswerk en chemicaliën kon leveren, dan wel bestellen. Ik hoop dat je uitbundig kan genieten van de vut die nu voor je ligt. Gert Buurman, bedankt voor het vervaardigen van diverse tekeningen en het omslagontwerp.

De secretariële en emotionele steun in wat voor situaties dan ook van Josie Zeevat en Wil Kleijne waren goud waard. En dat brengt me op het feit dat er ook veel mensen zijn die op een andere manier hebben bijgedragen. In de eerste plaats Wilfred, mijn trouwe kamergenoot, die ik zo dankbaar ben dat hij me niet voor de hele vakgroep voor schut heeft gezet toen ik in de zuurkast opgesloten zat. Maar ook hebben we samen wel lol

gehad. Verder wil ik ook Stefan van der Burgh bedanken, voor het leren bierbrouwen en het feit dat we een passie voor (Duitse) auto's hebben. Andere collega AIO's en medewerkers die ik vooral voor de gezellige jaren wil bedanken zijn in willekeurige volgorde: Wouter, Jos & Mireille, Jasper (de lay-out van dit boekje zal je wel bekend voorkomen), Joanne, Martijn, Anita, Mara, Stefan Janssen, Marijn, Desiree, Monique, Sonja, Natalie en Maykel.

Behalve binnen de leerstoelgroep zijn er ook mensen van buiten geweest die hebben bijgedragen aan de totstandkoming van dit proefschrift. Dat zijn de mensen van de werkplaats, Jan Theunissen en Henny van Beek, en de glasblazerij, Gert Nieuwboer. De mensen van Optel wil ik bedanken voor hun bijdrage aan het optimaliseren van de randhoekmeter. Zinnvolle wetenschappelijke discussies zijn gevoerd met Els de Hoog, Dirk Aarts, Henk Lekkerkerker, Marjolein Dijkstra en René van Roij.

Marloes Biermans, Nienke Geudeker en Mirjam Hibma wil ik bedanken voor het geven van commentaar op de samenvatting voor niet-vakgenoten. Behalve dat er de afgelopen jaren veel tijd in mijn proefschrift is gaan zitten, heb ik ook nog (misschien een beetje te veel) tijd kunnen besteden aan ontspanning. Ik wil dan ook de vrienden van het USKO, in het bijzonder Johan, en Arezzo, in het bijzonder Guido en Chris, bedanken dat ik met jullie zo fijn muziek heb kunnen maken. Daarnaast ook dank aan de bridgers van Dombo, in het bijzonder mijn viertalgenoten met wie wij dit seizoen ook op bridgegebied gepromoveerd zijn.

Verder wil alle familieleden bedanken die altijd interesse hebben getoond in mijn onderzoek. Opa Brouwer, hoe moeilijk voor jou de laatste jaren ook waren, je vroeg altijd hoe het met mijn onderzoek ging. Het is en was voor ons beiden toch wel bijzonder dat ik ruim 60 jaar na jou ook doctor in de scheikunde mag worden. Jammer dat je bij mijn verdediging niet meer aanwezig kan zijn. Karin, mijn oudste zus, bedankt voor het nemen van de foto's voor de kaft. Marleen en Carla, mijn andere twee zussen, jullie ook bedankt. Ik wil besluiten met mijn ouders te bedanken. Voor alles wat jullie voor me betekenen. Vooral de laatste maanden waren erg moeilijk voor mij, en ik ben blij dat jullie me daarin hebben willen ondersteunen. Daarom is dit proefschrift aan jullie opgedragen.



## Curriculum vitae

Wim Wijting werd geboren op 3 maart 1972 te Apeldoorn. In 1989 behaalde hij zijn HAVO-diploma aan de Christelijke Scholengemeenschap de Heemgaard te Apeldoorn. Na in 1992 zijn propaedeuse van het HLO in Deventer behaald te hebben, begon hij aan de studie scheikunde aan de Universiteit Utrecht. In 1998 behaalde hij zijn doctoraal diploma met als hoofdvak Fysische en Colloïdchemie. In januari 1999 begon hij aan het in dit proefschrift beschreven promotie-onderzoek aan de leerstoelgroep Fysische Chemie en Kolloïdkunde van Wageningen Universiteit. Naast zijn werkzaamheden heeft hij zich ook verdienstelijk gemaakt als organist in diverse orkesten, met name in de grote werken van Johann Sebastian Bach.

Het in dit proefschrift beschreven onderzoek is gefinancierd door de Nederlandse Organisatie voor Wetenschappelijk Onderzoek (NWO).